

**Dissertation zur Erlangung des Doktorgrades  
der Fakultät für Chemie und Pharmazie  
der Ludwig-Maximilians-Universität München**



**Novel Insights into the Pathophysiology of Peripherin-2  
Mutations in Rod and Cone Photoreceptors**

**Sybille Böhm**

**aus**

**Schäßburg, Rumänien**

**2018**

## **Erklärung**

Diese Dissertation wurde im Sinne von § 7 der Promotionsordnung vom 28. November 2011 von Herrn Prof. Dr. Martin Biel betreut.

## **Eidesstattliche Versicherung**

Diese Dissertation wurde eigenständig und ohne unerlaubte Hilfe erarbeitet.

München, den 12.10.2018

---

(Sybille Böhm)

Dissertation eingereicht am	12.10.2018
1. Gutachter:	Prof. Dr. Martin Biel
2. Gutachter:	PD Dr. Stylianos Michalakis
Mündliche Prüfung am	18.12.2018

## Table of contents

<b>1</b>	<b>Preface</b> .....	<b>7</b>
<b>2</b>	<b>Introduction</b> .....	<b>8</b>
2.1	<b>Anatomy of the retina</b> .....	<b>8</b>
2.2	<b>Anatomy of photoreceptors</b> .....	<b>9</b>
2.3	<b>Inherited retinal diseases</b> .....	<b>10</b>
2.3.1	Retinitis pigmentosa .....	10
2.4	<b>Peripherin-2</b> .....	<b>11</b>
2.5	<b>Rom-1</b> .....	<b>12</b>
2.6	<b>Mutations in <i>PRPH2</i> and <i>ROM1</i></b> .....	<b>12</b>
2.7	<b>Adeno-associated viruses</b> .....	<b>13</b>
<b>3</b>	<b>Aim of the study</b> .....	<b>15</b>
<b>4</b>	<b>Materials and methods</b> .....	<b>16</b>
3.1	<b>Animals</b> .....	<b>16</b>
3.2	<b>Chemicals, solutions and buffers</b> .....	<b>16</b>
3.3	<b>Molecular biology</b> .....	<b>16</b>
3.3.1	Plasmids .....	16
3.3.2	Polymerase chain reaction (PCR) .....	17
3.3.3	Precipitation of DNA fragments .....	17
3.3.4	Restriction analysis.....	18
3.3.5	Agarose gel electrophoresis and DNA fragment isolation.....	18
3.3.6	Dephosphorylation and ligation .....	18
3.3.7	Transformation .....	18
3.3.8	Inoculation of bacterial cells and isolation of plasmid DNA.....	19
3.3.9	RNA isolation and cDNA synthesis .....	20
3.3.10	Quantitative real-time PCR (qPCR).....	20
3.3.11	<i>In silico</i> prediction of splicing .....	20
3.3.12	Genomic DNA isolation .....	20

---

3.3.13	Construction and cloning of the <i>PRPH2</i> minigene .....	21
3.3.14	Side-directed mutagenesis .....	22
<b>3.4</b>	<b>Cell culture</b> .....	<b>22</b>
3.4.1	Cultivation of mammalian cell lines .....	22
3.4.2	Transfection.....	22
<b>3.5</b>	<b>Protein biochemistry</b> .....	<b>23</b>
3.5.1	Isolation and quantification of proteins .....	23
3.5.2	Membrane preparations .....	23
3.5.3	Co-immunoprecipitation (co-IP).....	24
3.5.4	SDS-PAGE .....	24
3.5.5	Western blotting.....	25
3.5.6	Native protease cleavage assay .....	26
3.5.7	Peptide competition assay .....	26
<b>3.6</b>	<b>Sucrose density gradient centrifugation</b> .....	<b>27</b>
<b>3.7</b>	<b>Production of rAAVs</b> .....	<b>27</b>
3.7.1	Transfection and harvest.....	27
3.7.2	Iodixanol gradient centrifugation .....	28
3.7.3	Anion exchange chromatography.....	29
3.7.4	Concentration of rAAVs.....	29
3.7.5	rAAV titer determination .....	30
<b>3.8</b>	<b>Subretinal injection</b> .....	<b>31</b>
<b>3.9</b>	<b>Immunohistochemistry</b> .....	<b>31</b>
<b>3.10</b>	<b>Confocal microscopy</b> .....	<b>32</b>
<b>3.11</b>	<b>Fluorescence-activated cell sorting (FACS)</b> .....	<b>32</b>
<b>3.12</b>	<b>Isolation of photoreceptor outer segments</b> .....	<b>33</b>
<b>3.13</b>	<b>Förster resonance energy transfer (FRET)</b> .....	<b>33</b>
<b>3.14</b>	<b>Statistics</b> .....	<b>35</b>
<b>4</b>	<b>Results</b> .....	<b>36</b>
4.1	rAAV <i>PRPH2</i> minigenes confer efficient protein expression in rods and cones ..	36
4.2	<i>In silico</i> mRNA splice analysis of exon 2-specific peripherin-2 point mutations..	37

---

4.3	Comparative splice analysis of WT and mutant peripherin-2 minigenes in rods and cones.....	38
4.4	Quantitative analysis of native peripherin-2 splice isoforms.....	41
4.5	Peripherin-2 isoform encoded by exon 1 is mislocalized in photoreceptors .....	43
4.6	Protein expression and localization of per <sup>MT</sup> in rods and cones .....	45
4.7	Splicing and protein expression of a rod-dominant per <sup>MT</sup> in cones and a cone-dominant per <sup>MT</sup> in rods .....	49
4.8	Impact of the disease-linked per <sup>MT</sup> on homo- and heteromeric protein-protein interactions .....	50
4.9	P210 and C214 are crucial for the proper folding of the distal D2 loop .....	50
4.10	Quantification of per <sup>WT</sup> , per <sup>MT</sup> , and Rom-1 protein-protein interactions in HEK293T cells using FRET .....	52
4.11	Subunit assembly of homo- and heteromeric per <sup>WT</sup> , per <sup>MT</sup> , and Rom-1 complexes. ....	54
4.12	Rod OS targeting of homo- and heteromeric per <sup>WT</sup> , per <sup>MT</sup> , and Rom-1 complexes ..	57
4.13	Analysis of the per <sup>WT</sup> -per <sup>MT</sup> binding properties in rod OSs using FRET .....	59
5	Discussion.....	61
6	Summary.....	67
7	Zusammenfassung.....	69
8	References.....	71
9	Appendix.....	77
9.1	Supplementary tables .....	77
9.2	Abbreviations .....	85
9.3	Curriculum vitae .....	88
9.4	Lebenslauf .....	89

---

<b>9.5</b>	<b>List of publications .....</b>	<b>90</b>
<b>9.6</b>	<b>Danksagung.....</b>	<b>91</b>

# 1 Preface

“What we know is a drop, what we don’t know is an ocean”. This is a quote by the English mathematician and physicist Sir Isaac Newton, one of the foremost scientists and a key player in the scientific revolution [1]. Almost 300 years later, substantial and constant progress has been made in virtually all fields of science to further broaden human knowledge and simultaneously reduce this “ocean” of ignorance. These fields of science also include the research on retinal disorders. Inherited retinal dystrophies (IRDs) are a major genetic cause of irreversible vision loss worldwide. Great advances have been made over the last decades in identifying genes and genetic defects leading to IRDs [2]. The peripherin-2 gene (*PRPH2*) was one of the first found to be associated with this disease [3]. Thereupon, constant research has been conducted to understand the precise function of peripherin-2, to identify additional disease-causing mutations in this gene, and to analyze their deleterious effects. However, despite great advances, many important questions concerning the pathophysiology of *PRPH2* mutations remained unclear, hampering the development of appropriate treatment strategies for the affected individuals. This PhD thesis was conducted to elucidate the disease mechanisms of enigmatic disease-linked peripherin-2 mutations. The results of this study gained unexpected and novel insights into the pathophysiology associated with this gene and may pave the way for future therapeutic interventions.

## 2 Introduction

### 2.1 Anatomy of the retina

The mammalian retina forms a thin sheet of neural tissue at the back of the eye. The fundamental, inverse organization of the retina is conserved across all vertebrates. The retina is composed of different neuronal and non-neuronal cell types. The five major neuronal cell types include the photoreceptors, bipolar cells, horizontal cells, amacrine cells and ganglion cells. The major non-neuronal retinal cell type are Müller glial cells, which provide metabolic and homeostatic support (Figure 1) [4]. Photoreceptors consist of rods and cones and convert the light into electrical signals, a process known as phototransduction. The photoreceptors are distally embedded in the retinal pigment epithelium (RPE) which is involved in phagocytosis of toxic products, in digestion of shed photoreceptor outer segments and in the regeneration of the visual pigment. The cell bodies of rods and cones form the outer nuclear layer (ONL) which is followed by the outer plexiform layer (OPL). In the OPL, electrical impulses generated in the photoreceptors are transmitted via synaptic connections to bipolar and horizontal cells [5]. Their cell bodies together with amacrine cells form the inner nuclear layer (INL). Proximal to the INL, bipolar and amacrine cells are connected to ganglion cells arranging the inner plexiform layer (IPL). Ganglion cells, shaping the ganglion cell layer (GCL), constitute the sole output neurons of the retina projecting their axons to higher visual centers in the brain [4].

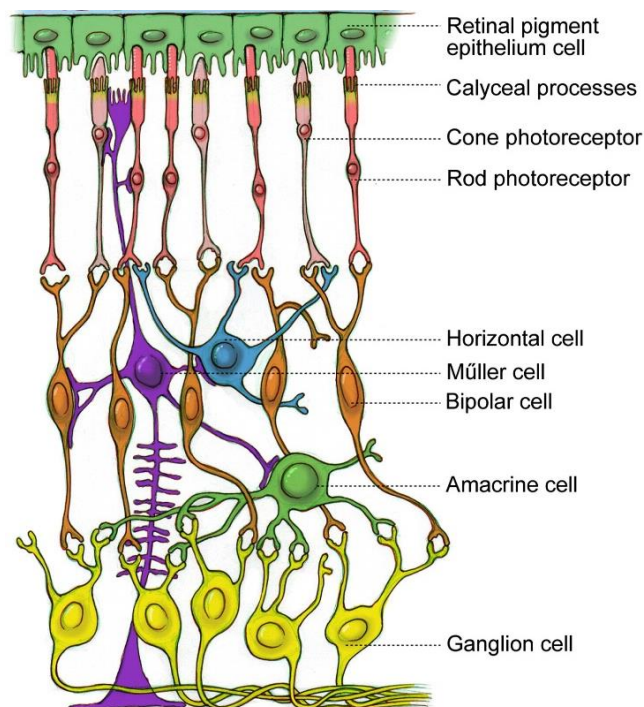
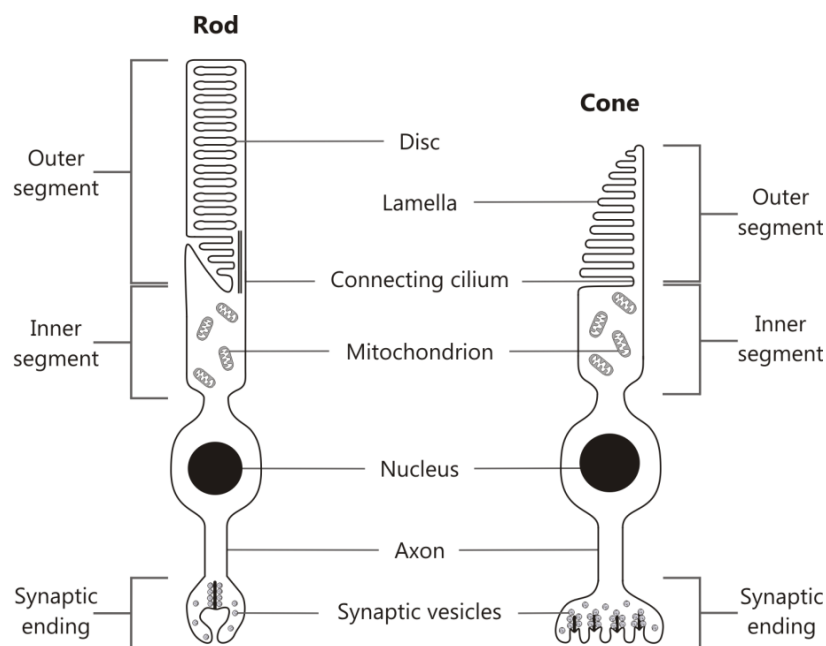


Figure 1 Cellular structure of the retina [5].

## 2.2 Anatomy of photoreceptors

Rods and cones are the primary light-sensing cells of the retina. Rods account for 95 % of the photoreceptors in the human retina [3]. They are highly sensitive to light as they can detect even a single photon. Due to this remarkable feature, rods are ideally suited for dim-light and night vision constituting the scotopic pathway [6, 7]. In contrast, cones are 100 times less sensitive than rods. However, they show much faster response kinetics during phototransduction. Depending on the species, different cone photoreceptor types can be found with each of them being most sensitive to light of a specific wavelength. Hence, cones are responsible for bright-light and color vision forming the photopic pathway [4]. Additionally, in primates they are highly concentrated in a specific region of the retina, termed macula, which mediates central high acuity vision [3].

Rods and cones share a very similar basic morphology. Both photoreceptor types consist of an outer segment (OS), an inner segment (IS), the cell body containing the nucleus, and the axon terminating in the synapse. In rods, the OS harbors tightly stacked, individualized discs that are largely disconnected from the ciliary plasma membrane. In contrast, cones do not possess distinctly separated discs, but lamellae formed by evaginations of the cell membrane [8]. The next compartment, the IS, contains the cell machinery required for protein synthesis and energy production. It is linked to the OS via a connecting cilium tightly regulating the transport of cargo between both segments. The IS is followed by the nucleus and the axon which finally terminates in the synapse transmitting the electrical signal generated during phototransduction to downstream neurons.



**Figure 2 Rod and cone photoreceptor structure.** Both cell types can be divided into three compartments: OS, IS, and the synaptic ending. OS and IS are coupled via the connecting cilium. Rod OSs contain discs, while cones have lamellae.

## 2.3 Inherited retinal diseases

Inherited retinal diseases (IRDs) are a large group of genetically and clinically heterogeneous disorders affecting more than two million people worldwide [9]. They are inherited as Mendelian traits or via mitochondrial DNA, and are a major cause of gradual vision loss characterized by a slow and progressive degeneration of the retina, ultimately resulting in blindness. IRDs can either affect the entire retina or can be restricted to the macula.

Cutting-edge treatment approaches including cell transplantation of retinal or stem cells, artificial retinal prostheses, and gene therapy have been researched through preclinical and clinical studies and have yielded significant progress during the recent decade [10]. On December 19, 2017, the first gene therapy treatment Voretigene Neparvovec (Luxturna, Spark Therapeutics) for Leber congenital amaurosis or retinitis pigmentosa, both IRDs, caused by a biallelic *RPE65* mutation, was approved for clinical commercial use in the United States [11]. However, there are still many challenges to overcome, as the heterogeneity of causative genes in IRDs precludes the development of a common, gene- or mutation-independent treatment [10].

### 2.3.1 Retinitis pigmentosa

Retinitis pigmentosa (RP) is the most common type of IRDs with an estimated incidence of 1:3500 to 1:4000 [12]. Despite the diverse genetic origin with more than 3000 mutations in approx. 70 genes, RP patients share many clinical hallmarks. These include an abnormal, punctuate pigmentation and thinning of the retina due to dysfunction and degeneration of the photoreceptors and, in some cases, the RPE [10]. In the majority of RP cases, an initial degeneration of rods is followed by a secondary atrophy of cones. The deterioration of cones in the advanced stages of the disease is due to the co-dependence between the two photoreceptor types [13, 14]. In addition to night blindness, patients suffering from RP display a gradual loss of the peripheral visual field leading to tunnel vision. In the later stage, when cones start to degenerate, patients also show daylight vision impairments resulting from the loss of both peripheral and central vision [10].

All forms of RP are progressive, however, the mode of inheritance as well as the age of disease onset ranging from childhood to middle age are highly variable. RP can be inherited in an autosomal dominant, autosomal recessive, X-linked, or in rare cases also digenic manner [15, 16]. To date, mutations in 22 different genes have been associated with autosomal dominant RP (adRP) [17]. However, only a few of these genes, including *PRPH2*, show a high prevalence in the populations examined so far [10].

## 2.4 Peripherin-2

Peripherin-2, also known as retinal degeneration slow (RDS), is a photoreceptor-specific transmembrane glycoprotein which is crucial for the formation, maintenance and renewal of both rod and cone OSs [8, 18]. Accordingly, peripherin-2 knock out mice (*rds*<sup>-/-</sup>) are lacking OSs and show strong impairments of retinal function [19, 20]. In the OSs, peripherin-2 is exclusively located at the rim regions of the rod discs and cone lamellae [8, 21].

The protein is encoded by the human peripherin-2 gene (*PRPH2*), which is localized on chromosome 6p21.2 and spans approx. 26 kb. *PRPH2* consists of three exons segregated by two large introns [22]. Peripherin-2 belongs to the super-family of tetraspanins, which share several highly conserved structural features such as four helical transmembrane domains (T1-T4), a cytoplasmic N- and C-terminus and two extracellular (cones) or intradiscal (rods) loops termed D1 and D2 (Figure 3) [23, 24]. Generally, tetraspanins are known to form functional membrane microdomains assembling via homo- and heteromeric protein-protein interactions [25]. Peripherin-2 forms high-order oligomers composed of dimers tethered to non-covalently linked tetramers. The tetramer formation is mediated by the large D2 loop [26, 27]. This tetrameric structure constituting the core unit of peripherin-2 is postulated to be crucial for proper trafficking to and incorporation into newly shaped rod OS disc membranes [28]. The D2 loop contains seven cysteine residues, of which six (C165, C166, C213, C214, C222 and C250) are stabilizing its structure via intramolecular disulfide bonds [25, 29]. The remaining cysteine (C150) is involved in intermolecular disulfide bonding. By forming this disulfide bond the assembly of peripherin-2 tetramers into covalently linked octamers and higher-order complexes is initiated. The high-order oligomerization of peripherin-2 tetramers occurs in OSs and is essential for the correct formation of this compartment [29-33].

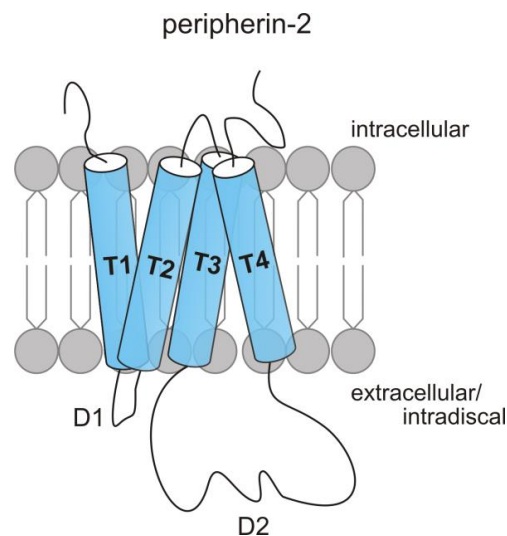


**Figure 3 Topology of peripherin-2.** Peripherin-2 consists of four transmembrane domains (T1-T4). N- and C-terminus are cytoplasmic whereas the D1 and D2 loop are located within the extracellular space (in cones) or within the discs (in rods).

## 2.5 Rom-1

Rom-1 (rod outer segment membrane protein 1) is a non-glycosylated homolog of peripherin-2. Akin to peripherin-2, Rom-1 is localized to the rim regions of both rod and cone OSs [34, 35]. Both proteins share an approx. 35 % sequence identity and are forming non-covalently linked heterotetramers and covalently linked higher-order complexes [26, 34]. However, despite the aforementioned similarities, Rom-1 cannot compensate for the function of peripherin-2 [19, 20]. The precise function of Rom-1 has not been clarified yet, but previous studies suggest that it likely regulates OS morphogenesis by fine tuning the peripherin-2/Rom-1 ratio and the distribution of peripherin-2 complexes to the rim regions of rod discs or cone lamellae [36].

## 2.6 Mutations in *PRPH2* and *ROM1*

Over 150 individual disease-causing mutations in *PRPH2* have been described in patients leading to a variety of clinical phenotypes. These are ranging from rod-dominant retinal disorders involving the peripheral retina such as RP or cone-rod dystrophy to multiple classes of cone-dominant macular dystrophies such as adult-onset foveomacular vitelliform dystrophy (AFVD), cone dystrophy and pattern dystrophy [22, 31, 37]. However, despite some progress in the past, the molecular mechanisms underpinning the differential penetrance of single *PRPH2* mutations in rods and cones are largely unknown. This is due to the fact that rod- or cone-dominant mutations do not correlate with the type or position of the mutation in the primary protein sequence [38].

Most of the *PRPH2* mutations have been implicated in adRP accounting for up to 10 % of all adRP cases: The majority of them are point mutations located in exon 2 [22, 39], which encodes for the distal half of the D2 loop domain and the proximal part of T4 (Figure 4).

In contrast to *PRPH2*, no monogenic disease-causing mutations have been found in *ROM1* so far [40]. However, a digenic form of RP has been associated with mutations in both *PRPH2* and *ROM1* [41]. The affected persons are double heterozygous for the *L185P* mutation in *PRPH2* and one of three different mutations in *ROM1* [41-43]. Although the causal mechanisms of this rare digenic form of RP are yet not fully understood, previous studies propose abnormalities in peripherin-2/Rom-1 subunit assembly and/or reduced total levels of peripherin-2 and Rom-1 [44, 45].



genome, AAVs can be easily manipulated by replacing viral *rep* and *cap* with a desired gene expression cassette thus making them a valuable multifunctional tool for different approaches in research including gene therapy [46, 47]. These recombinant adeno-associated virus (rAAV) vectors vary in their transduction efficiency and tropism, i.e. their preference for entering cells of a particular tissue, which is determined by their different serotypes. Among 12 human serotypes discovered to date, i.e. AAV1-12, AAV2 was the first serotype successfully applied in retinal gene transfer transducing the RPE and ganglion cells [46, 47]. Pseudotyping of rAAVs, i.e. the cross packaging of the genome of one ITR serotype into the capsid of a different serotype, has allowed broadening their tropism by creating novel hybrid vectors [48]. Thus, AAV2/8 containing the ITRs of AAV2 pseudotyped with the capsid of AAV8 has been shown to transduce murine photoreceptors very efficiently [49]. Rational design and directed evolution strategies led to the development of new AAV variants (e.g. AAV2/8Y33F or 7m8 AAV2) with improved transduction efficacies and/or widespread and faster transgene expression kinetics in retinal cells [50-52].

In conclusion, given the aforementioned properties and additional advantages of the rAAV vectors including the ability to infect both dividing and non-dividing cells, the lack of apparent pathogenicity, and episomal long-term expression, rAAV-mediated gene delivery is currently the most widely used approach for gene therapy in the retina [52-55].

### 3 Aim of the study

Point mutations in *PRPH2* are associated with severe retinal dystrophies deteriorating the structure or function of rod or cone photoreceptors. The molecular pathways underlying this differential penetrance of individual *PRPH2* mutants in rods and cones are currently unknown. However, the exact knowledge of these mechanisms is essential to develop appropriate treatment strategies for the affected individuals.

The initial hypothesis of this study is that the rod- or cone-dominance of disease-linked *PRPH2* mutants might correlate with their differential effects on distinct molecular mechanisms in rods and cones. In particular, these mechanisms include i) mRNA splicing, ii) protein expression, iii) protein transport/localization, and iv) protein-protein interactions. To address this hypothesis, this study is set out to examine six rod- and five cone-dominant point mutations in *PRPH2* in HEK293T cells and transduced murine photoreceptors. To achieve this goal, a variety of different methods will be applied. *PRPH2* wild type and mutant minigenes will be used in all experiments for a comprehensive analysis of mRNA splicing and protein expression *in vitro* and *in vivo*. For the latter, recombinant adeno-associated virus (rAAV) vectors will be produced and subretinally delivered into wild type mice. Analysis of the protein-protein interactions will be achieved using FRET measurements and sucrose density gradient centrifugation.

The results of this study will provide novel insights into the pathophysiology of *PRPH2* mutations and may offer new and innovative approaches for future therapies.

## 4 Materials and methods

### 3.1 Animals

For all experiments in this study, wild type C57Bl/6J mice were used. All procedures concerning animals were carried out with permission of local authorities (District Government of Upper Bavaria). Anesthesia was performed by intraperitoneal injection of ketamine (40 mg/kg body weight) and xylazine (20 mg/kg body weight). All mice received food (Ssniff; regular feed: R/M-H; breeding feed: M-Z Extrudat) and water *ad libitum* and were maintained in a 12 h light/dark cycle (lights on at 7 am). Euthanasia was performed by cervical dislocation.

### 3.2 Chemicals, solutions and buffers

All chemicals used had the quality “*pro analysi*” or “for molecular biological use” and were obtained from VWR, Sigma-Aldrich, Merck, Fluka, Roche, Bio-Rad or Roth if not mentioned otherwise. For all solutions, high pure and deionized water was used (Milli-Q Plus System, Millipore). Additionally, all solutions and buffers were autoclaved (Sterilisator, Münchener Medizin Mechanik).

### 3.3 Molecular biology

#### 3.3.1 Plasmids

##### pcDNA3.1

The standard pcDNA3.1 vector (Invitrogen) was designed for high-level stable and transient expression in mammalian cell lines. In this study, it was used for the transient transfection of transgenes in SV40 large T antigen expressing HEK293T cells (LentiX 293 T Cell Line, Clontech Laboratories).

##### pAAV2.1

For episomal *in vivo* expression of transgenes delivered by recombinant adeno-associated viruses (rAAVs), the pAAV2.1 *cis* [52, 53] plasmid was used. The DNA packaging capacity of rAAVs comprises approx. 4.7 kb including the inverted terminal repeats (ITRs), the coding sequence of the gene of interest and regulatory elements, such as promoter or transcriptional termination sequences [56, 57]. In this study, the vector contained the human rhodopsin

promoter (hRHO) [58] or murine short-wavelength opsin promoter (mSws) [53] for specific gene expression in murine rod or cone photoreceptors. The expression cassette was flanked by AAV2 ITRs. The ITRs encode all *cis*-acting elements for efficient replication (*rep*) and packaging (*cap*) of rAAVs in the presence of an additional AAV *trans* and adenovirus helper plasmid (pAD Helper). As AAV *trans* plasmid pAAV2/8YF [59] was used containing the AAV2 *rep* gene and capsid protein encoding genes from AAV8 for enhanced specific transduction of photoreceptors [58, 60, 61]. As adenovirus helper plasmid pAdDeltaF6 [62] was used.

### 3.3.2 Polymerase chain reaction (PCR)

PCR reaction conditions and pipetting schemes were adjusted for the different polymerases and the respective application according to the manual of the corresponding manufacturer. Standard PCR conditions of each polymerase are summarized in Table 1:

**Table 1 Standard PCR conditions for polymerases used in this study.**

Polymerase	Q5 (NEB)	Kapa HiFi (Roche)	Herculase II (Agilent Technologies)
Initial denaturation	98 °C 30 sec	95 °C 3 min	95 °C 2 min
Denaturation	98 °C 10 sec	98 °C 20 sec	95 °C 20 sec
Annealing	X °C 30 sec	X °C 15 sec	X °C 20 sec
Elongation	72 °C 30 sec/kb	72 °C 30 sec/kb	72 °C 30 sec/kb
Final elongation	72 °C 2 min	72 °C 1 min/kb	72 °C 3 min
Hold	10 °C 15 min	10 °C 15 min	10 °C 15 min

The annealing temperatures (X) were chosen with regard to the respective melting temperatures of the used primers purchased from Eurofins Genomics. The number of cycles used for denaturation, annealing and elongation was adjusted depending on the respective application.

### 3.3.3 Precipitation of DNA fragments

To purify a PCR product, H<sub>2</sub>O was added to a total volume of 100 µl followed by 10 µl of 3 M sodium acetate buffer pH 5.2 and 275 µl of cold ethanol (100 %). The mixture was incubated at -80 °C for 10 minutes. Afterwards, the solution was centrifuged at 20.000 x g at 4 °C for 15 minutes. The supernatant was discarded and the pellet was washed with 70 % (v/v) cold ethanol before centrifuging at 20.000 x g and 4 °C for another 5 minutes. The pellet was dried at 50 °C for 20 minutes before resuspension in an appropriate amount of H<sub>2</sub>O.

### 3.3.4 Restriction analysis

All restriction enzymes (FastDigest) used in this work were purchased from Thermo Fisher Scientific. Restriction digest conditions were conducted according to the manufacturer's instructions. The amount of DNA used for cloning applications was 3 µg. In contrast, 0.5 µg of isolated plasmid DNA were used for restriction analysis.

### 3.3.5 Agarose gel electrophoresis and DNA fragment isolation

To isolate or check for correct bands after restriction digest, the cut DNA was directly loaded on an appropriately concentrated agarose gel (peqGOLD Universal-Agarose, peqlab) containing peqGreen dye (peqlab) for visualization under UV light. GeneRuler 1 kb plus DNA ladder (Thermo Fisher Scientific) was used as DNA size reference. The DNA fragments were separated by size in 1x TBE buffer at 150 V. For cloning, desired DNA bands were excised from the gel and isolated using the QIAquick Gel Extraction Kit (Qiagen) according to the manufacturer's protocol.

#### 1x TBE buffer

0.5 M EDTA pH 8.0	20.0 ml
Boric acid	27.5 g
Tris	54.0 g
H <sub>2</sub> O	add to 5 l

### 3.3.6 Dephosphorylation and ligation

To prevent their re-ligation, vectors cut with a restriction enzyme generating blunt ends were dephosphorylated using the Rapid DNA Dephosphorylation Kit (Roche) according to the manufacturer's instructions.

For ligation, T4 DNA Ligase (Thermo Fisher Scientific) was utilized in accordance with the manufacturer's manual. The vector to insert molar ratios ranged from 1:3 to 1:6.

### 3.3.7 Transformation

For transformation, a 100 µl aliquot of chemically competent cells (10-beta competent *E. coli* strain, NEB) was thawed on ice. 1-10 ng of plasmid DNA or 3-5 µl of a ligation mixture were added to the cell suspension which was then gently mixed and incubated on ice for 5-30 minutes. After incubation, a heat shock at 42 °C for 30-45 seconds was performed. Heat-shocked cells were returned on ice for at least 2 minutes before plating them on LB(+) agar plates containing 100 µg/ml ampicillin (resistance depending on the plasmid). Afterwards, the plate was incubated overnight at 37 °C in an inverted position.

<u>LB(+) medium</u>		<u>LB(+) agar</u>	
Peptone	10 g	Agar	15 g
Yeast extract	5 g	LB(+) medium	add to 1 l
NaCl	5 g	Autoclave	
D-(+)-Glucose	1 g		
H <sub>2</sub> O	add to 1 l	Let the solution cool down to 50 °C and add	
Adjust pH to 7.2-7.5 and autoclave		Ampicillin	100 mg

### 3.3.8 Inoculation of bacterial cells and isolation of plasmid DNA

Bacterial colonies were picked from the agar plate and transferred to culture tubes (Sarstedt) containing 5 ml LB(+) medium and ampicillin (100 µg/ml). The bacterial cultures were incubated overnight at 37 °C while shaking at 225 rpm. On the next day, the cells were centrifuged at 3500 rpm and room temperature (RT) for 10 minutes. After discarding the supernatant, the cell pellet was resuspended in 250 µl resuspension buffer and transferred to a 1.5 ml Eppendorf tube. 250 µl lysis buffer was added to the solution which was then mixed by inverting the tube 5-6 times followed by an incubation for 5 minutes at RT. 250 µl neutralization buffer was added and the mixture was inverted 5-6 times before incubating it 15 minutes on ice. Then, the suspension was centrifuged at 20.000 x g and 4 °C for 15 minutes. The supernatant was transferred to a new 1.5 ml Eppendorf tube and 525 µl of cold isopropanol (100 %) was added to precipitate the DNA. After vortexing, the solution was centrifuged at 20.000 x g and 4 °C for 15 minutes. The supernatant was removed and 700 µl 70 % (v/v) ethanol was added before centrifuging at 20.000 x g and 4 °C for 5 minutes. The supernatant was discarded and the pellet was dried at 50 °C for 20 minutes before resuspension in 20 µl H<sub>2</sub>O. DNA concentration and purity were determined using a Nanodrop 2000c spectrophotometer (Thermo Fisher Scientific).

All constructs used in this study were sequenced at Eurofins Genomics prior to use. For large scale and high purity plasmid isolation the PureLink HiPure Plasmid Midiprep or Megaprep Kit (Invitrogen) was used. For this purpose, 100 ml or 1000 ml LB(+) medium was inoculated with single colonies according to the manufacturer's instructions.

<u>Resuspension buffer</u>		<u>Lysis buffer</u>	
Tris	6.06 g	NaOH	8.0 g
EDTA	3.72 g	10 % (w/v) SDS solution	100 ml
RNAse A	100 mg	H <sub>2</sub> O	add to 1 l
H <sub>2</sub> O	add to 1 l		
Adjust pH to 8.0			

<u>Neutralization buffer</u>	
3 M potassium acetate pH 5.5	500 ml
H <sub>2</sub> O	add to 1 l

### 3.3.9 RNA isolation and cDNA synthesis

RNA isolation from murine or human tissue was conducted using the RNeasy Plus Minikit (Qiagen) according to the instructions of the manufacturer. RNA concentration and purity were determined using the Nanodrop 2000c spectrophotometer. Subsequent reverse transcription was performed using the RevertAid First Strand cDNA Synthesis Kit (Thermo Fisher Scientific) following the manual of the manufacturer. For cDNA synthesis from transfected cell culture experiments, the amount of total RNA was 500 ng. Random hexamers as well as oligo(dT) primers were added to the reaction. For cDNA synthesis from sorted murine rods and cones (cf. chapter 3.11), 50 ng of isolated total RNA was used.

### 3.3.10 Quantitative real-time PCR (qPCR)

qPCR was performed using the SYBR Select Master Mix (Applied Biosystems) on a StepOnePlus Real-Time PCR System (Applied Biosystems). Pipetting scheme and reaction conditions were adapted from the manufacturer's manual and adjusted for every gene individually. Murine or human gene expression was normalized to the housekeeping gene aminolevulinic acid synthase (*Alas/ALAS*). Three technical replicates were run for each gene of interest. Relative quantification was performed according to the  $2^{-\Delta\Delta CT}$  method [63]. All relevant primer sequences for detection of murine and human transcripts can be found in the appendix (cf. Supplementary Table 8).

### 3.3.11 *In silico* prediction of splicing

Prior to examining the effects of potential splice mutations via minigenes, an initial *in silico* prediction of mRNA splicing of the mutations of interest was conducted [64]. Therefore, the free trial ASSEDA splice software ([splice.uwo.ca/](http://splice.uwo.ca/)) and the open access NNSplice software (Berkeley Drosophila Genome Project, [http://www.fruitfly.org/seq\\_tools/splice.html](http://www.fruitfly.org/seq_tools/splice.html)) were used. For *in silico* prediction, 40 bp flanking the respective point mutation from each side were chosen. The software can predict different effects on mRNA splicing, e.g. the potential generation of novel donor or acceptor splice sites and the generation or abolition of exonic splice enhancer (ESE) or silencer (ESS) motifs. In this study, 30 *PRPH2* point mutations were analyzed via this *in silico* approach (cf. Supplementary Table 1).

### 3.3.12 Genomic DNA isolation

Genomic DNA was extracted from buccal cells isolated from Dr. Elvir Becirovic using the Gentra Puregene Buccal Cell Kit (Qiagen) following the instructions of the manufacturer.

### 3.3.13 Construction and cloning of the *PRPH2* minigene

To generate the human *PRPH2* minigene overlap extension PCR was used. The genomic DNA isolated from Dr. Elvir Becirovic served as template (cf. chapter 3.3.12). First, the three exons including  $\geq 200$  bp of the flanking introns were amplified via standard PCR (Figure 5). The primers used for these PCRs encompass defined overhangs of approx. 20 bp. These overhangs are complementary to the corresponding PCR amplicon to be connected in the subsequent overlap extension PCR. Thus, 40 bp overlap regions are created which were used for the amplification of two fragments. In addition, to amplify the first minigene exon, an appropriate restriction site was added to the 5' end of the corresponding forward primer. For the amplification of the last exon, an appropriate restriction site was added to the 5' end of the corresponding reverse primer. The two amplicons PCR1 and PCR2 served as templates for the first overlap PCR. This new fragment was fused in the second overlap PCR to the remaining amplicon PCR3 yielding the final *PRPH2* minigene. Using the chosen restrictions sites, the minigene was cloned into the respective expression vector. A list of the used primers can be found in Supplementary Table 5.

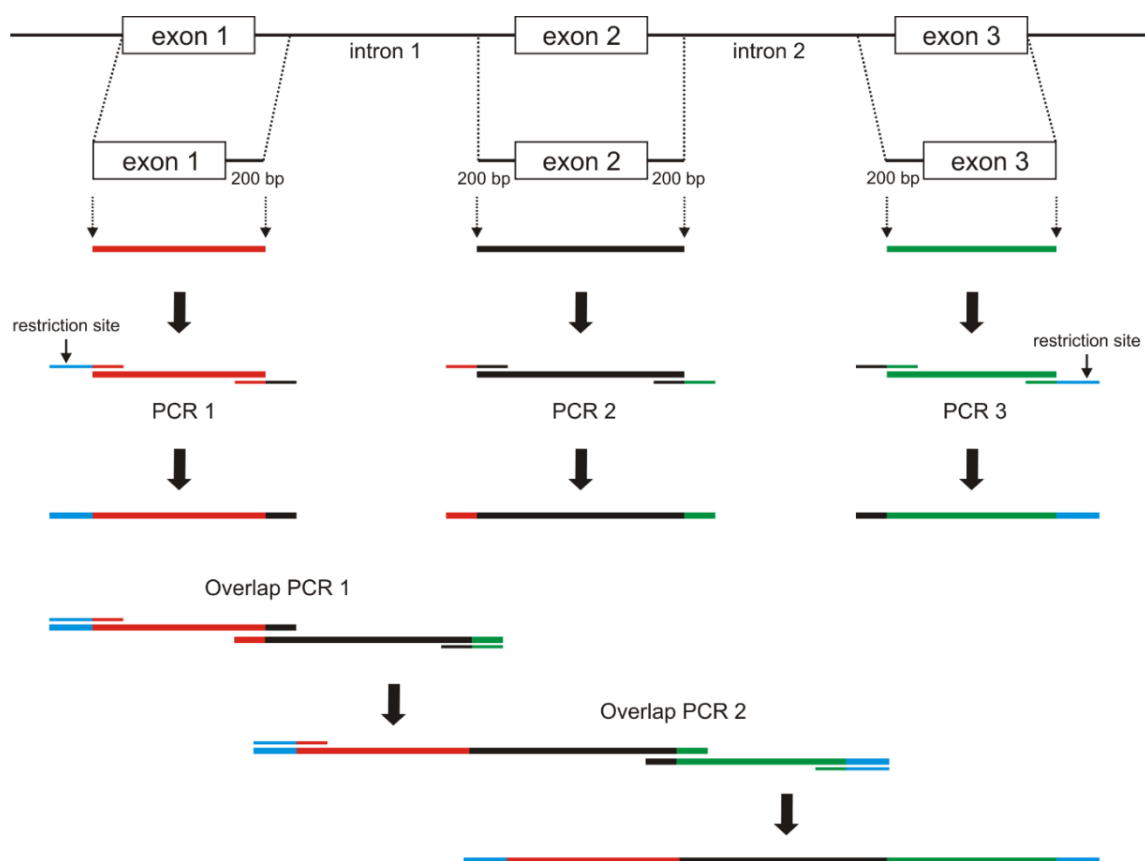


**Figure 5 Schematic of overlap extension PCR for creating the human *PRPH2* minigene consisting of three exons and two flanking introns that were shortened [64].**

For monitoring expression and performing FACS and FRET experiments, the fluorophores citrine or cerulean were fused to the 5' end of the *PRPH2* minigene.

### 3.3.14 Side-directed mutagenesis

Point mutations were introduced into the *PRPH2* minigene by side-directed mutagenesis using the QuikChange Lightning Site-Directed Mutagenesis Kit (Agilent Technologies) according to the manufacturer's manual. Mutagenic oligonucleotide primers were designed using the QuikChange primer design program ([www.agilent.com/genomics/qcpd](http://www.agilent.com/genomics/qcpd)) and purchased at Eurofins Genomics (cf. Supplementary Table 6). All mutant minigenes were sequenced prior to use.

## 3.4 Cell culture

### 3.4.1 Cultivation of mammalian cell lines

HEK293T cells (LentiX 293 T Cell Line, Clontech Laboratories) were used for *in vitro* transfections in this study. The cells were cultivated in DMEM + GlutaMAX™-I medium ((+) 4.5 g/l glucose, (-) pyruvate, (+) 10 % FBS, (+) 1 % penicillin/streptomycin (Thermo Fisher Scientific)) at 37 °C and 10 % CO<sub>2</sub>.

### 3.4.2 Transfection

HEK293T cells were either transiently transfected using the calcium phosphate technique [65] or the polymer-based transfection reagent TurboFect (Thermo Fisher Scientific). For the calcium phosphate based transfection of a 10 cm dish (Cellstar, Greiner), the following reagents were premixed in a 15 ml Falcon tube:

DNA	10 µg	<u>2x BBS solution</u>	
2.5 M CaCl <sub>2</sub>	50 µl	BES	10.65 g
H <sub>2</sub> O	add to 500 µl	NaCl	16.35 g
		Na <sub>2</sub> HPO <sub>4</sub> x 2H <sub>2</sub> O	0.21 g
		H <sub>2</sub> O	add to 1 l
		Adjust pH to 6.95 and filtrate sterilely	

While vortexing, 500 µl of 2x BBS solution were added dropwise to the mixture. After incubating for 5 minutes at RT, the transfection mix was evenly distributed on approx. 70 % confluent cells. The cells were then incubated at 37 °C and 5 % CO<sub>2</sub> for 8-16 hours before changing the medium and placing them back to 37 °C and 10 % CO<sub>2</sub> until harvesting.

TurboFect was used for the transfection of cells cultivated in glass bottomed 35 mm dishes (Cellvis) for subsequent FRET measurements. The required DNA and medium volumes were adjusted in accordance with the manufacturer's protocol. After vortexing, the mixture was

incubated for 15-20 minutes at RT. Finally, it was spread on the cells and incubated at 37 °C until proceeding with the FRET measurements.

### 3.5 Protein biochemistry

#### 3.5.1 Isolation and quantification of proteins

Proteins were isolated 48 hours after transfection of HEK293T cells. Afterwards, the medium was removed and cells were scraped off the dish and collected in a 1.5 ml Eppendorf tube. Cells were then centrifuged at 1000 x g at 4 °C for 10 minutes. After removing the remaining medium, the pellet was resuspended in an appropriate amount of lysis buffer, disrupted using the Potter S homogenizer (B. Braun Diessel Biotech) and rotated at 4 °C for 20 minutes. Subsequently, the cells were centrifuged at 5000 x g and 4 °C for 10 minutes before transferring the supernatant into a new 1.5 ml tube. For protein isolation from mouse tissue a similar protocol was used.

Total protein concentration was determined using the Bradford assay [66]. For this purpose, 5 µl of protein lysate were mixed with 95 µl of 0.15 M NaCl solution and transferred to a 1 ml PMMA cuvette (Brand). 5 µl of lysis buffer served as blank control. 1 ml of Coomassie blue solution was added and incubated at RT for 2 minutes before measuring the concentration via a BioPhotometer (Eppendorf).

<u>Lysis buffer</u>		<u>Coomassie blue solution</u>	
Triton X-100	2.5 ml	Coomassie brilliant blue G250	50 mg
5 M NaCl	15 ml	95 % (v/v) ethanol	25 ml
2.5 M CaCl <sub>2</sub>	0.4 ml	85 % (v/v) phosphoric acid	50 ml
H <sub>2</sub> O	add to 500 ml	H <sub>2</sub> O	add to 500 ml

#### 3.5.2 Membrane preparations

Membrane preparations were performed to enrich membrane proteins from transfected HEK293T cells or transduced murine retinas. For this purpose, harvested cells or tissue were lysed in an appropriate amount of 1x membrane preparation buffer containing a cComplete EDTA-free Protease Inhibitor Cocktail (Roche) using the Potter S homogenizer. The solution was centrifuged at 5000 x g at 4 °C for 10 minutes before transferring the supernatant into a 6.5 ml clean thick wall polycarbonate tube (16 x 64 mm, Beckman Coulter). 1x membrane preparation buffer was added to the tube to a final volume of 4 ml prior to centrifugation at 30.000 rpm and 4 °C for 45 minutes in a Sorvall Discovery 90 ultracentrifuge using a 45 Ti rotor (Beckman Coulter). The supernatant was discarded and the pellet was resuspended in

50-100  $\mu$ l of 1x membrane preparation buffer. 5  $\mu$ l were used for protein quantification via the Bradford assay (cf. chapter 3.5.1).

3x membrane preparation buffer

MOPS	3.15 g
Sucrose	77 g
0.5 M EDTA pH 7.4	6 ml
H <sub>2</sub> O	add to 250 ml

### 3.5.3 Co-immunoprecipitation (co-IP)

To analyze protein-protein interactions via co-IP experiments protein G dynabeads (novex by Life Technologies) were used. 5  $\mu$ g of an appropriate antibody was added to 30  $\mu$ l of dynabeads. This mixture was filled up to a final volume of 500  $\mu$ l with PBS. To allow a binding of the antibodies to the beads, the solution was rotated at 4 °C for 30 minutes. Afterwards, the fluid was removed from the beads by withholding them with a magnet. The beads were then washed in 200  $\mu$ l PBS followed by adding 1 mg of the protein lysate (cf. chapter 3.5.1 or 3.5.2) and filling up the reaction to a final volume of 500  $\mu$ l with PBS. While rotating, the solution was incubated for 30-60 minutes at 4 °C before washing the beads three times with 200  $\mu$ l PBS. After the last washing step, the complete bead suspension was transferred to a new 1.5 ml Eppendorf tube and the fluid was discarded. Beads were resuspended in 10  $\mu$ l PBS and 6x Lämmli buffer with or without DTT (depending on the application) was added. The suspension was incubated at 75 °C for 10 minutes to elute bound proteins from the bead-antibody complexes. The resulting protein-enriched solution was removed from the beads and loaded on a SDS-PAGE gel (cf. chapter 3.5.4).

6x Lämmli buffer

Tris-HCl pH 6.8	7 ml
Glycerol	3 ml
SDS	1.0 g
Bromophenol blue	1.2 mg
(DTT	0.93 g)
H <sub>2</sub> O	add to 10 ml

### 3.5.4 SDS-PAGE

To separate isolated proteins according to their molecular weight SDS-PAGE was used. For this, 6-12 % gradient gels were prepared using the Mini Protean 3 gel system (Bio-Rad). First, 4.25 ml of a 6 % gel solution were aspirated using a 10 ml pipette followed by 4.25 ml of a 12 % gel solution. The gradient was generated by carefully aspirating one air bubble prior to pouring the gel solution into the gel system.

As molecular weight standard PageRuler Prestained Protein Ladder (Thermo Fisher Scientific) was used. Electrophoresis was run in electrophoresis buffer at 140 V for 1 hour.

1x Electrophoresis buffer

Tris base	3.03 g
Glycin	14.4 g
SDS	1.0 g
H <sub>2</sub> O	add to 1 l

4x Tris-HCl/SDS buffer 0.5 M

Tris base	0.5 M
SDS	0.4 %
H <sub>2</sub> O	add to 500 ml
Adjust pH to 6.8 with HCl	

4x Tris-HCl/SDS buffer 1.5 M

Tris base	1.5 M
SDS	0.4 %
H <sub>2</sub> O	add to 500 ml
Adjust pH to 8.8 with HCl	

Stacking gel (for 2 gels)

30 % acrylamide/bis-acrylamide	1 ml
4x Tris-HCl/SDS buffer 0.5 M	1.9 ml
H <sub>2</sub> O	4.6 ml
APS	37.5 µl
TEMED	7.5 µl

<u>Gradient separation gel (for 2 gels)</u>	<u>6 %</u>	<u>12 %</u>
30 % acrylamide/bis-acrylamide	2.3 ml	4.6 ml
4x Tris-HCl/SDS buffer 1.5 M	2.8 ml	2.8 ml
H <sub>2</sub> O	6.2 ml	3.9 ml
APS	22.5 µl	22.5 µl
TEMED	7.5 µl	7.5 µl

### 3.5.5 Western blotting

Following SDS-PAGE, separated proteins were blotted on a PVDF membrane (peqlab) equilibrated in methanol using the Mini Trans-Blot Cell (Bio-Rad). Western blotting was performed at 100 V for 90 minutes in transfer buffer. After blotting, the membrane was incubated in blocking solution for 1 hour at RT while rotating. The membrane was then incubated in the appropriate primary antibody solution for 1 hour at RT followed by 3 washing steps in TBST for 5 minutes. Afterwards, the membrane was transferred to the secondary antibody solution and incubated for 1 hour at RT while rotating. Subsequently, the membrane was washed 3 times in TBST and once in H<sub>2</sub>O prior to chemiluminescence detection via the Western Blotting Luminol Reagent (Santa Cruz) using the Chemidoc MP Imaging system (Bio-Rad) and the ImageLab software. A list of all antibodies used in this study can be found in Table 2.

Transfer buffer

Tris	3.0 g
Glycin	14.4 g
H <sub>2</sub> O	add to 1 l

TBST

Tris	1.2 g
NaCl	8.0 g
Tween 20	1 ml
H <sub>2</sub> O	add to 1 l

Blocking solution

TBST	15 ml
Non-fat dried milk powder	0.75 g

Primary/secondary antibody solution

TBST	5 ml
Non-fat dried milk powder	0.05 g
Antibody stock solution	x $\mu$ l
x: depending on the concentration	

**Table 2 Antibodies used for western blotting.**

Antibody	Source	Dilution
rb anti-CNGB1a	in-lab production	1:5000
ms anti-GFP JL-8	Clontech	1:2000
ms anti-myc 9B11	Cell Signaling Technology	1:2000
ms anti-Na <sup>+</sup> /K <sup>+</sup> ATPase $\alpha$ 6F-c	Developmental Studies Hybridoma Banks, University of Iowa	1:1000
ms anti-ATPase $\alpha$ 3	Abcam	1:2000
rb anti-flag	Sigma	1:2000
gt anti-mouse HRP	Santa Cruz	1:2000
gt anti-rabbit HRP	Santa Cruz	1:2000

### 3.5.6 Native protease cleavage assay

For the native protease cleavage assay, membrane preparations (cf. chapter 3.5.2) from transfected HEK293T cells were performed in absence of protease inhibitors. This membrane protein solution was incubated for 5 hours at RT to allow for endogenously expressed proteases to cleave exposed domain regions of the isolated proteins. Subsequently, they were further processed for western blotting (cf. chapter 3.5.5).

### 3.5.7 Peptide competition assay

The peripherin-2 peptide (sequence: DGRYLVDGVPFSCCNPSSPR) used for the peptide competition assay was purchased at jpt Innovative Peptide Solutions. It was added to the respective membrane preparations (cf. chapter 3.5.2) before starting with the co-IP experiments (cf. chapter 3.5.3) using an anti-myc antibody (cf. Table 2).

### 3.6 Sucrose density gradient centrifugation

A sucrose density gradient centrifugation (SDGC) facilitates the separation of different covalently or non-covalently linked protein complexes across a sucrose gradient according to their specific molecular weight. For SDGC, HEK293T cells were transiently transfected (cf. 3.4.2) with the respective peripherin-2 and Rom-1 constructs. 48 hours post transfection, cells were harvested and processed as described in chapter 3.5.1. Continuous density gradients of 5-20 % (w/v) sucrose were prepared by underlayering 0.5 ml of 5 %, 10 %, 15 % and 20 % sucrose solutions containing 10 mM N-ethylmaleimide (Sigma-Aldrich) and 0.1 % Triton X-100 into a centrifuge tube (Beranek Laborgeräte). To allow for diffusion, the gradient was left at RT for 1 hour and chilled on ice for another 30 minutes prior to sample application. DNA standards of defined molecular weights (75-20.000 bp, i.e. 49-13.000 kDa, GeneRuler 1 kb Plus (Thermo Fisher Scientific)) were added to lysates containing 200 µg of the respective proteins to be able to determine the weight of the single peripherin-2 and Rom-1 complexes in subsequent immunoblots. The mix was then carefully layered on top of the gradient and centrifuged at 46.700 rpm at 4 °C for 2 hours in a Beckman Coulter Optima L-80K Ultracentrifuge (Beckman Coulter). Hereafter, the centrifuge tube was punctured at the bottom and fractions were collected dropwise (5 drops/tube). Fractions from every sucrose gradient were used separately for western blotting (cf. chapter 3.5.5) utilizing anti-flag- or -myc-specific antibodies (cf. Table 2) and for agarose gel electrophoresis to detect the DNA standards.

### 3.7 Production of rAAVs

#### 3.7.1 Transfection and harvest

Single-stranded rAAVs were produced by triple calcium phosphate transfection of HEK293T cells (cf. chapter 3.4.2) with the pAAV2.1 vector containing the transgene as well as the pAD Helper and pAAV2/8YF plasmids (cf. chapter 3.3.1). To achieve higher transfection efficiencies, dextran 500 (Sigma) and polybrene (hexadimethrine bromide, Sigma) were mixed with the regular transfection compounds [67]. 15x 15 cm dishes of HEK293T cells were transfected to generate one batch of rAAVs according to the following reaction mixture:

#### Transfection mixture

pAAV2.1 vector	270 µg
pAD Helper	X µg
pAAV2/8YF	Y µg
Polybrene (8 mg/ml)	15 µl
Dextran (10 mg/ml)	1.5 ml
2.5 M CaCl <sub>2</sub>	1.5 ml
H <sub>2</sub> O	add to 15 ml

The necessary amounts of pAD Helper and pAAV2/8YF plasmids were calculated as follows:

$$X \mu\text{g} = 270 \mu\text{g} \times \text{MM of pAD Helper} / \text{MM of pAAV2.1 vector} \quad (1)$$

$$Y \mu\text{g} = 270 \mu\text{g} \times \text{MM of pAAV2/8YF} / \text{MM of pAAV2.1 vector} \quad (2)$$

MM = molar mass of double stranded plasmid

MM of pAD Helper = 9509 g/mol

MM of pAAV2/8 YF = 4523 g/mol

The transfection mixture was vortexed while adding 15 ml 2x BBS dropwise. 2 ml of the solution were evenly distributed on each of the 15 culture dishes. Cells were incubated overnight at 37 °C and 5 % CO<sub>2</sub>. On the next day, the medium was exchanged and cells were incubated overnight at 37 °C and 10 % CO<sub>2</sub>.

The cells were harvested by scraping them from each dish and collecting them together with the medium in a 500 ml centrifuge tube. After centrifugation at 4000 rpm at 4 °C for 15 min (JA-10 rotor, J2-MC High speed centrifuge, Beckman Coulter), the medium was discarded and the pellet was resuspended in 7.5 ml lysis buffer. Cells were disrupted by three cycles of shock-freezing in liquid nitrogen and thawing at 37 °C in a water bath.

#### Lysis buffer

NaCl 150 mM

Tris-HCl pH 8.5 50 mM

H<sub>2</sub>O add to 50 ml

Filtrate sterilely

### 3.7.2 Iodixanol gradient centrifugation

Benzonase (VWR) was added to the virus-containing solution from step 3.7.1 to a final concentration of 50 U/ml and incubated for 30 minutes at 37 °C. After centrifugation at 4000 rpm at 4 °C for 25 minutes, the pellet was discarded and the supernatant was transferred into a Quick-Seal Polypropylene Tube (39 ml, Beckman Coulter). Then, a gradient was prepared by underlayering the virus-containing supernatant with 7 ml of 15 %, 5 ml of 25 %, 5 ml of 40 % and 6 ml of 60 % iodixanol using a long glass pipette and a Gilson MINIPULS3 pump. The tube was sealed with a Beckman Tube Topper and centrifuged at 70.000 rpm at 18 °C for 105 minutes in an Optima L-80K ultracentrifuge using a 70 Ti rotor (Beckman Coulter). To collect the virus which migrated into the 40 % iodixanol layer, the tube top was perforated several times for pressure compensation. Afterwards, the tube was laterally punctured with a 21-gauge needle directly above the 60 % layer. Then, the 40 % layer (approx. 5 ml) was extracted with a syringe.

<u>15 % iodixanol</u>		<u>25 % iodixanol</u>	
10x PBS	5 ml	10x PBS	5 ml
1 M MgCl <sub>2</sub>	50 µl	1 M MgCl <sub>2</sub>	50 µl
2.5 M KCl	50 µl	2.5 M KCl	50 µl
5 M NaCl	10 ml	Optiprep	20.9 ml
Optiprep (Progen)	12.5 ml	1 % phenol red	50 µl
1 % phenol red	37.5 µl	H <sub>2</sub> O	add to 50 ml
H <sub>2</sub> O	add to 50 ml		
 <u>40 % iodixanol</u>		 <u>60 % iodixanol</u>	
10x PBS	5 ml	1 M MgCl <sub>2</sub>	50 µl
1 M MgCl <sub>2</sub>	50 µl	2.5 M KCl	50 µl
2.5 M KCl	50 µl	Optiprep	50 ml
5 M NaCl	10 ml	1 % phenol red	37.5 µl
Optiprep	33.3 ml		
H <sub>2</sub> O	add to 50 ml		

### 3.7.3 Anion exchange chromatography

Anion exchange chromatography was applied to further purify the rAAVs using the ÄKTAprime plus system (GE Healthcare), the HiTrap Q FF sepharose column (GE Healthcare) and the PrimeView 5.31 software (GE Healthcare) according to the manufacturer's instructions. Prior to use, the column was equilibrated with buffer A which was also used to dilute the virus suspension 1:1 before loading it onto the column via a loop injector (Superloop, 50 ml, GE Healthcare). Conductance and UV curves were recorded during the process providing information about the properties of the collected fractions. The bound molecules were eluted from the column with 2.5 M NaCl (buffer B, pH = 8.5). Desired virus-containing fractions, i.e. fractions within the plateau of the conductance curve, were combined for further processing.

#### Buffer A

Tris	20 mM
NaCl	15 mM
H <sub>2</sub> O	add to 500 ml
Adjust pH to 8.5	

### 3.7.4 Concentration of rAAVs

To increase the concentration of rAAVs, combined fractions from step 3.7.3 were transferred into an Amicon Ultra-4 Centrifugal Filter Unit (100 kDa, Millipore) and centrifuged at 4000 rpm (JA-10 rotor, J2-MC High speed centrifuge, Beckman Coulter) at 20 °C for 20 minutes until the volume of the virus-containing solution was reduced to 500 µl. Then, the filter unit was washed with 1 ml 0.014 % Tween/PBS-MK and centrifugation was continued until 100 µl of concentrated virus suspension remained within the filter unit. 10 µl aliquots were prepared and stored at -80 °C until titer determination and subretinal injection.

Tween/PBS-MK

10x PBS	50 ml
1 M MgCl <sub>2</sub>	500 µl
2.5 M KCl	500 µl
Tween 20	0.014 % (v/v)
H <sub>2</sub> O	add to 500 ml

## 3.7.5 rAAV titer determination

Genomic rAAV titers were determined by qPCR using a standard curve generated by a serial dilution of the WPRE fragment which was amplified from the pAAV2.1 vector using the following primers:

WPRE\_F: AGTTCCGCCGTGGCAATAGG

WPRE\_R: CAAGGAGGAGAAAATGAAAGCC

The WPRE element was purified (cf. chapter 3.3.3) and its concentration was measured via Nanodrop. The following equation (3) was used to calculate the concentration of the standard for 10<sup>10</sup> copies of viral genome per 5 µl:

$$c \text{ (pg/}\mu\text{l)} = 10^{10} \times 660 \times 10^{12} \text{ pg/mol} \times \text{WPRE fragment size} / (6.022 \times 10^{23} / \text{mol} \times 5 \mu\text{l}) \quad (3)$$

660 × 10<sup>12</sup> pg/mol is the mean molar mass of one base pair and 6.022 × 10<sup>23</sup>/mol is the Avogadro constant.

Based on this concentration, a 10-fold serial dilution was prepared with the first dilution comprising 10<sup>10</sup> copies/5 µl and the last dilution containing 10<sup>1</sup> copies/5 µl. Subsequently, qPCR was run with triplicates of all ten dilutions and the standard curve was calculated by plotting the CT values against the logarithm of the dilution factors. The purified and concentrated rAAVs obtained in chapter 3.7.4 were diluted 1:500 in H<sub>2</sub>O and qPCR was performed. The genomic titers could be inferred from the resulting CT values and the corresponding values obtained in the standard curve.

qPCR reaction mix

SYBR Select Master Mix	10 µl
WPRE_F (10 µM)	1 µl
WPRE_R (10 µM)	1 µl
Template	5 µl
H <sub>2</sub> O	add to 20 µl

### 3.8 Subretinal injection

For subretinal injection of titer-matched rAAVs ( $10^9$  particles/ $\mu$ l), 14-day-old wild type C57Bl/6J mice were weighted and anesthetized via an intraperitoneal injection of ketamine (40 mg/kg body weight) and xylazine (20 mg/kg body weight). The pupil was dilated by administering 1 % atropine- and 0.5 % tropicamide-containing eye drops (Mydriaticum Stulln, Pharma Stulln GmbH). For injection, the eye fundus was focused using a surgical microscope (OPMI 1 FR pro, Zeiss). 1  $\mu$ l of the virus solution was then applied subretinally using a NanoFil 10  $\mu$ l syringe equipped with a 34-gauge beveled needle (World Precision Instruments). A correct subretinal application is indicated by the formation of a bleb, i.e. a temporal detachment of the retina at the injection site. Finally, the injected eye was treated with a gentamicin 5 mg/g and dexamethasone 0.3 mg/g containing eye salve (Dexamytrex, Dr. Gerhard Mann GmbH) and the mouse was kept in a cage heated to 37 °C until full anesthesia recovery.

### 3.9 Immunohistochemistry

Four weeks post injection, mice were euthanized and eyes were collected and transferred into 0.1 M PB. Using a stereomicroscope (Stemi 2000, Zeiss) the eye was punctured at the *ora serrata* with a cannula (21G, Sterican, B. Braun) and fixed for 5 minutes in 4 % PFA. Afterwards, the cornea and lens were excised by cutting along the *ora serrata* with micro-scissors (SuperFine Vannas, World Precision Instruments). Subsequently, the vitreous body was removed and the remaining retina-containing eyeball was fixed for 45 minutes in 4 % PFA. Hereafter, the eye was washed thrice for 5 minutes in 0.1 M PB. For cryoprotection, the eyeball was placed in 30 % sucrose and incubated overnight at 4 °C. After this, the eyeball was embedded in tissue freezing medium (Electron Microscopy Sciences) and frozen on dry ice. Then, 10  $\mu$ m retinal cryosections were prepared using a cryostat (Leica CM3050 S, Leica), mounted on coated glass object slides (Superfrost Plus microscopic slides, Thermo Fisher Scientific) and stored at -20 °C prior to use.

For immunohistochemistry, retinal cryosections were thawed at RT and rimmed by a hydrophobic barrier using a liquid blocker (Super PAP Pen Liquid Blocker, Science Services). Cryosections were rehydrated with 0.1 M PB for 5 minutes followed by a fixation step with 4 % PFA for 10 minutes. After washing thrice with 0.1 M PB for 5 minutes, the cryosections were incubated with the primary antibody diluted in 0.1 M PB containing 5 % ChemiBlocker (Millipore) and 0.3 % Triton X-100 overnight at 4 °C. On the next day, the cryosections were washed three times with 0.1 M PB for 5 minutes and incubated with the secondary antibody diluted in 0.1 M PB containing 2 % ChemiBlocker for 1.5 hours at RT. Then, cryosections were washed three times with 0.1 M PB for 5 minutes and the nuclei were stained with 5  $\mu$ g/ml

Hoechst 33342 solution (Invitrogen) for 5 minutes. After a final washing step with 0.1 M PB for 5 minutes, the sections were covered with Fluoromount-G Slide Mounting Medium (Thermo Fisher Scientific) and a cover slip. The cryosections were stored at 4 °C until analysis. All antibodies used are displayed in Table 3.

<u>0.1 M PB</u>		<u>4 % PFA</u>	
Na <sub>2</sub> HPO <sub>4</sub> x 2H <sub>2</sub> O	28.48 g	Paraformaldehyde	6 g
NaHPO <sub>4</sub> x H <sub>2</sub> O	5.52 g	0.1 M PB	add to 150 ml
H <sub>2</sub> O	add to 2 l	Dissolve at 60 °C and filtrate sterilely	
Adjust pH to 7.4			

**Table 3 Antibodies used for immunohistochemical stainings.**

Antibody	Source	Dilution
rb anti-CNGB1a	in-lab production	1:5000
dk Cy-3 anti-rabbit IgG	Jackson Laboratories	1:400
rb anti-M-opsin	Millipore	1:300

### 3.10 Confocal microscopy

Images of immunolabeled retinal cryosections and isolated rod outer segments (cf. section 3.12) were obtained by the TCS SP8 confocal laser scanning microscope (Leica) equipped with the following lasers: 552 nm, 514 nm, 488 nm, 405 nm. Images were acquired as confocal z-stacks using the LASX software (Leica) and processed with the ImageJ software (National Institutes of Health).

### 3.11 Fluorescence-activated cell sorting (FACS)

FACS was performed by Oliver Borsch and Tiago Santos-Ferreira in the group of Prof. Marius Ader at the TU Dresden. For FACS of rods and cones, the two different reporter mice neural retina leucine zipper- (Nrl-) EGFP [68] and cone-GFP [69] mice were used. In the Nrl-EGFP mice, reporter expression was driven by the rod-specific Nrl promoter. In the cone-GFP mice, GFP was driven by a 5' regulatory sequence of the human red/green opsin gene. Two retinas per reporter mouse (6-8-week-old) were isolated and dissociated using the Papain Dissociation System (Worthington Biochemical Corporation) following the manufacturer's instructions. Dissociated retinal cells were sorted with the BD FACSAria II SORP (BD Bioscience) device and collected according to their reporter fluorescence [70].

### 3.12 Isolation of photoreceptor outer segments

Mice were sacrificed four weeks post injection for isolation of transduced photoreceptor outer segments. For this purpose, retinas were isolated and collected in a 1.5 ml reaction tube filled with 100  $\mu$ l PBS. OSs were detached from the retina by vortexing 15-30 seconds and by centrifuging at 500 x g for 30 seconds. The OS-enriched supernatant was collected and used for subsequent FRET measurements.

### 3.13 Förster resonance energy transfer (FRET)

FRET is a commonly used method in optical microscopy to analyze protein-protein interactions and to determine atomic-scale distances (limited to approx. 10 nm) in living cells [71]. To perform FRET, each of the two putative interaction partners has to be tagged with a fluorescent molecule, one with the donor and the other one with the acceptor fluorophore. The excitation spectrum of the acceptor should overlap with the emission spectrum of the donor. One of the most popular fluorescent FRET pairs is cerulean (donor) and citrine (acceptor) [72, 73]. When both molecules are in close proximity, following photoexcitation the donor transfers parts of this excitation energy in a non-radiative fashion via long-range dipole-dipole interactions to the acceptor. This event results in a quenched donor and an augmented acceptor fluorescence. In this setting, fluorescent signals are measured via three different filter cubes (3<sup>3</sup>- or three cube FRET). The fractional increase in the acceptor intensity also referred to as sensitized emission, can be utilized to calculate the FRET efficiencies ( $E_A$ ) [74-76]. The method enables a non-destructive qualitative and quantitative analysis of protein-protein interactions.

In this study, FRET was used to quantify the effects of disease associated peripherin-2 point mutations on homomeric and heteromeric protein-protein interactions, i.e. oligomerization of peripherin-2 and its interaction with Rom-1, in HEK293T cells and in isolated rod outer segments.

FRET measurements were conducted using a Leica DMI6000B inverted fluorescent microscope equipped with a R1527 photomultiplier detection system including a photomultiplier tube (Horiba). A xenon short arc lamp (UXL-75XE, Ushio Inc. Japan) combined with a DeltaRamX monochromator (Horiba) served as excitation source. Data were acquired with the FelixGX software (Horiba) and processed using MATLAB (MathWorks. Inc.) and Excel (Microsoft Corporation) [71]. Switching of filter cubes was done manually via a motorized filter wheel and with the following cubes being used: A donor cube containing a cerulean excitation filter (426-446 nm), a T455lp dichroic mirror and a cerulean emission filter (460-500 nm); an acceptor cube equipped with a citrine excitation filter (490-510 nm), a T515lp dichroic mirror and a citrine emission filter (510-550 nm); a FRET cube with a cerulean excitation filter

(426-446 nm), a T455lp dichroic mirror and a citrine emission filter (510-550 nm) (Chroma Technology).

For FRET experiments, transfected HEK293T cells (cf. chapter 3.4.2) as well as isolated rod OSs (cf. section 3.12) were measured in a FRET imaging solution at RT. Fluorescence intensities were acquired from single cells co-expressing varying levels of donor- and acceptor-tagged proteins with each filter cube. First, FRET ratios ( $FR$ ) were calculated from the signal intensities according to the 3<sup>3</sup>-FRET equation:

$$FR = (S_{FRET} - R_{D1} \times S_{cer}) / (R_{A1} \times (S_{citr} - R_{D2} \times S_{cer})) \quad (4)$$

$R_{D1}$ ,  $R_{A1}$ , and  $R_{D2}$  represent experimentally predetermined constants obtained from measured cells expressing only cerulean- or citrine-tagged molecules. These constants correct for bleed-through of cerulean into the citrine channel (donor bleed-through,  $R_{D1}$ ), direct excitation of citrine by cerulean excitation (acceptor cross excitation,  $R_{A1}$ ), and the small proportion of cerulean excitation at the citrine excitation wave-length (donor cross talk,  $R_{D2}$ ) [76].  $S_{FRET}$ ,  $S_{cer}$ , and  $S_{citr}$  are the fluorescence signals measured from cells co-expressing cerulean- and citrine-tagged molecules through the respective filter cube.

FRET efficiencies ( $E_A$ ) at given cerulean/citrine molar ratios (MR) were derived from the following equation (5):

$$E_A = [FR - 1] \times \epsilon_{citrine} (436) / \epsilon_{cerulean} (436) \quad (5)$$

The two factors  $\epsilon_{citrine}$  and  $\epsilon_{cerulean}$  are the FRET setup-specific average molar extinction coefficients for citrine and cerulean.

Binding curves were generated using equation (6):

$$E_A = E_{Amax} \times MR / [K + MR] \quad (6)$$

$E_{Amax}$  represents the maximal FRET efficiency that can be calculated for saturated donor concentrations.  $K$  is an analog to the dissociation constant.

#### FRET imaging solution

NaCl	140 mM
KCl	5 mM
MgCl <sub>2</sub>	1 mM
CaCl <sub>2</sub>	2 mM
Glucose	10 mM
HEPES sodium salt	10 mM
H <sub>2</sub> O	add to 50 ml
Adjust pH to 7.4	

### 3.14 Statistics

For the comparison of two groups, the unpaired Student's t-test was applied. For multiple comparisons, one-way ANOVA followed by Tukey's or Dunett's test were used. All values are given as mean  $\pm$  SEM, and n is the number of independent measurements. Statistical significance is given as follows: \*,  $p < 0.05$ ; \*\*,  $p < 0.01$ ; \*\*\*,  $p < 0.001$ .

## 4 Results

### 4.1 rAAV *PRPH2* minigenes confer efficient protein expression in rods and cones

The entire human *PRPH2* gene including the 5' and 3' untranslated region, the exons, and the introns comprises approx. 26 kb (Figure 6A, upper panel). Due to its large size and the limited genomic packaging capacity of rAAV vectors (4.7 kb), mRNA splicing cannot be analyzed on the native *PRPH2* transcript. To overcome this issue, a peripherin-2 minigene (P-mg) was generated which contains the coding sequence of all three exons and shortened introns bearing the native splice sites (Figure 6A, lower panel). To enable monitoring of minigene-derived protein expression, the P-mg was N-terminally fused to a citrine tag. The corresponding rAAV vector contained either a rod-specific human rhodopsin promoter (hRHO) or a cone-specific murine short wavelength opsin promoter (mSws) yielding the minigene vectors rP-mg and cP-mg, respectively (Figure 6B). The resulting rAAV particles were subretinally injected into two-week-old (P14) wild type (WT) mice. Correct splicing of rP-mg and cP-mg results in a peripherin-2 protein with a molecular weight of approx. 66.5 kDa (Figure 6C). The expression was analyzed three weeks post injection by monitoring the citrine fluorescence on retinal slices from injected animals. As expected, in transduced rods and cones, citrine signal was exclusively found in the outer segments (Figure 6D and E).



generation of novel donor or acceptor splice sites and the abolition or generation of binding sites for exonic splice enhancers (ESEs) or exonic splice silencers (ESSs) (cf. Supplementary Table 1). Among the mutations with predicted splice defects, 11 were randomly chosen for further experimental analysis. Six of these mutants are associated with rod-dominant adRP, whereas the remaining five are found in patients suffering from different types of cone diseases (Table 4). Some of these mutations have been functionally characterized on protein level in previous studies (e.g. C214S) [77, 78], however, none of these studies addressed the potential impacts of the single mutants on mRNA splicing.

**Table 4 Exon 2-specific peripherin-2 point mutations analyzed in this study [43, 79-88].**

Mutation	Disease	References
<i>c.584G&gt;T; p.R195L</i>	cone and cone-rod dystrophy	Yanagihashi <i>et al.</i> 2003
<i>c.594C&gt;G; p.S198R</i>	adRP	Sullivan <i>et al.</i> 2006
<i>c.625G&gt;A; p.V209I</i>	adult foveomacular vitelliform dystrophy	Coco <i>et al.</i> 2010
<i>c.629C&gt;T; p.P210L</i>	adRP	Budu <i>et al.</i> 2001
<i>c.635G&gt;C; p.S212T</i>	adult foveomacular vitelliform dystrophy	Felbor <i>et al.</i> 1997
<i>c.641G&gt;C; p.C214S</i>	adRP	Saga <i>et al.</i> 1993
<i>c.658C&gt;T; p.R220W</i>	pattern dystrophy	Payne <i>et al.</i> 1998
<i>c.659G&gt;A; p.R220Q</i>	pattern dystrophy	Jacobson <i>et al.</i> 1996
<i>c.676C&gt;G; p.Q226E</i>	adRP	Rodriguez <i>et al.</i> 1994
<i>c.736T&gt;C; p.W246R</i>	adRP	Kohl <i>et al.</i> 1997
<i>c.745G&gt;A; p.G249S</i>	adRP	Renner <i>et al.</i> 2009

### 4.3 Comparative splice analysis of WT and mutant peripherin-2 minigenes in rods and cones

Viral particles containing the different mutant minigenes were subretinally injected into WT mice on P14. To analyze mRNA splicing of WT (per<sup>WT</sup>) and mutant peripherin-2 (per<sup>MT</sup>) transgenes, RNA was isolated and pooled from four retinas of four injected animals three weeks after injection. RT-PCR (Figure 7A) was performed with minigene-specific primers, indicated as arrows in Figure 7B. Three different splice isoforms were detected for per<sup>WT</sup> and per<sup>MT</sup> minigenes in rods and cones: 1) the unspliced variant containing both introns (1699 bp), 2) the variant with retained intron 1 (1319 bp), and 3) the correctly spliced transcript (919 bp) (Figure 7A, B). One mutation, per<sup>G249S</sup>, associated with adRP gave rise to a fourth splice product containing an in-frame deletion of 90 bp at the 3' end of exon 2 due to the use of a novel donor splice site (DS) (Figure 7A, B).

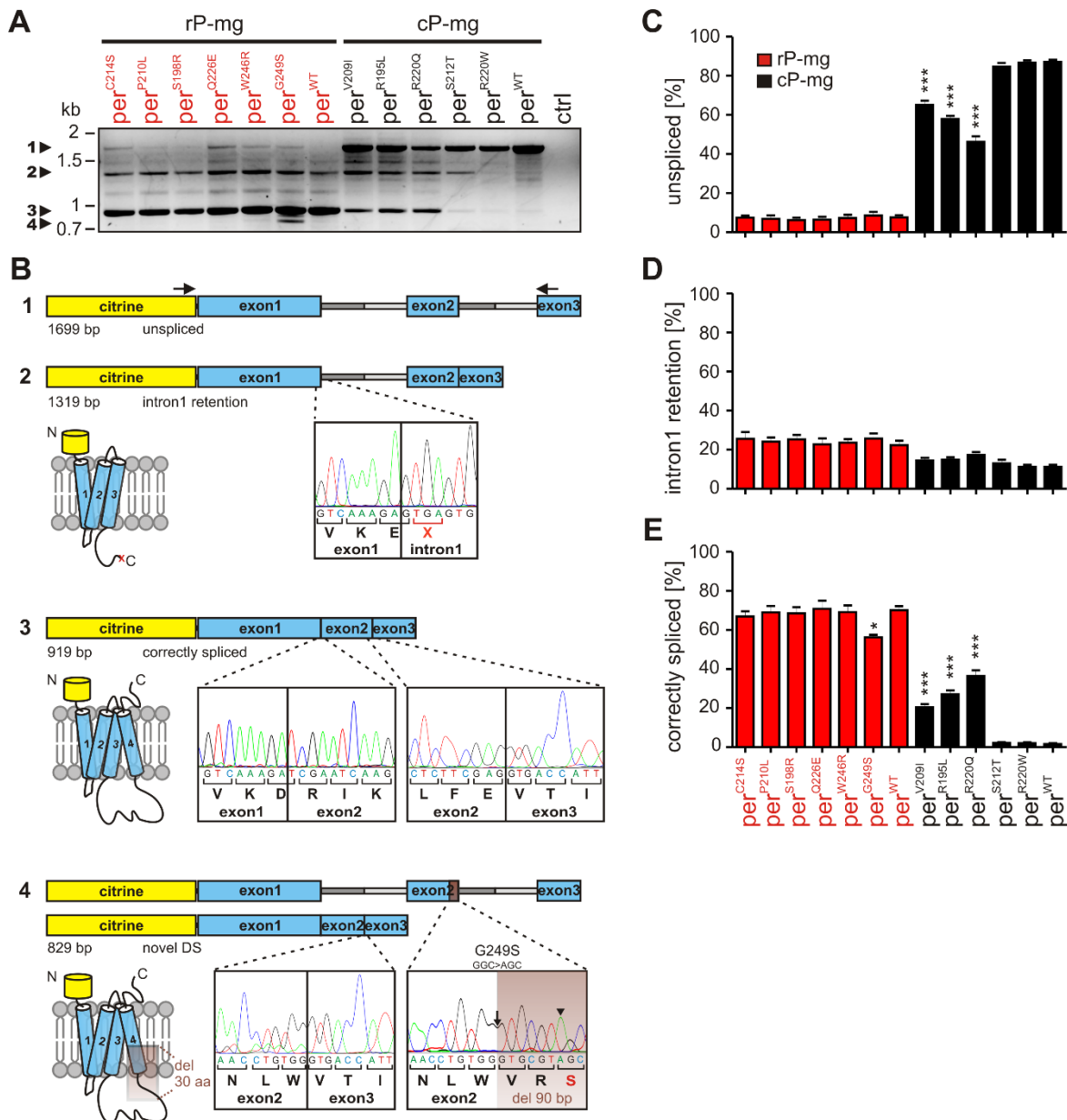


**Figure 7 Splice analysis of  $per^{WT}$  and  $per^{MT}$  minigenes in rods and cones.** (A) Representative RT-PCR from cDNA generated from total RNA isolated from transduced retinas of WT mice three weeks after injection with WT and mutant rP-mg (left) or cP-mg (right) on P14. Ctrl, control containing cDNA from non-transduced retina. The individual bands of the relevant splice products are numbered (1-4) and marked by arrowheads. (B) Schematic representation and sequence analyses of the single minigene-derived splice variants detected in (A). For RT-PCR, primers were used binding to the 3' end of citrine and 5' end of exon 3 of peripherin-2 as indicated by the arrows. **1** and **2**, Unspliced (**1**) and intron 1 retention (**2**) transcripts lead to a frameshift resulting in a premature stop codon immediately after exon 1. The corresponding protein lacks the distal half of the D2 loop, T4, and the C-terminus. N, N-terminus; C, C-terminus. **3**, Sequence results displaying the exon boundaries of the correctly spliced transcript. Left, topology of correctly spliced peripherin-2. **4**, Sequencing results obtained for  $per^{G249S}$ . Upper panel, scheme showing  $per^{G249S}$  before (top) and after splicing (bottom). Lower panel, left, predicted impact of  $per^{G249S}$  on protein level. The generation of a novel donor splice site (DS) results in an in-frame deletion of 30 amino acids (aa) comprising the part of peripherin-2 covered by the brown transparent rectangle. Middle and right, Electropherograms showing the impact of  $per^{G249S}$  before and after splicing. Right, the position of the novel DS is indicated by an arrow and the position of the mutation is highlighted by an arrowhead. All sequencing reactions were performed on bands isolated from (A). (C-E) Semi-quantitative analysis of the relative intensities obtained for the unspliced (C), intron 1 retention (D), and correctly spliced (E) peripherin-2 transcripts. For each  $per^{WT}$  and  $per^{MT}$  minigene, the mean percentage of the band intensities of these three variants relative to the total band intensity (given as sum of the single band intensities) was calculated from five RT-PCR analyses performed with a variable number of cycles (20-28 for rods and 26-33 for cones, cf. Figure 8). Differences in intensities between the rod and cone  $per^{MT}$  to the corresponding  $per^{WT}$  minigene were analyzed for significance using one-way ANOVA followed by Dunett's test. All data were shown as mean values and error bars represent the standard of the mean (SEM). \*,  $p < 0.05$ ; \*\*,  $p < 0.01$ ; \*\*\*,  $p < 0.001$ .

To allow for more precise statements concerning the relative amounts of the three different splice isoforms (unspliced, intron 1 retention, and correctly spliced) in rods and cones, quantitative real-time PCR (qPCR) was used. qPCR was performed with the pooled RNA isolated from retinas transduced with WT rP-mg and cP-mg utilizing the minigene-specific primers. The linear range of amplification was detected between 20-28 cycles for WT rP-mg in rods and between 26-33 cycles for WT cP-mg in cones (Figure 8).

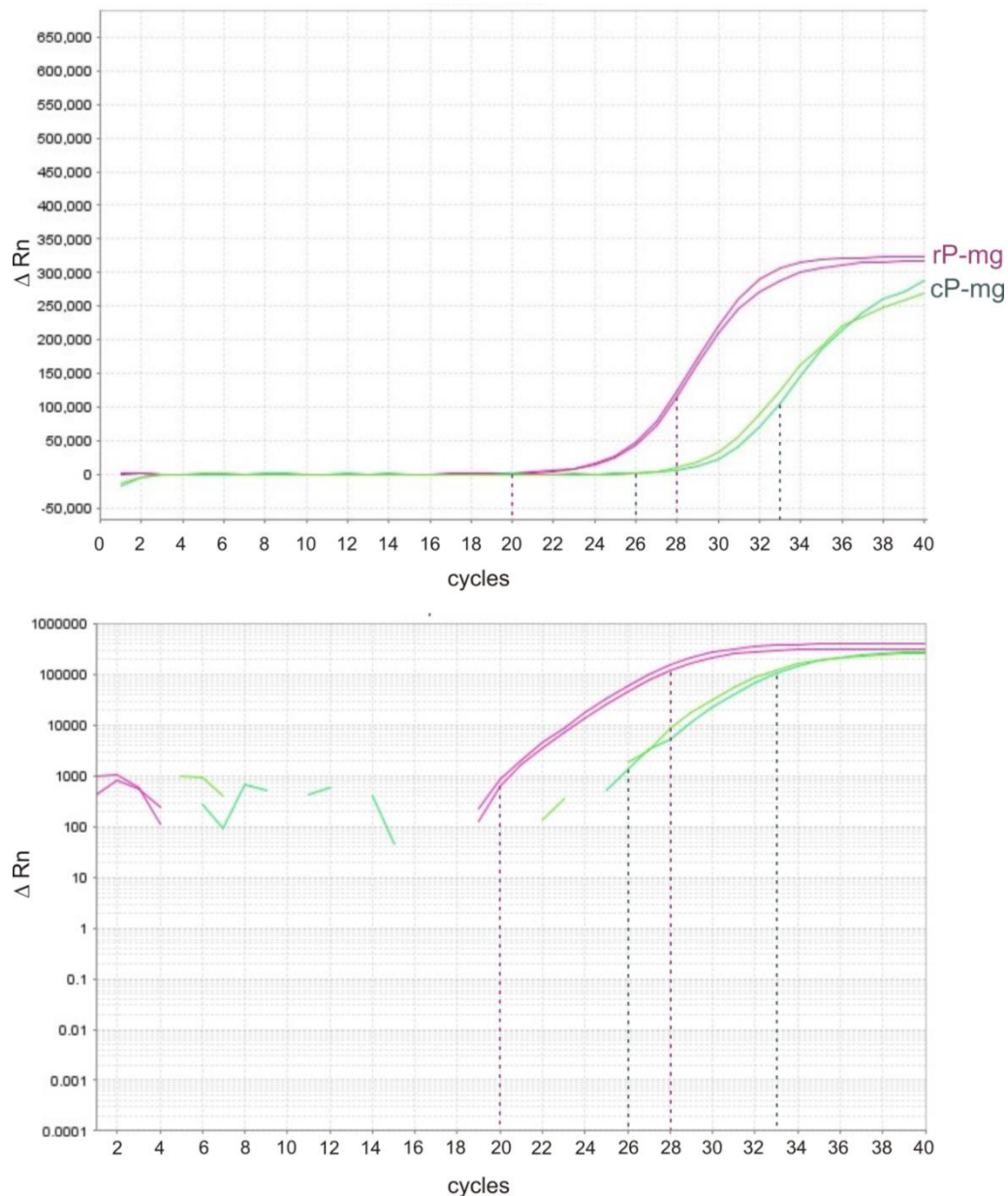


**Figure 8 Determination of the linear amplification range of RT-PCR for peripherin-2 minigenes using qPCR.** Representative qPCR from retinas injected with per<sup>WT</sup> minigenes harboring a rod- (hRHO, rP-mg) or a cone- (mSws, cP-mg) promoter. For qPCR, the same pooled retina samples and the same primers were used as described in Figure 7B. The dashed lines represent the window of cycles falling within the linear amplification range for rP-mg (cycles 20-28, magenta) and cP-mg (cycles 26-33, green).  $\Delta Rn$  (delta Rn), the magnitude of the signal generated by the given set of PCR conditions.

Based on these findings, five technical RT-PCR replicates were performed for each peripherin-2 construct with cycle numbers lying within the respective range of linear amplification in rods and cones. The mean percentage of unspliced, intron 1 retention, and correctly spliced transcripts relative to the sum of band intensities was calculated for all peripherin-2 minigenes (cf. Supplementary Table 2). This analysis revealed profound differences in the relative percentage of the different splice isoforms in rods and cones. These differences were not only observed when comparing the splicing of per<sup>WT</sup> minigenes in rods and cones, but also when relating the effect of each per<sup>MT</sup> to the corresponding per<sup>WT</sup> in the given cell type. Regarding per<sup>WT</sup> in rods, the major splice isoform was the correctly spliced transcript with 70.1 %, whereas splicing of per<sup>WT</sup> in cones yielded only very low amounts of this variant (1.64 %, Figure 7E). In contrast to rods, splicing of per<sup>WT</sup> in cones predominantly resulted in the unspliced isoform with 87.1 % (Figure 7C). For the intron 1 retention variant, a moderate, but not significant difference was found in rods and cones (Figure 7D). For the per<sup>G249S</sup> mutant, the correctly spliced isoform was reduced to 56.2 % in rods (Figure 7E). This reduction most likely results from the generation of the novel donor splice site observed for this mutation (Figure 7B). In cones, the three mutants per<sup>V209I</sup>, per<sup>R195L</sup>, and per<sup>R220Q</sup> resulted in a strong increase in the correctly spliced isoform accompanied by a simultaneous decrease in the unspliced transcript (Figure 7C, E). Taken together, these results indicate cell type- and mutation-specific effects on mRNA splicing of peripherin-2 in rod and cone photoreceptors.

#### 4.4 Quantitative analysis of native peripherin-2 splice isoforms

The splicing analysis shown in Figure 7A was performed with human peripherin-2 minigenes expressed in murine photoreceptors. However, it is conceivable that the endogenous ratios of the single peripherin-2 splice isoforms might differ in human and in mouse photoreceptors, which in turn would impede the interpretation of this minigene-based assay. To investigate whether mRNA splicing of peripherin-2 in mouse photoreceptors is similar to that of human peripherin-2, endogenous levels of peripherin-2 splice isoforms in human and murine retina were assessed via qPCR using human or mouse retinal WT cDNA. For this purpose, two primer sets were utilized specific for the two human (hPRPH2) or murine (mPrph2) peripherin-2 transcripts mirroring the splice isoforms detected in the minigene-based splicing assay (Figure 9A). For the detection of the correctly spliced transcript, primers binding to exon 1 and exon 3 (P-cs\_F and P-cs\_R) were used. Due to the large size of the interjacent native introns (23 kb for human and 12 kb for murine intron 1 and intron 2, cf. Figure 6A and Figure 9A), peripherin-2 isoforms containing the introns are most likely not amplified under the qPCR conditions. To specifically amplify the unspliced peripherin-2 isoform, primers binding to the intronic regions flanking exon 2 were selected (P-us\_F and P-us\_R). Both primer sets led to

detectable qPCR products in human and mouse retina with the relative expression being slightly higher for each of the two peripherin-2 transcripts in the human retina (Figure 9B). As rods account for  $\geq 95\%$  of the photoreceptor population in both, the human and mouse retina, these results most likely reflect the splicing of peripherin-2 minigenes in rods. Accordingly, the correctly spliced peripherin-2 transcript was much higher expressed compared to the unspliced variant ( $10.6 \pm 0.68$  vs  $0.21 \pm 0.03$  in the human retina, and  $5.60 \pm 0.29$  vs  $0.14 \pm 0.03$  in the murine retina). No differences between the human and mouse peripherin-2 expression were identified when plotting the ratio of the unspliced to the correctly spliced isoforms ( $0.10 \pm 0.01$  for human retina vs  $0.13 \pm 0.02$  for murine retina, Figure 9C). These results strongly indicate that in both qualitative and quantitative terms, splicing of peripherin-2 is very similar in the human and mouse retina.

The minigene-based splicing analysis revealed that cones significantly differ from rods in the relative abundance of the correctly spliced and the unspliced peripherin-2 isoforms (Figure 7). To investigate whether this is also the case in a more native setting, fluorescence-activated cell sorting (FACS) was used to purify rods and cones from 6-8-week-old reporter mice. The purity of sorted rods and cones was assessed by comparing the transcript levels of cell type-specific genes, i.e. rhodopsin (*Rho*) as marker for rods and M-opsin (*Opn1mw*) as marker for cones. Sorted cones were only slightly contaminated with rods (about 3.6 %, Figure 9D). This minor contamination is not expected to have noticeable impacts on the interpretation of the results. In accordance with the qPCR results obtained for the native retina shown in Figure 9B, the correctly spliced peripherin-2 transcript in sorted rods was much higher expressed compared to the unspliced variant ( $16.7 \pm 20.71$  vs  $0.95 \pm 0.07$ ). Unlike rods, in sorted cones the correctly spliced peripherin-2 isoform was only moderately increased compared to the unspliced transcript ( $5.45 \pm 0.44$  vs  $2.71 \pm 0.19$ ). Additionally, the data reveals that the expression level of correctly spliced peripherin-2 is markedly decreased in cones which was accompanied by an increase in the expression of the unspliced transcript. The differential expression of the single peripherin-2 isoforms in the two cell types was further emphasized by comparing the ratios of the unspliced to the correctly spliced variants ( $0.06 \pm 0.004$  in rods vs  $0.49 \pm 0.04$  in cones, Figure 9E). These results are largely compatible with the data acquired from the minigene-based splicing analysis demonstrating that the relative endogenous levels of the correctly spliced and unspliced peripherin-2 isoforms differ significantly between rods and cones.

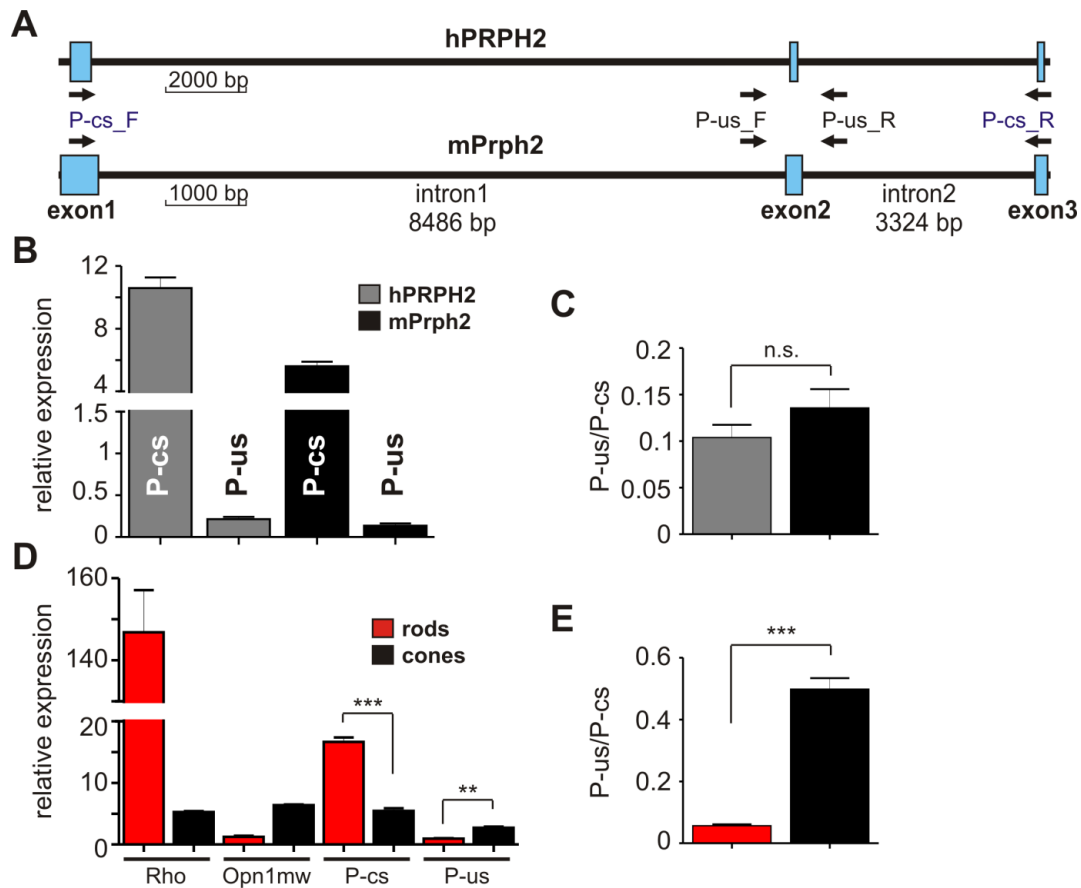


**Figure 9 Quantification of peripherin-2 splice isoforms in native human and murine retinas.** (A) Exon-intron structure of human *PRPH2* (hPRPH2, upper panel) and mouse *Prph2* (mPrph2, lower panel). Binding positions of primers used for qPCR are indicated by arrows. To detect correctly spliced human (hP-cs) or murine peripherin-2 (mP-cs), the P-cs\_F and P-cs\_R primer combination was used. For the detection of unspliced human (hP-us) or murine peripherin-2 (mP-us), the P-us\_F and P-us\_R primer set was applied (cf. Supplementary Table 8). (B) qPCR from pooled human (gray boxes) or murine (black boxes) total retinal RNA, isolated from two (human) or four (mouse) biological samples. The single values are as follows: hP-cs,  $10.6 \pm 0.67$ ; hP-us,  $0.21 \pm 0.03$ ; mP-cs,  $5.60 \pm 0.29$ ; mP-us,  $0.13 \pm 0.03$ . All data are given as mean values and error bars represent the SEM. Three technical replicates were performed for each primer set. (C) Relative ratios given as mean values  $\pm$  SEM of the single unspliced transcripts to the corresponding correctly spliced isoform from human ( $0.10 \pm 0.01$ ) or murine ( $0.13 \pm 0.02$ ) retina. A significance test was conducted using the two-tailed t-test ( $p = 0.26$ ). n.s., not significant. (D) qPCR from sorted murine rods (red boxes) and cones (black boxes). It was performed with cDNA obtained from pooled rods sorted from six animals (yielding 100.000 cells) and pooled cones sorted from four animals (yielding 27.000 cells). For cDNA synthesis, identical total RNA concentrations of isolated rods and cones (50 ng each) were used. Three technical replicates were conducted for each primer combination. All data are given as mean values and error bars represent the SEM. The single values for sorted rods are as follows: Rho,  $146.9 \pm 10.2$ ; Opn1mw,  $1.25 \pm 0.16$ ; P-cs,  $16.7 \pm 0.71$ ; P-us,  $0.95 \pm 0.07$ . Expression in sorted cones yielded following values: Rho,  $5.27 \pm 0.14$ ; Opn1mw,  $6.38 \pm 0.13$ ; P-cs,  $5.45 \pm 0.44$ ; P-us,  $2.71 \pm 0.19$ . P-cs rods vs cones:  $p = 0.0002$ ; P-us rods vs cones:  $p = 0.001$ . (E) Relative ratios of the unspliced transcripts to the corresponding correctly spliced isoform from sorted rods and cones. Significance analysis was conducted with the two-tailed t-test ( $p = 0.0003$ ).

#### 4.5 Peripherin-2 isoform encoded by exon 1 is mislocalized in photoreceptors

Expression of *PRPH2* minigenes shown in Figure 6D and E indicates that the citrine-tagged peripherin-2 protein is properly expressed and localized in the OSs of murine rods and cones. However, considering that all three minigene-derived splice isoforms harbor the fluorophore,

the detection of citrine fluorescence does not allow discriminating which of the isoforms and to which extent they are expressed on protein level. Correctly spliced, fluorophore-tagged full-length peripherin-2 is known to be properly localized in OSs [89]. However, unspliced peripherin-2 and the intron 1 retention isoform contain a premature stop codon directly after exon 1 (cf. Figure 7B) and their OS localization has not been analyzed in previous studies. The translation of these two transcripts would yield a truncated protein lacking the distal part of the D2 loop, transmembrane domain 4, and subsequent downstream sequence (Figure 10A). Translation and protein expression of these peripherin-2 isoforms could lead to one of the four following scenarios: i) The two splice variants are translated into protein, which is stably expressed, but mislocalized to the inner segments. ii) Both isoforms are translated into protein showing correct localization. iii) The two variants are translated into protein, but the protein is degraded. iv) The isoforms are degraded on mRNA level via the nonsense-mediated mRNA decay (NMD) mechanism due to the presence of a premature stop codon. The first option can be excluded as no mislocalized protein was detected in transduced photoreceptors expressing the  $per^{WT}$  minigene. To differentiate between the remaining three alternatives, the peripherin-2 variant harboring a stop codon directly after exon 1 (Figure 10A) was expressed in rods and cones. This truncated peripherin-2 mirrors the protein translated from the unspliced or intron 1 retention isoforms. However, unlike the two minigene-born transcripts, this variant does not contain a premature stop codon and the mRNA can thus not be degraded by the NMD mechanism. This truncated peripherin-2 was completely mislocalized in the inner segments of rods (rP-trunc) and cones (cP-trunc) (Figure 10B and C). Hence, scenarios ii) and iii) proposing correct localization or protein degradation of the two isoforms can be excluded. Consequently, the most likely scenario is that the two splice isoforms bearing the premature stop codon are not translated into protein, presumably as a result of mRNA degradation due to NMD.

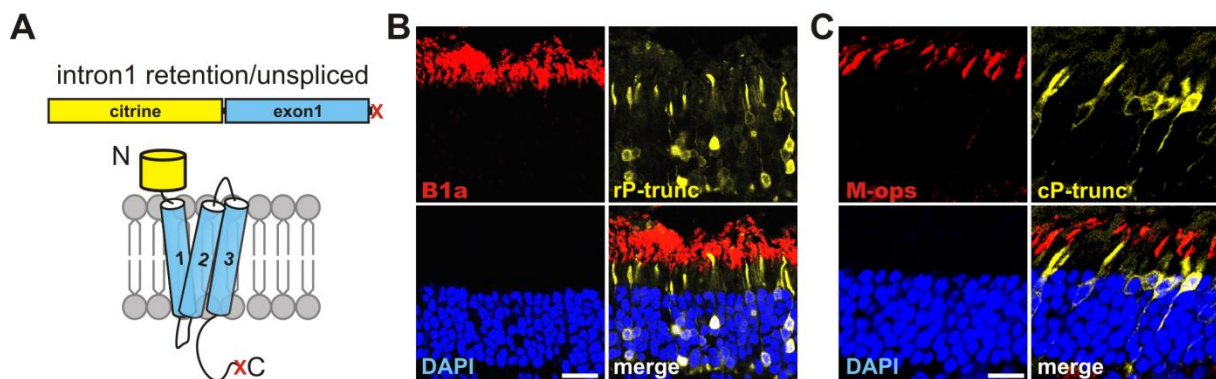


**Figure 10 Impaired OS targeting of truncated peripherin-2.** (A) The truncated peripherin-2 construct contains only exon 1 followed by a downstream stop codon (indicated by "X") mimicking translation from the intron 1 retention and unspliced isoforms (upper panel). Lower panel, Topology of the truncated peripherin-2 protein. (B and C) Immunohistology of transduced murine retinas showing rod- (B) and cone-specific (C) expression of the truncated peripherin-2. In both, rods and cones, truncated peripherin-2 is not transported to the OSs and is almost exclusively present in the ISs and somas of the photoreceptors. B1a and M-ops (red) served as rod and cone OS markers, respectively. Scale bar represents 20  $\mu$ m.

#### 4.6 Protein expression and localization of per<sup>MT</sup> in rods and cones

Next, protein expression and localization of the disease-associated peripherin-2 mutations were addressed in transduced rods and cones (Figure 12 and 11). The mutant expression was assessed on retinal sections three weeks after the subretinal delivery of rAAVs to P14 WT mice. Cone dominant mutations were correctly localized to the cone OSs (Figure 11A-E). In the western blot analysis, all mutant proteins migrated at the same size as per<sup>WT</sup> (approx. 66.5 kDa), however, their expression levels differed among each other (Figure 11F). Particularly, the three mutants per<sup>V209I</sup>, per<sup>R195L</sup>, and per<sup>R220Q</sup> displayed a strongly increased protein expression compared to per<sup>WT</sup> (Figure 11F and G). These findings are consistent with the strongly increased splicing efficiency of the correctly spliced *PRPH2* isoform that was observed for these mutants in cones (cf. Figure 7E).

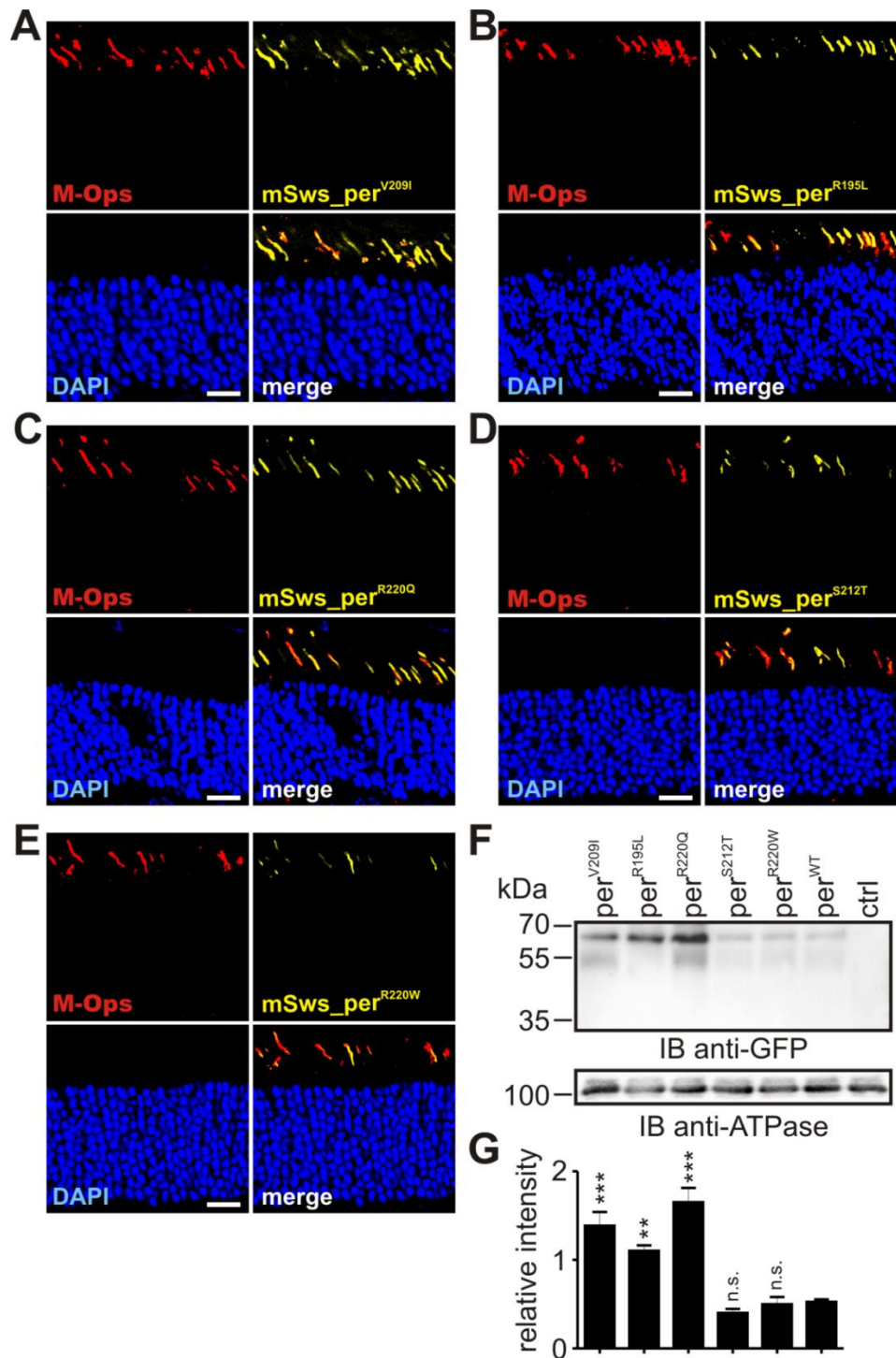


**Figure 11** *In vivo* expression of cone-dominant peripherin-2<sup>MT</sup>. (A-E) Immunohistology of transduced retinas expressing the single cone-disease associated peripherin-2 constructs under the control of the mSws promoter as indicated. A M-opsin antibody (M-ops, red) served as cone OS marker. Scale bar represents 20  $\mu$ m. (F) Western blot analysis from membrane preparations of four murine retinas transduced with the minigenes shown in A-E. All retinas were dissected three weeks post injection. Ctrl, Membrane preparation from non-injected control retinas. Peripherin-2 was detected via an anti-GFP antibody recognizing the citrine tag. An antibody detecting the murine alpha subunit of ATPase (anti-ATPase) served as loading control. (G) Semi-quantitative analysis of the results shown in (F). For determining the relative band intensities, three technical replicates were performed and peripherin-2 expression was normalized to the expression of ATPase. All data are given as mean values  $\pm$  SEM. Statistical analysis was done with one-way ANOVA followed by the Dunnett's test. \*,  $p < 0.05$ ; \*\*,  $p < 0.01$ ; \*\*\*,  $p < 0.001$ . n.s., not significant.

When compared to the cone-dominant  $\text{per}^{\text{MT}}$ , rod-dominant  $\text{per}^{\text{MT}}$  revealed more diverse effects. Two out of the six mutants,  $\text{per}^{\text{C214S}}$  and  $\text{per}^{\text{P210L}}$ , were completely mislocalized to the rod inner segments (Figure 12A and B). In contrast to  $\text{per}^{\text{C214S}}$  showing an evenly distributed cytosolic expression,  $\text{per}^{\text{P210L}}$  was found in large vesicular-like structures.

Additionally, in the western blot analysis and in retinal cryosections,  $\text{per}^{\text{C214S}}$  and  $\text{per}^{\text{P210L}}$  together with two further mutants,  $\text{per}^{\text{S198R}}$  and  $\text{per}^{\text{G249S}}$ , showed lower expression compared to  $\text{per}^{\text{WT}}$  (Figure 12G, H). The strongest reduction was observed for  $\text{per}^{\text{C214S}}$  and  $\text{per}^{\text{S198R}}$ , followed by the  $\text{per}^{\text{P210L}}$  and the  $\text{per}^{\text{G249S}}$  mutant. The remaining two mutants,  $\text{per}^{\text{Q226E}}$  and  $\text{per}^{\text{W246R}}$ , displayed  $\text{per}^{\text{WT}}$ -like protein levels (Figure 12G, H).

Furthermore, the strong reduction of the 66.5 kDa band for the  $\text{per}^{\text{S198R}}$  and  $\text{per}^{\text{P210L}}$  mutants was accompanied by an increased expression of an additional band at approx. 42 kDa. This band was only weakly detectable for  $\text{per}^{\text{WT}}$  and most likely results from protein degradation.

The moderate decrease in protein expression observed for the  $\text{per}^{\text{G249S}}$  mutation is presumably due to the generation of a novel donor splice site (cf. Figure 7B, E) as this reduces the relative amount of the correctly spliced peripherin-2 transcript for this mutant. This novel donor splice site leads to a deletion of 30 amino acids comprising the most distal part of the D2 loop domain and the proximal half of the transmembrane domain 4 (Figure 7B). This deletion reduces the molecular size of the protein by approx. 3.5 kDa, yielding a molecular mass of 63 kDa. However, as no band was detected for  $\text{per}^{\text{G249S}}$  at this size in the western blot, the aberrantly spliced isoform is most likely either degraded on the mRNA or protein level.

Taken together, diverse disease mechanisms were observed for four out of the six adRP-linked  $\text{per}^{\text{MT}}$  including aberrant mRNA splicing, protein degradation, and protein mislocalization. However, all of these mechanisms lead to a decreased protein expression for these mutants in rods. In contrast, three out of the five  $\text{per}^{\text{MT}}$  associated with cone diseases result in increased protein expression in this photoreceptor type.

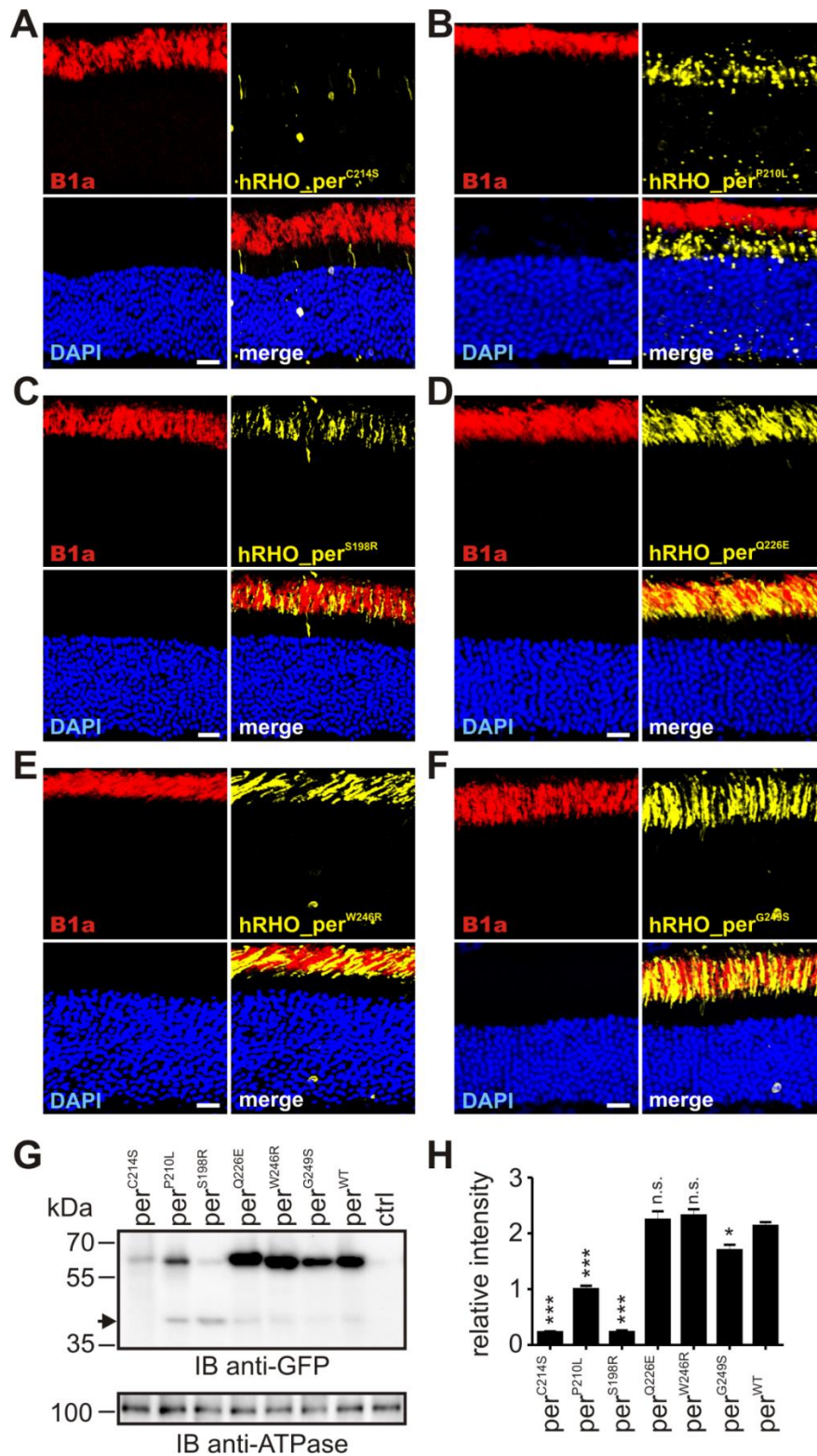


**Figure 12** *In vivo* expression of rod-dominant per<sup>MT</sup>. (A-F) Immunohistology of transduced retinas expressing the single adRP-linked peripherin-2 constructs under the control of the hRHO promoter as indicated. A CNGB1a antibody (B1a, red) served as rod OS marker. Scale bar represents 20 μm. (G) Western blot analysis from membrane preparations of four murine retinas transduced with the minigenes shown in (A-F). All retinas were dissected three weeks post injection. Ctrl, Membrane preparation from non-injected control retinas. The arrow indicates a degradation band detected at 42 kDa. Peripherin-2 was detected via an anti-GFP antibody recognizing the citrine tag. An antibody detecting the murine alpha subunit of ATPase (anti-ATPase) served as loading control. (H) Semi-quantitative analysis of the results shown in (G). For determining the relative band intensities, three technical replicates were performed and peripherin-2 expression was normalized to the expression of ATPase. All data are given as mean values ± SEM. Statistical analysis was assessed using one-way ANOVA followed by the Dunnett's test. \*, p < 0.05; \*\*, p < 0.01; \*\*\*, p < 0.001. n.s., not significant.

#### 4.7 Splicing and protein expression of a rod-dominant $per^{MT}$ in cones and a cone-dominant $per^{MT}$ in rods

So far, mRNA splicing and protein expression of the rod- and cone-specific  $per^{MT}$  were exclusively analyzed in the photoreceptor type reported to be affected by the given mutation. In order to exclude the possibility that mutations also impact on these processes in the photoreceptor type that is not primarily affected by the mutation, the rod-dominant  $per^{W246R}$  mutant was expressed in cones while the cone-dominant  $per^{R220W}$  mutant was expressed in rods (Figure 13). However, for both mutants, protein localization (Figure 13A, F), mRNA splicing (Figure 13B, C, G, H), and protein expression levels (Figure 13D, E, I, J) remained unaffected and were indistinguishable from the corresponding  $per^{WT}$ .

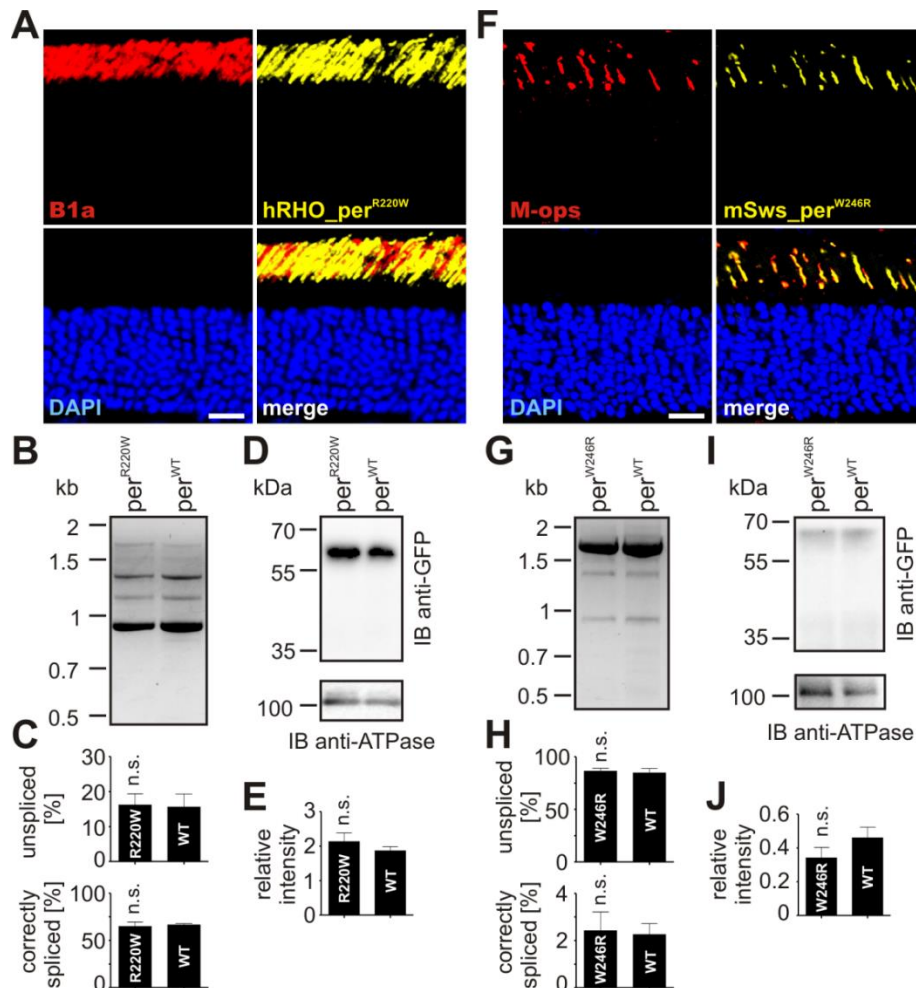


**Figure 13 Cross-expression of a rod-dominant  $per^{MT}$  in cones and a cone-dominant  $per^{MT}$  in rods.** Protein localization (A, F), mRNA splicing (B, C, G, H), and protein expression (D, E, I, J) of the cone-specific  $per^{R220W}$  mutant in rods (A-E) and the rod-specific  $per^{W246R}$  mutant in cones (F-J). All experimental conditions (age and number of injected mice, immunolabeling of retinal slices, time points of RNA and protein isolation, number of cycles used for RT-PCR, and type of data presentation) were identical to those described in Figure 6, 7, 11 and 12. For the semi-quantitative analysis of mRNA splicing (C, H) and protein expression (E, J) in rods and cones, three technical replicates were performed. Significance test was conducted using the two-tailed t-test. p-values are as follows: C,  $p_{\text{unspliced}} = 0.91$ ; C,  $p_{\text{correctly spliced}} = 0.76$ ; H,  $p_{\text{unspliced}} = 0.74$ ; H,  $p_{\text{correctly spliced}} = 0.87$ ; E,  $p = 0.87$ ; J,  $p = 0.25$ . Scale bars in A and F represent 20  $\mu\text{m}$ .

#### 4.8 Impact of the disease-linked per<sup>MT</sup> on homo- and heteromeric protein-protein interactions

As demonstrated in Figure 11 and Figure 12 in chapter 4.6, in contrast to per<sup>C214S</sup> and per<sup>P210L</sup>, none of the other nine mutants affected rod OS targeting. One possible mechanism explaining the mislocalization of per<sup>C214S</sup> and per<sup>P210L</sup> in rod photoreceptors could be that these mutations impact on the binding of the mutant protein to per<sup>WT</sup> and/or to Rom-1. As mentioned in the introduction, peripherin-2 can form homomeric peripherin-2/peripherin-2 and heteromeric peripherin-2/Rom-1 complexes. To investigate whether the disease-linked peripherin-2 mutations affect these complexes, co-immunoprecipitation experiments from HEK293T cells co-transfected with the single mutants and per<sup>WT</sup> or Rom-1 were performed. As the two mutations per<sup>R220Q</sup> and per<sup>R220W</sup> affect the same arginine residue at position 220, only one of these mutants (per<sup>R220Q</sup>) was analyzed in this experiment.

As is evident from Figure 14, only the two rod-dominant mutations per<sup>C214S</sup> and per<sup>P210L</sup> showed a markedly reduced binding to both per<sup>WT</sup> and Rom-1 (Figure 14B, C). In accordance with previous studies [28, 77], this suggests that peripherin-2 mislocalization might correlate with impaired protein complex formation.

#### 4.9 P210 and C214 are crucial for the proper folding of the distal D2 loop

The proline at position 210 (P210) and the cysteine at position 214 (C214) are located within a highly conserved motif among tetraspanins, the PxxCC motif whose function has not been fully clarified yet [90]. The reduced binding of per<sup>C214S</sup> and per<sup>P210L</sup> to per<sup>WT</sup> suggests that these residues might either be crucial for proper folding of peripherin-2 or could represent the protein-protein interaction interface. A recent study utilizing CD spectroscopy indicated that per<sup>C214S</sup> impairs protein folding by increasing the percentage of  $\beta$ -sheets accompanied by a decrease in helices in the D2 loop [91]. However, it was not fully clarified which part(s) of the D2 loop is (are) affected by this mutation. In order to address this issue more directly, a protease cleavage assay was designed and performed on membrane preparations from HEK293T cells expressing the citrine-tagged per<sup>WT</sup> and per<sup>MT</sup> transgenes (Figure 14D). Membrane preparations are expected to preserve the native protein structure as they are performed without any detergents or reducing agents [92]. Improper folding can lead to the masking of existing or to an exposure of hidden protease cleavage sites and therefore alter the number of cleavage sites accessible for the endogenously expressed proteases present in the membrane preparations.

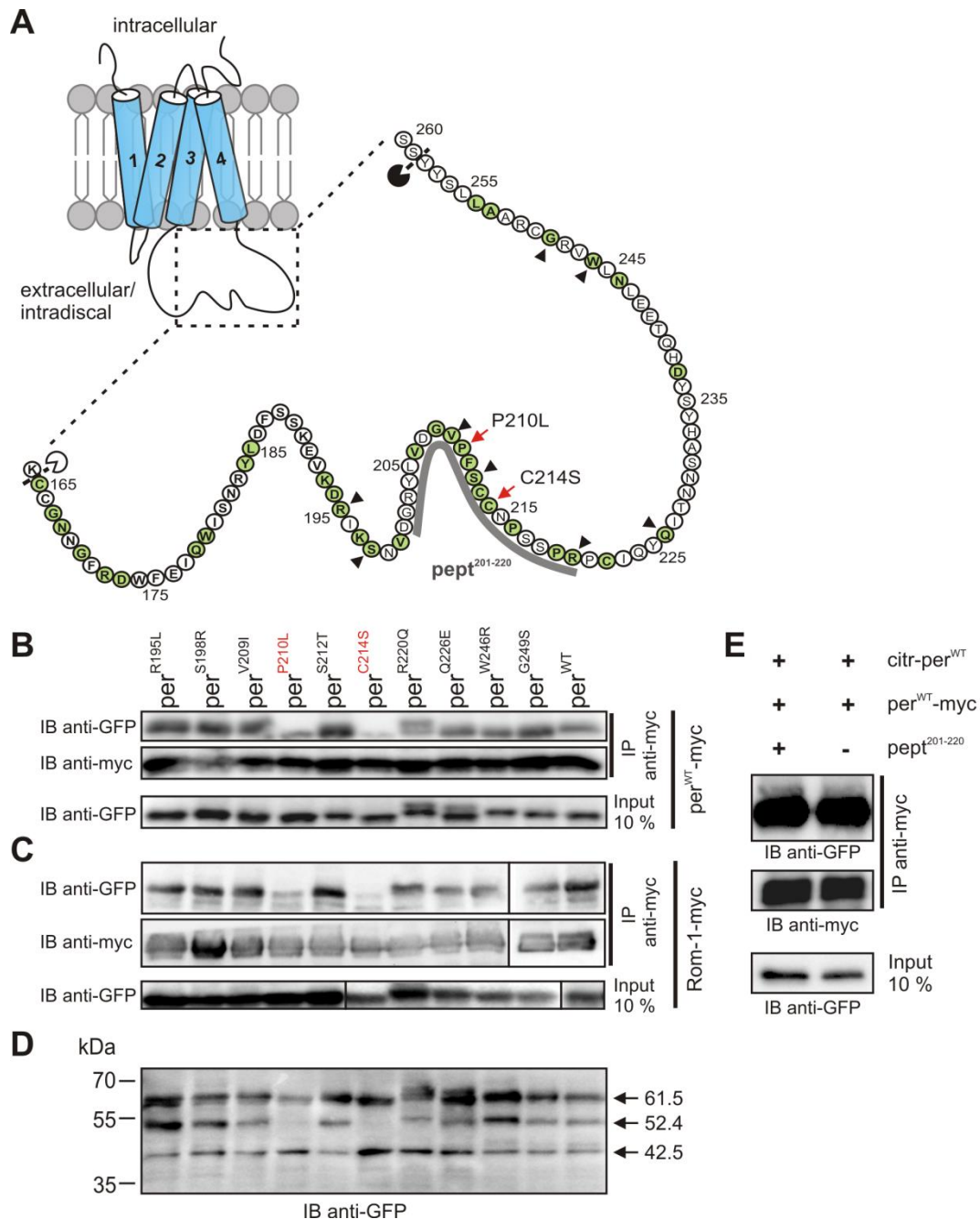


**Figure 14 Effects of peripherin-2 mutants on protein-protein interactions and D2 loop folding.** (A) The dashed rectangle marks the distal part of the D2 loop which is schematically enlarged below. The hitherto identified disease-associated peripherin-2 mutations in this region are highlighted in green. The positions of the mutants analyzed in (B-D) are indicated by red arrows (for per<sup>P210L</sup> and per<sup>C214S</sup>) or by black arrowheads in case of the remaining mutants. The calculated protease cleavage sites from (D) are marked by a white (corresponding to the 42.5 kDa band) or black (corresponding to the 52.4 kDa band) pacman. The position of the peptide (amino acids 201-220) used in the competition assay shown in (E) (pept<sup>201-220</sup>) is highlighted by the gray line. (B-C) Co-IPs from membrane preparations of HEK293T cells transiently transfected with the respective N-terminally citrine-tagged mutants and C-terminally myc-tagged per<sup>WT</sup> (per<sup>WT</sup>-myc, B) or Rom-1 (Rom-1-myc, C). The mutants were detected using a GFP antibody (anti-GFP) recognizing the citrine-tag whereas per<sup>WT</sup>-myc and Rom-1-myc were detected via a myc-specific antibody (anti-myc). IB, Immunoblotting. (D) Protease cleavage assay performed with membrane preparations from HEK293T cells transiently transfected with the citrine-tagged per<sup>MT</sup> and per<sup>WT</sup> as indicated. The molecular weight of the single bands (marked by arrows) was calculated from five independent western blot experiments. (E) Co-IPs from membrane preparations of HEK293T cells co-transfected with citrine- and myc-tagged per<sup>WT</sup> in presence (left lane, 10mM) or absence of the peptide.

Using the same GFP antibody recognizing the N-terminally citrine-tagged peripherin-2 constructs (cf. chapter 4.8), three bands at 61.5 kDa, 52.4 kDa and 42.5 kDa could be detected. The 61.5 kDa band represents the full-length citrine-tagged peripherin-2. Its calculated size is 66.5 kDa; however, in the presence of protease inhibitors, full-length per<sup>WT</sup> always migrated as a 61.5 kDa band. The 52.4 kDa and 42.5 kDa bands could only be detected in the absence of protease inhibitors and upon incubation of the samples at 37 °C. Using the 61.5 kDa per<sup>WT</sup> band as reference, the putative cleavage sites for the 52.4 kDa and 42.5 kDa bands were calculated. The 42.5 kDa band indicates protein cleavage around the highly conserved tetraspanin CCG motif (Figure 14A) [90]. This band could be observed for all peripherin-2 constructs suggesting proper folding in this part of the protein. In contrast, the 52.4 kDa band was completely absent for per<sup>C214S</sup> and per<sup>P210L</sup>. The putative protease cleavage site for the 52.4 kDa band is calculated to be located within the distal part of the D2 loop next to the transmembrane domain 4 (Figure 14A). Collectively, these findings indicate that per<sup>C214S</sup> and per<sup>P210L</sup> lead to a structural rearrangement of the distal part of the D2 loop.

A recent study postulated that peripherin-2 residues 165-182 are crucial for homomeric protein-protein interactions [93]. However, it has not been clarified whether flanking regions involving the per<sup>C214S</sup> and per<sup>P210L</sup> residues could also have an impact on this type of interaction. To investigate this possibility, a peptide competition assay was performed using a peptide corresponding to the residues 201-220 of native human peripherin-2 (Figure 14A and E). In case the positions P210 and C214 are involved in peripherin-2 homomerization, the peptide should compete with this binding and, thus, lead to a reduction of homomeric protein-protein interactions. In subsequent co-IP experiments, however, even in the presence of a very high peptide concentration (10 mM), no changes in the per<sup>WT</sup>-per<sup>WT</sup> interaction compared to the peptide-free approach were detectable (Figure 14E). These results indicate that the region comprising the residues 201-220 is most likely not directly involved in homomerization of peripherin-2.

#### 4.10 Quantification of per<sup>WT</sup>, per<sup>MT</sup>, and Rom-1 protein-protein interactions in HEK293T cells using FRET

<sup>3</sup>FRET can be used to quantify homo- and heteromeric interactions of photoreceptor-specific proteins such as peripherin-2 [89, 94]. In particular, this method can be applied to determine the relative binding affinities of these proteins in HEK293T cells [89]. Thus, FRET was used in this study to examine the specific binding characteristics of the different homo- and heteromeric per<sup>WT</sup>, per<sup>MT</sup>, and Rom-1 protein complexes (Figure 15). To calculate the binding curves, the relative expression of cerulean and citrine (given as molar ratio, cer/citr MR) needs to vary between the single cells co-expressing these FRET fluorophores. When plotting the FRET

efficiency ( $E_A$ ) values against the corresponding cer/citr MR, sufficient variabilities in the expression of both fluorophores for each FRET combination were obtained.  $E_{Amax}$ , representing the maximal FRET efficiency, was calculated according to equation (6) in chapter 3.13 and is proportional to the binding strength of the respective protein complex in the equilibrium. Analysis of  $E_{Amax}$  for the different per<sup>WT</sup> and per<sup>MT</sup> combinations provided several important conclusions:

i) Robust and unusually high  $E_{Amax}$  values for the per<sup>WT</sup> only FRET pair were obtained (34.2 %, Figure 15A and Supplementary Table 3). These  $E_{Amax}$  values almost reach the highest theoretically possible FRET efficiency of 40 % for proteins fused to bulky fluorophores like cerulean or citrine emphasizing the strength of homomeric peripherin-2 protein-protein interactions [95].

ii) In comparison to per<sup>WT</sup>, the per<sup>P210L</sup> only (30.7 %, Figure 15B and Supplementary Table 3) and per<sup>C214S</sup> only (26.5 %, Figure 15C and Supplementary Table 3) FRET pairs displayed just a slight decrease in  $E_{Amax}$ , indicating that both mutants are still largely able to self-interact.

iii) In line with the findings obtained from the co-IP experiments shown in Figure 14B, per<sup>WT</sup>-per<sup>P210L</sup> (9.44 %) as well as per<sup>WT</sup>-per<sup>C214S</sup> (8.58 %) complexes resulted in a robust decrease in  $E_{Amax}$  (Figure 15D, E and Supplementary Table 3). This indicates that the protein complex formation is strongly impaired but not completely abolished for the per<sup>WT</sup>-per<sup>P210L</sup> and per<sup>WT</sup>-per<sup>C214S</sup> combinations.

Next, the  $E_{Amax}$  values of peripherin-2-Rom-1 combinations were analyzed.  $E_{Amax}$  of the per<sup>WT</sup>-Rom-1 interaction was considerably decreased (15.6 %) compared to the per<sup>WT</sup> only (34.2 %) interaction suggesting that heteromeric per<sup>WT</sup>-Rom-1 complexes bind less tight than their homomeric per<sup>WT</sup> only counterparts (Figure 15F and Supplementary Table 3). Furthermore, both combinations, per<sup>P210L</sup>-Rom-1 and per<sup>C14S</sup>-Rom-1, exhibited a reduction in their  $E_{Amax}$  values compared to the per<sup>WT</sup>-Rom-1 interaction (6.58 % and 6.32 %, respectively, Figure 15G, H and Supplementary Table 3).

Finally, also the percentage of  $E_{Amax}$  reduction for both mutants relative to the per<sup>WT</sup> only and the per<sup>WT</sup>-Rom-1 FRET pairs were calculated. The  $E_{Amax}$  values were reduced to 28 % of the per<sup>WT</sup> only value for the per<sup>WT</sup>-per<sup>P210L</sup> and to 25 % for the per<sup>WT</sup>-per<sup>C214S</sup> complexes. In contrast,  $E_{Amax}$  values were only reduced to 42 % of the per<sup>WT</sup>-Rom-1 FRET pair value in the case of the per<sup>P210L</sup>-Rom-1 and to 40 % for the per<sup>C14S</sup>-Rom-1 combinations (Supplementary Table 3). These results indicate that the binding of both peripherin-2 mutants to Rom-1 is less severely affected than their binding to per<sup>WT</sup>. However, despite more or less strongly reduced efficiencies, per<sup>P210L</sup> and per<sup>C14S</sup> in principal retain their ability to self-interact and to form complexes with both, per<sup>WT</sup> and Rom-1.

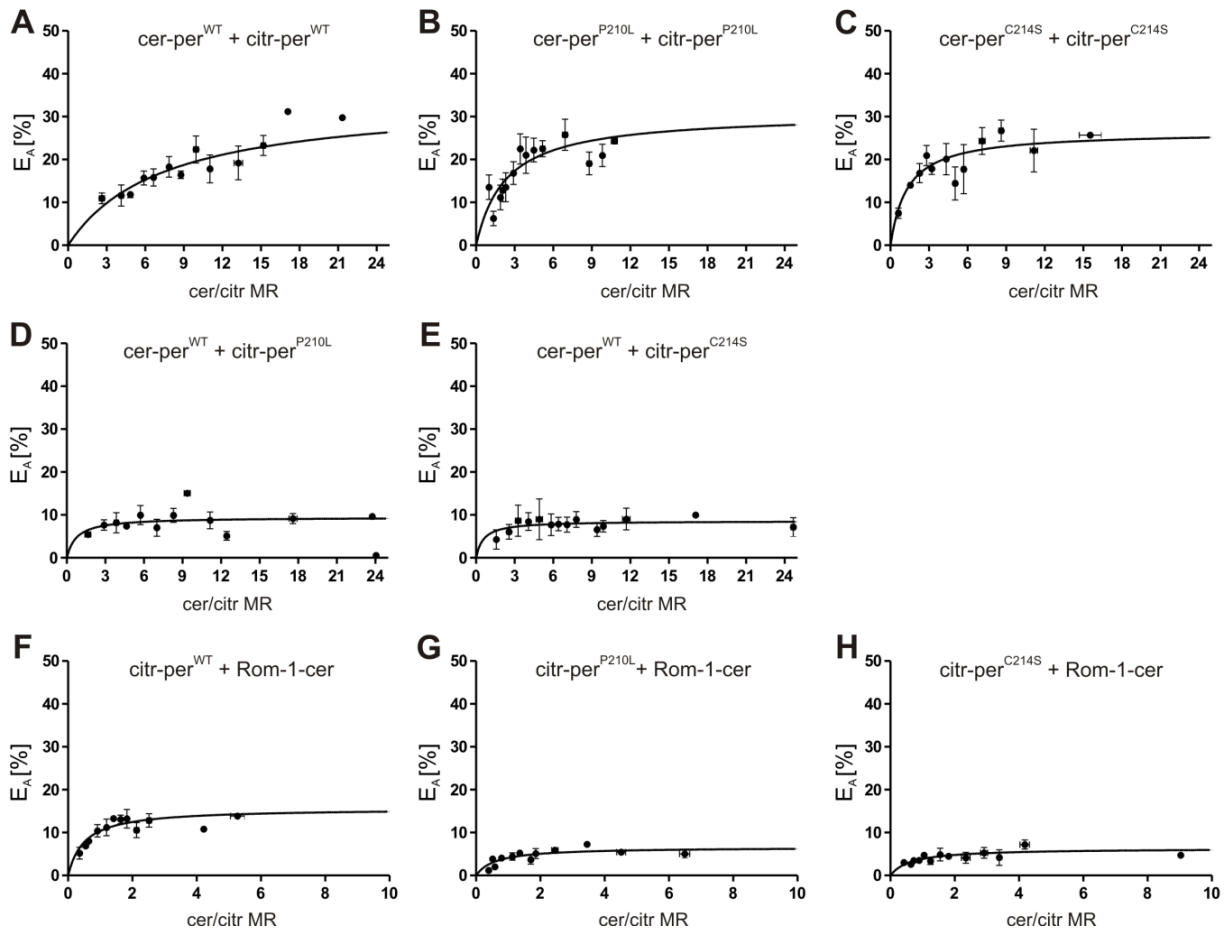


**Figure 15 Quantification of per<sup>WT</sup>, per<sup>MT</sup>, and Rom-1 protein-protein interactions in HEK293T cells using FRET.** (A-H) FRET experiments performed in living HEK293T cells transiently transfected with the respective cerulean- (cer) or citrine- (citr) tagged peripherin-2 or Rom-1 constructs as indicated. Binding curves were generated by plotting the FRET efficiency ( $E_A$ ) against the cer/citr molar ratio (MR). The dots represent mean values of 1-7 single FRET measurements  $\pm$  SEM. The single  $E_A$  values,  $E_{Amax}$ , and numbers of independent measurements (n) for each combination are summarized in Supplementary Table 3.

#### 4.11 Subunit assembly of homo- and heteromeric per<sup>WT</sup>, per<sup>MT</sup>, and Rom-1 complexes

Sucrose density gradient centrifugation (SDGC) is a commonly used technique allowing the separation of covalently or non-covalently linked proteins across a sucrose gradient corresponding to their specific molecular weight. In previous studies, this method was already successfully applied to examine the impact of peripherin-2 mutants including per<sup>C214S</sup> on homomeric per<sup>MT</sup>-per<sup>MT</sup> or heteromeric per<sup>MT</sup>-Rom-1 interactions [28, 29, 77, 96]. However, due to the autosomal dominant fashion of *PRPH2*-linked adRP, many different combinations of peripherin-2 complexes can be formed in heterozygous patients: per<sup>WT</sup>-per<sup>WT</sup>, per<sup>MT</sup>-per<sup>MT</sup>, per<sup>WT</sup>-per<sup>MT</sup>, per<sup>WT</sup>-Rom-1, and per<sup>MT</sup>-Rom-1. Additionally, each of these combinations can exist in different equilibria of mono-, di-, and tetramers as well as higher-order oligomers. So far, this high complexity has prevented a more detailed investigation of how subunit assembly

might influence the rod OS targeting of the single peripherin-2 protein complexes. To examine the complexes that can be formed in heterozygous patients more systematically, a set of SDGC experiments was conducted with differentially tagged  $\text{per}^{\text{WT}}$ ,  $\text{per}^{\text{MT}}$ , and Rom-1 combinations transiently expressed in HEK293T cells.

In good agreement with previous work [97],  $\text{per}^{\text{WT}}$  was only detected in the fractions corresponding to the non-covalent tetramers and disulfide-linked octamers under non-reducing conditions (Figure 16A). In contrast,  $\text{per}^{\text{P210L}}$  was predominantly found as monomer, non-covalent dimer, and aggregates, but some complexes were also found as disulfide-linked tetramers and octamers (Figure 16B).  $\text{per}^{\text{C214S}}$  exhibited a similar pattern as  $\text{per}^{\text{P210L}}$  and was mainly detected as monomer, non-covalent dimer, and aggregates (Figure 16C). However, when co-expressed with  $\text{per}^{\text{WT}}$ , the subunit assembly pattern of both mutants changed.  $\text{per}^{\text{P210L}}$  was primarily found in the fractions containing monomers as well as non-covalent dimers, and a weak signal was also observed in the non-covalent tetramer fraction (Figure 16D). Interestingly, compared to  $\text{per}^{\text{WT}}$  only, in presence of  $\text{per}^{\text{P210L}}$  the pattern of  $\text{per}^{\text{WT}}$  also slightly changed as a considerable amount of  $\text{per}^{\text{WT}}$  appeared in the non-covalent dimer fraction (Figure 16D, cf. Figure 16A). As non-covalent dimers were virtually undetectable in the  $\text{per}^{\text{WT}}$  only situation, this suggests that the corresponding fraction at least partially consists of  $\text{per}^{\text{WT}}$ - $\text{per}^{\text{P210L}}$  dimers. Co-expression of  $\text{per}^{\text{WT}}$  with  $\text{per}^{\text{C214S}}$  led to a substantial decrease in the formation of  $\text{per}^{\text{C214S}}$  aggregates and mainly non-covalent dimers and monomers could be detected (Figure 16E). Moreover, unlike the  $\text{per}^{\text{WT}}$ - $\text{per}^{\text{P210L}}$  combination, in presence of  $\text{per}^{\text{WT}}$   $\text{per}^{\text{C214S}}$  could also be found in the non-covalently linked tetramer fractions. However, similar to the  $\text{per}^{\text{WT}}$ - $\text{per}^{\text{P210L}}$  combination, when co-expressed with  $\text{per}^{\text{C214S}}$   $\text{per}^{\text{WT}}$  signal was also detected in the non-covalent dimer fractions (Figure 16E). Considering that  $\text{per}^{\text{WT}}$  alone virtually does not form any non-covalent dimers (cf. Figure 16A) and that  $\text{per}^{\text{C214S}}$  alone does not form any non-covalent tetramers (cf. Figure 16C), it is most likely that these complexes consist of  $\text{per}^{\text{WT}}$ - $\text{per}^{\text{C214S}}$  dimers and tetramers, respectively (Figure 16E).

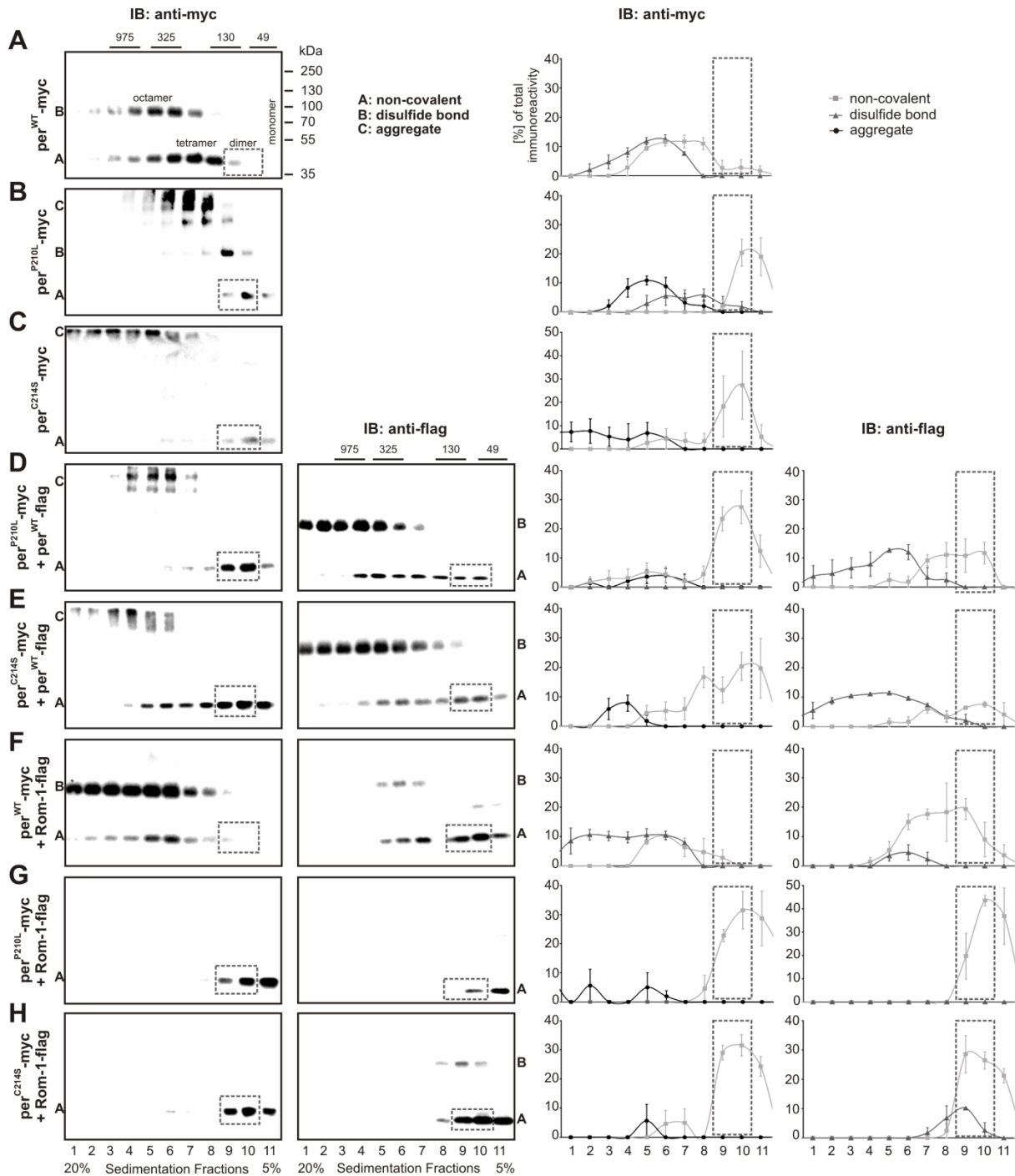


**Figure 16 SDGC experiments from different  $per^{WT}$ ,  $per^{MT}$ , and Rom-1 combinations.** (A-H) Shown are representative immunoblots (left panel) and the corresponding statistics (right panel) of each C-terminally myc- or flag-tagged combination as indicated. Each blot contains eleven fractions collected across the 5-20 % sucrose gradient. All fractions were normalized to the DNA standard mixed to the protein solution prior to SDGC as described in the materials and methods section 3.6. Fractions correlating to the DNA standard (975 kDa, 325 kDa, 130 kDa, and 49 kDa) are marked accordingly. The single peripherin-2 or Rom-1 complexes were found in following fractions: octamers, fraction 3-6; tetramers, fraction 6-8; dimers: fraction 9-10; monomers, fraction 10-11. Western blots were performed with antibodies recognizing either the myc-tag (first row of the left panel) or the flag-tag (second row of the left panel). For quantification (right panel), the percentage of total immunoreactivity related to the number of single fractions for non-covalent or covalent complexes and aggregates was plotted against the eleven collected fractions. The fractions containing non-covalent dimers are highlighted by a dashed rectangle. The single values (percentages and numbers of independent experiments) for all combinations are summarized in Supplementary Table 4.

Following the analysis of the homomeric peripherin-2 combinations, the SDGC fractions of the heteromeric peripherin-2-Rom-1 complexes were examined. In accordance with previous reports [26, 97, 98], the co-expression of Rom-1 and per<sup>WT</sup> resulted in a robust Rom-1 signal detected in the non-covalent tetramer and covalently linked octamer fractions (Figure 16F). Additionally, Rom-1 was also found as non-covalent dimers and monomers. However, since virtually no per<sup>WT</sup> signal could be identified in these fractions, it is very likely that no per<sup>WT</sup>-Rom-1 heterodimers are present under these conditions (Figure 16F). After co-expressing Rom-1 with each mutant, both, per<sup>P210L</sup> and per<sup>C214S</sup> were almost exclusively found as non-covalent dimers and monomers (Figure 16G, H). Similar results were obtained for Rom-1 in the corresponding fractions. Unlike the Rom-1-per<sup>WT</sup> combination, in presence of per<sup>P210L</sup> and per<sup>C214S</sup> Rom-1 signal was almost exclusively detected in the dimer and monomer fractions indicating that Rom-1 predominantly forms heteromeric non-covalent dimers with both mutants (Figure 16G, H). Taken together, the results obtained from this SDGC analysis indicate that homomeric per<sup>WT</sup>-per<sup>MT</sup> and heteromeric per<sup>MT</sup>-Rom-1 complexes are primarily built of non-covalent dimers.

#### 4.12 Rod OS targeting of homo- and heteromeric per<sup>WT</sup>, per<sup>MT</sup>, and Rom-1 complexes

The FRET (cf. chapter 4.10) and SDGC (cf. chapter 4.11) experiments from HEK293T cells indicate that per<sup>P210L</sup> and per<sup>C214S</sup> are in principle able to interact with per<sup>WT</sup> and Rom-1, albeit with markedly changed complex formation patterns. In this part of the study, it was assessed how the single complexes contribute to the protein transport/protein localization in the rod photoreceptors.

Subretinal co-administration of two rAAVs encoding different transgenes yields very high co-transduction efficiencies in rods [89]. Based on this, rAAV-mediated gene delivery was used to (co-)express the different combinations of per<sup>WT</sup>, per<sup>MT</sup>, and Rom-1 in mouse rod photoreceptors. To distinguish between the different transgenes, per<sup>WT</sup> and Rom-1 were N-terminally fused to cerulean while per<sup>P210L</sup> and per<sup>C214S</sup> retained the citrine tag at their N-terminus. The rAAVs harboring the different peripherin-2 and Rom-1 constructs were subretinally injected into WT mice on P14. Four weeks post injection, the protein localization was examined on corresponding retinal slices from injected animals.

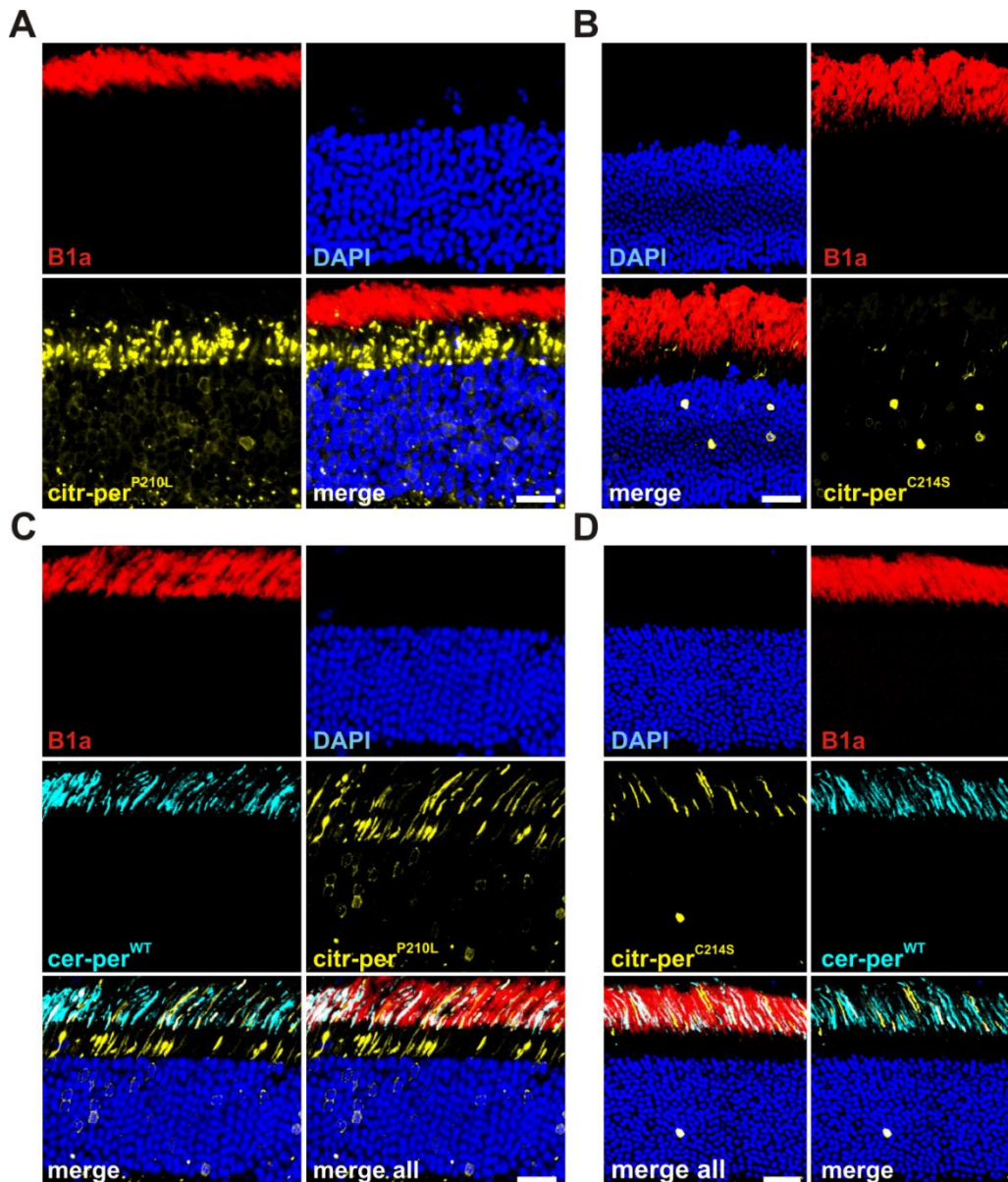


**Figure 17 Rod OS targeting of per<sup>MT</sup> and per<sup>WT</sup>-per<sup>MT</sup> complexes.** (A-D) Immunohistology of retinas injected with citrine-tagged mutants (per<sup>P210L</sup>, A, and per<sup>C214S</sup>, B), or co-injected with the respective mutants and N-terminally cerulean-tagged per<sup>WT</sup> (cer-per<sup>WT</sup>, C-D). B1a (red) was used as rod OS marker. Scale bar represents 30  $\mu$ m.

Similar to the results shown in Figure 12A and 12B in chapter 4.6, both mutants were retained in the inner segments when expressed alone (Figure 17A, B). However, simultaneous co-administration of titer-matched per<sup>WT</sup> and per<sup>MT</sup> resulted in a substantial rescue of rod OS targeting for per<sup>P210L</sup> and per<sup>C214S</sup> (Figure 17C, D). Additionally, co-expression of per<sup>WT</sup> also rescued the vesicular-like expression pattern of per<sup>P210L</sup> in the rod inner segments (Figure 17C) and increased the expression of per<sup>C214S</sup> protein (Figure 17D).

To investigate whether similar rescue effects could be achieved in the presence of Rom-1, transgenic Rom-1 and peripherin-2 constructs were co-delivered to murine rods (Figure 18).

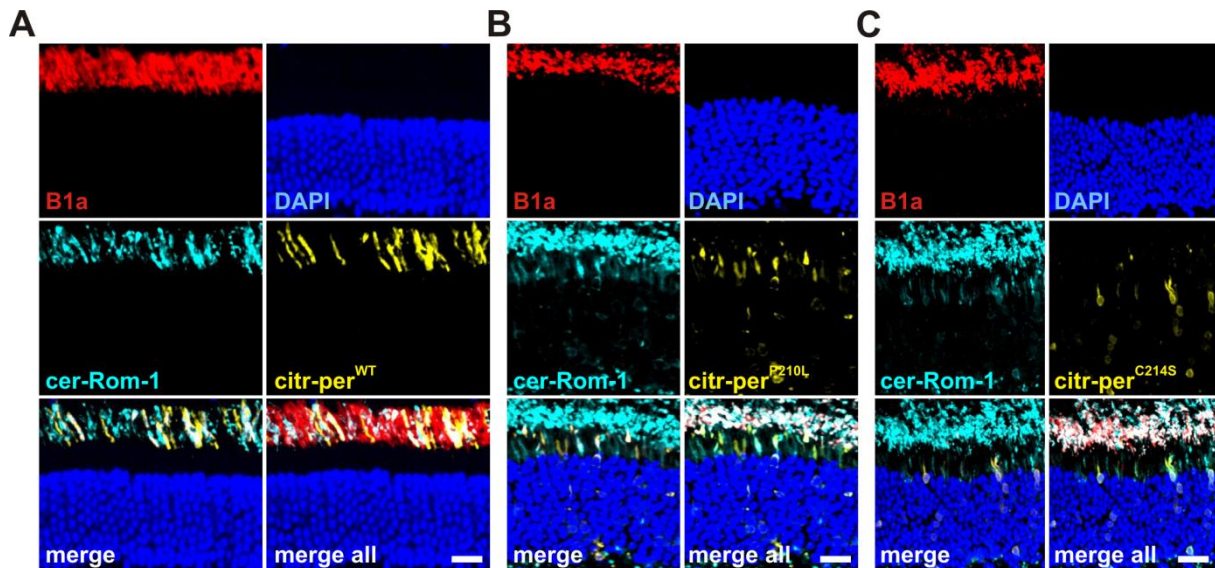


**Figure 18 Rod OS targeting of Rom-1-per<sup>WT/MT</sup> complexes.** Immunohistology of retinas co-injected with N-terminally cerulean-tagged Rom-1 (cer-Rom-1) and citr-per<sup>WT</sup> (A), citr-per<sup>P210L</sup> (B), and citr-per<sup>C214S</sup> (C). B1a (red) was used as rod OS marker. Scale bar represents 30  $\mu\text{m}$ .

After co-administration of Rom-1 and per<sup>WT</sup>, both proteins were exclusively detected in rod OSs (Figure 18A). However, in contrast to per<sup>WT</sup>, Rom-1 could not noticeably rescue the per<sup>MT</sup> OS targeting (Figure 18B and C). Nevertheless, a significant portion of transgenic Rom-1, most likely the Rom-1-per<sup>MT</sup> heterodimers, was withheld in the rod ISs (Figure 18B, C).

In summary, the co-administration of transgenic per<sup>WT</sup> rescued the OS targeting of per<sup>P210L</sup> and per<sup>C214S</sup> in rod photoreceptors. Conversely, co-delivery of transgenic Rom-1 with per<sup>P210L</sup> or per<sup>C214S</sup> led to a partial retention of Rom-1 in the rod ISs. These findings in combination with the results obtained from the SDGC experiments strongly indicate that per<sup>WT</sup>-per<sup>MT</sup>, but not per<sup>MT</sup>-Rom-1 heterodimers can be efficiently targeted to rod OSs.

#### 4.13 Analysis of the per<sup>WT</sup>-per<sup>MT</sup> binding properties in rod OSs using FRET

The results obtained from the co-IP and FRET experiments performed in HEK293T cells (cf. chapter 4.8 and 4.10) revealed that both peripherin-2 mutants display a reduced binding to per<sup>WT</sup>. This finding can be explained by a decreased binding affinity of the per<sup>WT</sup>-per<sup>MT</sup> interaction and/or decreased initial binding kinetics of both mutants to per<sup>WT</sup>. However, as seen in the SDGC experiments, in HEK293T cells transiently co-transfected with per<sup>WT</sup> and per<sup>MT</sup>, in addition to the per<sup>WT</sup>-per<sup>MT</sup> complexes, each mutant can also exist as monomers or can undergo self-interaction forming dimers and aggregates (cf. Figure 16B-E). Considering that all these combinations would contribute to the overall FRET signal, the reduction of  $E_{Amax}$  in HEK293T cells does not allow discriminating between the mechanisms described above. However, the fact that rod OS targeting of both mutants is rescued upon co-delivery of per<sup>WT</sup>

provides an opportunity to address this issue directly: In contrast to HEK293T cells, each of the mutant proteins found in rod OSs must be arranged in complexes with  $\text{per}^{\text{WT}}$ . This happenstance allows for drawing direct conclusions about the  $\text{per}^{\text{WT}}$ - $\text{per}^{\text{MT}}$  binding characteristics under close-to-native conditions by performing FRET measurements on isolated “rescued” rod OSs. For this purpose, WT mice were subretinally co-injected on P14 with rAAVs containing the respective  $\text{per}^{\text{WT}}$  and  $\text{per}^{\text{MT}}$  FRET pairs. Four weeks post injection, rod OSs were isolated and FRET measurements were performed on single transduced OSs simultaneously expressing cerulean-tagged  $\text{per}^{\text{WT}}$  and citrine-tagged  $\text{per}^{\text{MT}}$  (Figure 19).

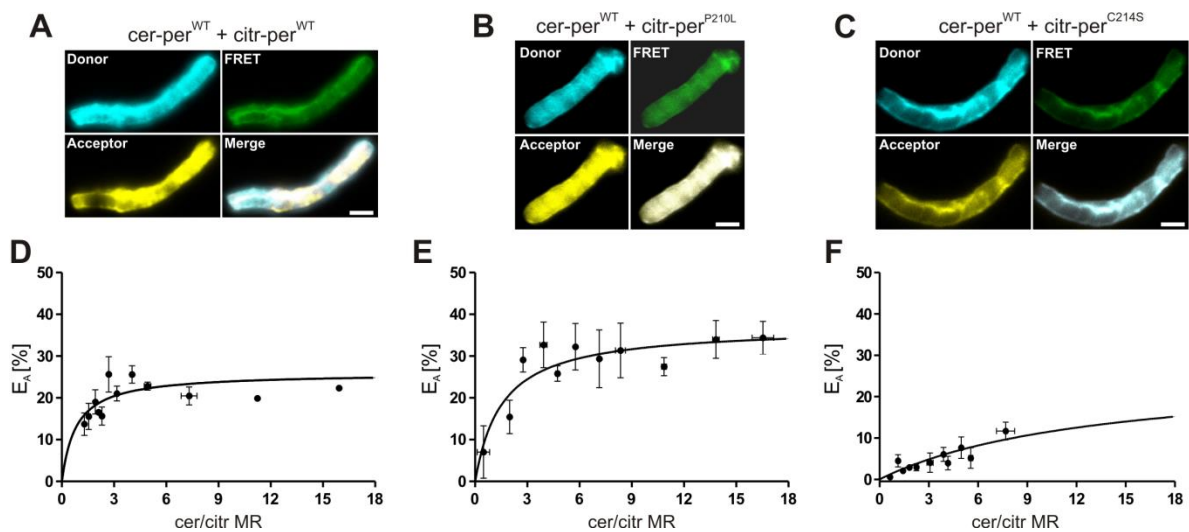


**Figure 19 FRET experiments from rod OSs of retinas co-injected with  $\text{per}^{\text{WT}}$  and  $\text{per}^{\text{MT}}$  rAAVs.** (A-C) Representative confocal images of FRET channels showing a single rod OS co-expressing cer- $\text{per}^{\text{WT}}$  and citr- $\text{per}^{\text{WT}}$  (A), cer- $\text{per}^{\text{WT}}$  and citr- $\text{per}^{\text{P210L}}$  (B), or cer- $\text{per}^{\text{WT}}$  and citr- $\text{per}^{\text{C214S}}$  (C). Scale bar represents 2  $\mu\text{m}$ . (D-F) Binding curves obtained from the corresponding FRET measurements of the different combinations displayed in (A-C). The dots represent mean values of 1-7 single FRET measurements  $\pm$  SEM. The single  $E_A$  values,  $E_{Amax}$ , and numbers of independent measurements ( $n$ ) for each combination are summarized in Supplementary Table 3.

For all three combinations (cer- $\text{per}^{\text{WT}}$  + citr- $\text{per}^{\text{WT}}$ , cer- $\text{per}^{\text{WT}}$  + citr- $\text{per}^{\text{P210L}}$ , and cer- $\text{per}^{\text{WT}}$  + citr- $\text{per}^{\text{C214S}}$ ), robust FRET signals could be measured. Moreover, as the cer/citr MR distinctively varied among the single rod OSs, the calculation of binding curves was possible. Strikingly, the  $E_{Amax}$  values from the isolated rod OSs strongly differed from the FRET results obtained from HEK293T cells (cf. Figure 15D, E).  $E_{Amax}$  was either increased for the  $\text{per}^{\text{WT}}$ - $\text{per}^{\text{P210L}}$  FRET pair or very close to that of the  $\text{per}^{\text{WT}}$  only interaction in case of the  $\text{per}^{\text{WT}}$ - $\text{per}^{\text{C214S}}$  combination (Figure 19D-E, Supplementary Table 3). These results suggest that the robust decrease in the  $\text{per}^{\text{WT}}$ - $\text{per}^{\text{MT}}$  interaction observed in FRET and co-IP experiments (cf. Figure 14 and 15) in HEK293T cells most likely results from a decrease in the initial binding kinetics of both mutants to  $\text{per}^{\text{WT}}$ .

## 5 Discussion

This study unveiled several molecular mechanisms regarding the differential impact of rod- and cone-dominant *PRPH2* mutations in the respective photoreceptor type.

In the first part of the study, the rAAV-mediated expression of per<sup>WT</sup> and per<sup>MT</sup> minigenes in murine photoreceptors uncovered a novel role of mRNA splicing in peripherin-2 pathophysiology in rods and cones. Minigene-derived per<sup>WT</sup> and per<sup>MT</sup> transcripts yielded three distinct isoforms in rods and cones: 1) the correctly spliced, 2) the intron 1 retention, and 3) the unspliced peripherin-2. Importantly, the existence of correctly spliced and unspliced transcripts was confirmed by qPCR from native human and murine retina as well as in FAC-sorted murine rods and cones. Furthermore, the relative amounts of the two isoforms obtained from the rAAV-mediated expression of *PRPH2* minigenes correlated with those from sorted photoreceptors. In FAC-sorted rods, the amount of correctly spliced transcript by far exceeded the amount of unspliced peripherin-2. In contrast, FAC-sorted cones displayed a considerably higher amount of unspliced transcript relative to the correctly spliced variant. These findings indicate that the splicing machinery is somewhat different in rods and cones. It remains unclear why the two photoreceptor types require differential mRNA splicing of *PRPH2*. As only the correctly spliced isoform is translated into protein (cf. chapter 4.5), low levels of this transcript in cones might have evolved to keep peripherin-2 expression rather low in this cell type. Previous studies could demonstrate that peripherin-2 is required for rod and cone OS morphogenesis. Rods from peripherin-2 deficient mice do not show OS-like structures, whereas cones develop atypical OSs [18, 20, 99-101]. Given these findings, the divergent peripherin-2 expression levels in rods and cones might also be relevant for the differential OS structure development in these cells. However, additional studies are necessary to reveal the exact function of differential peripherin-2 expression in photoreceptors.

A comparison of the splicing pattern and protein expression of the per<sup>MT</sup> in rods and cones uncovered a novel genotype-phenotype correlation (Table 5). Three out of the five per<sup>MT</sup> linked to cone defects led to a strong increase of correctly spliced peripherin-2 compared to per<sup>WT</sup>. Accordingly, this increased mRNA splicing efficiency yielded elevated protein expression levels as observed in immunostainings and western blotting of transduced retinas. None of the cone-dominant per<sup>MT</sup> impaired cone OS localization or affected the protein expression pattern. A previous study demonstrated that a moderate overexpression of peripherin-2 in cones (approx. 50 %) does not affect their morphology or function [102]. However, the results of this study indicate that peripherin-2 point mutations could result in protein levels far beyond of the 50 % overexpression analyzed in the aforementioned study, which in turn might very well have negative impacts on cones. The remaining two of the five analyzed cone-dominant per<sup>MT</sup>,

per<sup>S212T</sup> and per<sup>R220W</sup>, did not exhibit any effects on mRNA splicing or protein expression. This indicates that increased protein expression is not a general mechanism solely explaining the penetrance of all cone disease-linked per<sup>MT</sup>. This is in line with a previous study that analyzed per<sup>R172W</sup>, another cone-specific mutation located in the D2 loop of peripherin-2. This mutant led to cone degeneration in mice without affecting the protein expression [103]. Additional studies need to be performed to identify whether protein overexpression, functional defects caused by the per<sup>MT</sup>, or both mechanisms contribute to the disease phenotype.

**Table 5 Summary of the effects caused by the single mutants analyzed in this study.**

	rods						cones				
	C214S	P210L	S198R	Q226E	W246R	G249S	V209I	R195L	R220Q	S212T	R220W
<b>Protein expression</b>	↓↓↓	↓↓	↓↓↓	n.c.	n.c.	↓	↑↑↑	↑↑↑	↑↑↑	n.c.	n.c.
<b>Protein localization</b>	IS	IS	OS	OS	OS	OS	OS	OS	OS	OS	OS
<b>mRNA splicing</b>	n.c.	n.c.	n.c.	n.c.	n.c.	novel donor splice site	increased splice efficiency	increased splice efficiency	increased splice efficiency	n.c.	n.c.

↑, increase, ↓, decrease in protein expression compared to the WT.

IS, inner segment.

OS, outer segment.

n.c., no change.

In comparison to per<sup>MT</sup> linked to cone diseases, four out of the six per<sup>MT</sup> associated with adRP (per<sup>S198R</sup>, per<sup>P210L</sup>, per<sup>C214S</sup>, and per<sup>G249S</sup>) affected the protein expression via one of three distinct mechanisms: protein degradation, protein mislocalization and altered mRNA splicing (Table 5). Despite their diversity, these mechanisms collectively result in decreased protein expression levels in rods.

Among these, per<sup>G249S</sup> was the only mutant that affected mRNA splicing. This mutant gave rise to an additional fourth splice isoform due to the generation of a novel donor splice site within exon 2 (cf. Figure 7B). Except for correctly spliced peripherin-2, all other splice variants detected in this study including this new isoform seemed to be degraded on the mRNA level, most of them probably due to the NMD mechanism. Nevertheless, this aberrantly spliced isoform led to a decrease in the relative amount of the correctly spliced transcript for per<sup>G249S</sup> by approx. 20 %. A previous study using transgenic mice showed that the critical level of peripherin-2 expression required for maintaining proper morphology and function of rods is about 80 % of the native peripherin-2 expression [102]. This suggests that the 20 % reduction of protein expression caused by per<sup>G249S</sup> is very close to this critical level and might be sufficient to cause retinal degeneration in the affected patient.

The per<sup>S198R</sup> mutant appeared to be prone to degradation as it gave rise to an intense additional band in the western blot performed on transduced retinas (cf. Figure 12). Such degradation could be due to improper protein folding resulting in the exposure and/or the masking of existing native protease cleavage sites. The protease cleavage assay performed on membrane preparations from transfected HEK293T cells did not reveal any changes in the protein structure of this mutant (cf. Figure 14D). However, it is conceivable that in the native context other factors contribute to the degradation of per<sup>S198R</sup> resulting in its strongly reduced protein expression in rods.

The remaining two mutants that led to a reduction of protein expression in rods were adRP-linked per<sup>C214S</sup> and per<sup>P210L</sup>. Among all mutants analyzed in this study, only these two were mislocalized to the ISs of rod photoreceptors (cf. Figure 11 and Figure 12). In line with the aforementioned dose-dependency, transgenic mice expressing per<sup>C214S</sup> also exhibited reduced levels of mutant protein in rod OSs resulting in haploinsufficiency [77]. Interestingly, genetic supplementation of per<sup>WT</sup> on the per<sup>C214S</sup> mutant background by generating double transgenic mice resulted in a noticeable rescue of the retinal function [78]. Although helpful in initial stages of therapy development, genetic supplementation is restricted to model organisms. In contrast, rAAV-mediated gene delivery has proven to be a very promising approach for a therapeutic intervention in retinal diseases like RP in mammals [52, 104-106]. Using a rAAV-based approach, this study shows for the first time that rod OS targeting of per<sup>MT</sup> can be rescued *in vivo* upon simultaneous co-delivery of per<sup>WT</sup> (Figure 17). The co-supplementation of per<sup>WT</sup> led to the rescue of protein expression and protein localization of both, per<sup>C214S</sup> and per<sup>P210L</sup>. This finding helps deepening the understanding of *PRPH2*-linked disease mechanisms in photoreceptors and could support the development of future gene therapies for patients with mislocalizing peripherin-2 mutants. However, it remains unclear whether the rescue of per<sup>MT</sup> rod OS targeting caused by the delivery of per<sup>WT</sup> has any detrimental effects in patients heterozygous for these mutations. Consequently, prior to gene therapy, the long-term effects of the mutant rescue on retinal degeneration need to be evaluated in appropriate animal models.

WT mice transduced with the single transgenic per<sup>WT</sup> or per<sup>MT</sup> constructs also express peripherin-2 endogenously. Apparently, as per<sup>C214S</sup> and per<sup>P210L</sup> were completely mislocalized in the absence of transgenic per<sup>WT</sup>, endogenous peripherin-2 is insufficient to rescue protein localization. In line with this, in a recent study using heterozygous transgenic knock-in mice expressing per<sup>C214S</sup>, this mutant also remained in the ISs and was highly prone to degradation [77]. Hence, rAAV-mediated delivery of per<sup>C214S</sup> to WT mice leads to effects comparable to those obtained from mice heterozygous for this mutant. The fact that per<sup>C214S</sup> mutant protein is not targeted to rod OSs indicates that under these conditions per<sup>WT</sup>-per<sup>C214S</sup> complexes are

most likely not formed in considerable amounts. However, additional rAAV-mediated supplementation of per<sup>WT</sup> very likely exceeds the critical levels necessary for efficient per<sup>WT</sup>-per<sup>C214S</sup> complex formation. This further emphasizes the highly critical role of peripherin-2 dosage in the pathophysiology of photoreceptors.

This study also provides novel insights into the structural impacts of per<sup>C214S</sup> and per<sup>P210L</sup> on peripherin-2 folding. Both mutants rearrange the distal part of the D2 loop with the affected region being located around the aa position 260 (cf. Figure 14). The per<sup>C214S</sup> and per<sup>P210L</sup> mutants may also structurally rearrange other parts of this domain which could not be covered by the protease cleavage assay performed in this study. However, based on this assay it is very unlikely that they lead to folding changes in the proximal part of the D2 loop around the highly conserved tetraspanin CCG motif.

Furthermore, per<sup>C214S</sup> and per<sup>P210L</sup> affect residues that are located within the PxxCC motif, which is conserved among tetraspanins [90]. Previous studies demonstrated that both cysteine residues (C213 and C214) of this motif are crucial for the formation of intramolecular disulfide bonds [29, 107], whereas the role of the proline residue (P210) remained unknown. This study shows that the PxxCC motif and its flanking regions (6-9 aa) are not involved in homomeric peripherin-2 interactions. However, the P210 and C214 residues appear to be critical for the proper folding of the D2 loop as no other mutants in close proximity to these positions (e.g. per<sup>V209I</sup> or per<sup>S212T</sup>) changed the accessibility of the protease cleavage site in this part of peripherin-2.

In addition, per<sup>C214S</sup> and per<sup>P210L</sup> show reduced binding to per<sup>WT</sup> and its interaction partner Rom-1 in co-IP and FRET experiments performed in HEK293T cells (cf. Figure 14 and Figure 15). The results of this study indicate that this reduction is based on the misfolding of the D2 loop induced by the two mutants. It is conceivable that this structural change might decrease the affinity of the per<sup>MT</sup> to bind to per<sup>WT</sup> and Rom-1. However, the FRET measurements from isolated rod OSs uncovered that reduced initial binding kinetics of per<sup>C214S</sup> and per<sup>P210L</sup> rather than decreased binding affinities are most likely causative for the decreased interaction with per<sup>WT</sup> (cf. Figure 19). This suggests that the mutant misfolding interferes with the initial binding of per<sup>MT</sup> to per<sup>WT</sup>, but once bound, there is hardly any change in their affinity to per<sup>WT</sup>. These findings are also in line with the results from the peptide competition assay suggesting that the PxxCC motif is not part of the interface for homomeric peripherin-2 interactions.

SDGC experiments performed to analyze the effects of per<sup>C214S</sup> and per<sup>P210L</sup> on protein subunit assembly revealed that in the presence of per<sup>WT</sup> they just form considerably low amounts of tetramers (cf. Figure 16). Instead, both mutants preferentially formed dimers with per<sup>WT</sup> and Rom-1. However, only non-covalent transgenic per<sup>WT</sup>-per<sup>MT</sup> and no per<sup>MT</sup>-Rom-1 heterodimers could be transported to rod OSs (Figure 20). This finding is very surprising for two reasons:

First, non-covalent peripherin-2 tetramerization has been postulated to be crucial for rod OS targeting [28]. However, this conclusion was indirectly drawn from two findings: 1) Tetramerization-deficient peripherin-2 mutants could not be trafficked to rod OSs [28]. 2) No dimers among  $\text{per}^{\text{WT}}$  complexes isolated from rod OSs could be detected [98]. These experiments, however, are insufficient to state whether  $\text{per}^{\text{WT}}\text{-per}^{\text{WT}}$  or  $\text{per}^{\text{WT}}\text{-per}^{\text{MT}}$  dimers can in principle be targeted to rod OSs. This study for the first time demonstrates that  $\text{per}^{\text{WT}}\text{-per}^{\text{MT}}$  dimers can be transported to rod OSs.

The second surprising finding of this part of the study is that, in contrast to  $\text{per}^{\text{WT}}$ , rAAV-mediated co-delivery of Rom-1 and the corresponding increase in Rom-1 levels did not result in any rescue of  $\text{per}^{\text{C214S}}$  or  $\text{per}^{\text{P210L}}$ . This indicates that Rom-1 is not able to fully compensate for the function of peripherin-2 in rod photoreceptors. So far, one can only speculate about the physiological role of these opposing effects of peripherin-2 and Rom-1 in terms of binding and trafficking misfolded  $\text{per}^{\text{MT}}$ .

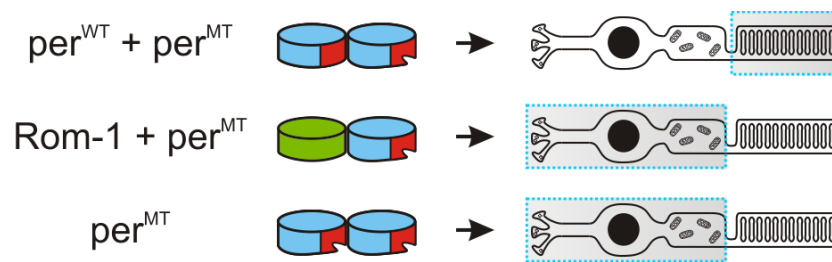


**Figure 20 Rod OS targeting of  $\text{per}^{\text{MT}}$  homo- and heteromeric dimeric complexes.** The localization of the different complexes ( $\text{per}^{\text{WT}}\text{-per}^{\text{MT}}$ ,  $\text{Rom-1-per}^{\text{MT}}$ , and  $\text{per}^{\text{MT}}$  only) in the rod photoreceptors is indicated by a dashed gray rectangle. The position of the D2 loop is highlighted in red and  $\text{per}^{\text{MT}}$  induced misfolding is highlighted via an incision.  $\text{per}^{\text{WT/MT}}$ , blue; Rom-1, green.

In the SGDC experiments (cf. Figure 16), the presence of Rom-1 entirely prevented the formation of  $\text{per}^{\text{MT}}$  aggregates and shifted their complex composition almost completely towards  $\text{per}^{\text{MT}}\text{-Rom-1}$  heterodimers. As these heterodimers were not targeted to rod OSs, it is conceivable that Rom-1 could be acting as a kind of gate keeper preventing the transport of incorrectly folded peripherin-2 mutants to the OSs. Previous studies have shown that digenic RP-linked *ROM1* mutations prevent the forming of peripherin-2 homotetramers and higher-order oligomers [44, 108]. In combination with the results of this study, this indicates that Rom-1 might play an important role in fine-tuning the ratio of peripherin-2/peripherin-2 and peripherin-2/Rom-1 complexes [36].

This study provides a novel experimental design allowing a more accurate analysis of disease mechanisms of point mutations in photoreceptors. Typically, studies focusing on the functional consequences of exonic point mutations are utilizing the full coding sequence (or just single exons) of the respective gene lacking any intronic sequences [109-111]. Here,

by means of *PRPH2* minigenes containing the full coding sequence and the flanking intronic regions, additional disease mechanisms were identified which cannot be found using the classical coding-sequence-only approach. These results strongly suggest that, whenever possible, analysis of disease-associated exonic point mutations should be performed on minigenes.

The disease mechanisms of *PRPH2* mutants identified in this study include the effects on mRNA splicing, protein expression, protein targeting/localization, and protein-protein interactions. The majority of *per*<sup>MT</sup> linked to cone diseases lead to an upregulated peripherin-2 expression in cones by increasing the mRNA splicing efficiency. In contrast, the majority of *per*<sup>MT</sup> associated with rod disorders results in a downregulation of peripherin-2 expression in rods via different mechanisms including aberrant mRNA splicing. It remains unclear why rod defects correlate with lowered amounts of peripherin-2 whereas cones seem to be susceptible to a high expression of this protein. Nevertheless, the latter finding suggests that strong overexpression of *PRPH2* in cones should be avoided in future gene therapy approaches. Finally, the results from the second part of this study indicate that Rom-1 might act as a molecular gate keeper preventing misfolded peripherin-2 from being transported to rod OSs. This raises the possibility that the efficiency of gene supplementation therapy of *PRPH2*-linked RP could be improved by co-delivering peripherin-2 and Rom-1.

## 6 Summary

The tetraspanin peripherin-2 is a transmembrane protein regulating the development, maintenance and renewal of the light-sensing compartments of photoreceptors termed outer segments (OSs). Mutations in the human peripherin-2 gene (*PRPH2*) are associated with severe retinal dystrophies leading to the degeneration or dysfunction of rods or cones. The molecular pathways underpinning this differential penetrance of the mutants in both photoreceptor types are largely unknown. The initial hypothesis of this study was that the rod- or cone-dominance of the *PRPH2* mutants correlates with their differential effects on mRNA splicing, protein expression, protein transport and/or protein-protein interaction in these cells. To address this issue, six rod- and five cone-dominant exonic *PRPH2* point mutations were analyzed in cell culture and in transduced photoreceptors.

In the first part of this study, the impacts of the *PRPH2* mutations on mRNA splicing and concomitant protein expression were investigated in rods and cones. For this purpose, wild type (per<sup>WT</sup>) and mutant (per<sup>MT</sup>) human *PRPH2* minigenes were expressed in murine photoreceptors using recombinant adeno-associated virus (rAAV)-mediated gene delivery. Three different *PRPH2* splice isoforms were found in rods and cones: 1) Correctly spliced 2) Intron 1 retention 3) Unspliced. Among these, only the correctly spliced transcript resulted in detectable protein expression. Surprisingly, differential splicing of *PRPH2* led to high levels of the correctly spliced isoform in rods and to low levels in cones. Three out of the five cone-dominant per<sup>MT</sup> considerably enhanced correct splicing of *PRPH2*, which correlated with a strongly elevated mutant protein expression in these cells. In contrast, four out of the six rod-dominant per<sup>MT</sup> resulted in reduced protein expression via different pathways including aberrant mRNA splicing, protein degradation, and protein mislocalization. These findings unveil novel disease mechanisms of *PRPH2* mutations in photoreceptors and identify the molecular determinants underlying the differential penetrance of rod- and cone-dominant mutations in these cells. Furthermore, these results suggest differential strategies for the treatment of rod- and cone-dominant *PRPH2* mutations.

Peripherin-2 forms homomeric peripherin-2/peripherin-2 and heteromeric complexes with its homolog Rom-1. The contribution of these complexes and the specific role of Rom-1 in the pathophysiology of *PRPH2* mutations remained unclear so far. In the second part of this study, the impact of the aforementioned *PRPH2* mutations on homo- and heteromeric peripherin-2 protein assembly was addressed. Two rod-dominant mutations (per<sup>P210L</sup> and per<sup>C214S</sup>) largely prevented the core peripherin-2/peripherin-2 and peripherin-2/Rom-1 tetramerization resulting predominantly in dimer formation. Surprisingly, however, in contrast to their per<sup>WT</sup>/per<sup>MT</sup> counterparts, the per<sup>MT</sup>/Rom-1 dimers could not be properly targeted to the OSs. This finding

---

uncovered unexpected opposing roles of per<sup>WT</sup> and Rom-1 in OS targeting of rod-dominant peripherin-2 mutations suggesting novel treatment strategies for the affected patients.

## 7 Zusammenfassung

Das Tetraspanin Peripherin-2 ist ein Transmembranprotein, das die Entwicklung, Aufrechterhaltung und Erneuerung der Licht-sensitiven Kompartimente von Photorezeptoren, der sogenannten Außensegmente, reguliert. Mutationen im humanen Peripherin-2 Gen (*PRPH2*) sind mit schweren retinalen Erkrankungen assoziiert, die zur Degeneration oder dem Funktionsverlust von Stäbchen oder Zapfen führen. Die molekularen Ursachen, die zu dieser differenziellen Ausprägung der Mutationen in Stäbchen und Zapfen führen, sind weitestgehend unbekannt. Die Ausgangshypothese dieser Studie war, dass die Stäbchen- bzw. Zapfendominanz der *PRPH2* Mutationen mit deren Auswirkungen auf mRNA Spleißen, Proteinexpression, -transport oder Protein-Protein-Interaktionen zusammenhängt. Um diese Fragestellung zu adressieren, wurden sechs Stäbchen- und fünf Zapfen-spezifische exonische *PRPH2* Punktmutationen in Zellkulturexperimenten und in transduzierten Photorezeptoren analysiert.

Im ersten Teil dieser Studie wurden die Effekte von *PRPH2* Mutationen auf das mRNA Spleißen und die daraus resultierende Proteinexpression in Stäbchen und Zapfen untersucht. Zu diesem Zweck wurden wildtypische ( $\text{per}^{\text{WT}}$ ) und mutierte ( $\text{per}^{\text{MT}}$ ) humane *PRPH2* Minigene mittels rekombinantem Adeno-assoziiertem Virus (rAAV)-vermittelten Gentransfers in murinen Photorezeptoren exprimiert. Drei verschiedene *PRPH2* Spleißisoformen wurden in Stäbchen und Zapfen vorgefunden: 1) Korrekt gespleißt 2) Intron 1 Retention 3) Ungespleißt. Von diesen Isoformen führte nur das korrekt gespleißte Transkript zu einer detektierbaren Proteinexpression. Überraschenderweise führte das differenzielle Spleißen von *PRPH2* in Stäbchen zu großen Mengen an korrekt gespleißter Isoform und zu vergleichsweise sehr geringen Mengen dieses Transkripts in Zapfen. Drei der fünf Zapfen-spezifischen  $\text{per}^{\text{MT}}$  steigerten deutlich den Anteil an korrekt gespleißter *PRPH2* mRNA, was mit einer stark erhöhten Expression an mutiertem Protein in diesen Zellen einherging. Im Gegensatz hierzu resultierten vier der sechs Stäbchen-spezifischen  $\text{per}^{\text{MT}}$  aufgrund verschiedener Mechanismen wie aberrantem mRNA-Spleißen, Proteindegradierung und Proteinefehllokalisation in einer verminderten Proteinexpression. Durch diese Erkenntnisse werden neue Krankheitsmechanismen aufgezeigt, die *PRPH2* Mutationen zu Grunde liegen, und legen die molekularen Mechanismen dar, die zur differenziellen Penetranz in Stäbchen und Zapfen führen können. Gleichzeitig deuten diese Ergebnisse darauf hin, dass zur Therapie Stäbchen- und Zapfen-dominanter *PRPH2* Mutationen unterschiedliche Strategien angewendet werden müssten.

Peripherin-2 kann homomere Peripherin-2/Peripherin-2 und heteromere Komplexe mit seinem Homolog Rom-1 formen. Der genaue Beitrag dieser Komplexe und die spezifische Rolle von Rom-1 in der RP-Pathophysiologie von *PRPH2* Mutationen blieben bisher weitestgehend

ungeklärt. Im zweiten Teil dieser Studie wurde der Einfluss der zuvor genannten *PRPH2* Mutationen auf die Homo- und Heteromerbildung von Peripherin-2 untersucht. Zwei Stäbchen-spezifische Mutationen ( $\text{per}^{\text{P210L}}$  und  $\text{per}^{\text{C214S}}$ ) verhinderten größtenteils die zentrale Peripherin-2/Peripherin-2 und Peripherin-2/Rom-1 Tetramerisierung und formten stattdessen präferentiell Dimere. Überraschenderweise konnten jedoch die  $\text{per}^{\text{MT}}$ -Rom-1 Dimere, im Gegensatz zu ihren  $\text{per}^{\text{WT}}$ - $\text{per}^{\text{MT}}$  Gegenstücken, nicht korrekt in die Außensegmente transportiert werden. Diese Erkenntnis deckt unerwartete gegensätzliche Rollen von  $\text{per}^{\text{WT}}$  und Rom-1 beim Transport von Stäbchen-spezifischen Peripherin-2 Mutationen in die Außensegmente auf. Dies bietet die Grundlage zur Entwicklung neuer Therapieansätze für Patienten, die von Mutationen in *PRPH2* betroffen sind.

## 8 References

1. *Isaac Newton's Life*. Isaac Newton Institute for Mathematical Sciences [Internet] 1998 [cited 2018 August 20]; Available from: <https://www.newton.ac.uk/about/isaac-newton/life>.
2. Veleri, S., et al., *Biology and therapy of inherited retinal degenerative disease: insights from mouse models*. *Dis Model Mech*, 2015. **8**(2): p. 109-29.
3. Broadgate, S., et al., *Unravelling the genetics of inherited retinal dystrophies: Past, present and future*. *Progress in Retinal and Eye Research*, 2017. **59**: p. 53-96.
4. Hoon, M., et al., *Functional architecture of the retina: development and disease*. *Prog Retin Eye Res*, 2014. **42**: p. 44-84.
5. Mathur, P. and J. Yang, *Usher syndrome: Hearing loss, retinal degeneration and associated abnormalities*. *Biochimica et Biophysica Acta (BBA) - Molecular Basis of Disease*, 2015. **1852**(3): p. 406-420.
6. Rieke, F., *Mechanisms of single-photon detection in rod photoreceptors*. *Methods Enzymol*, 2000. **316**: p. 186-202.
7. Sampath, A.P. and F. Rieke, *Selective transmission of single photon responses by saturation at the rod-to-rod bipolar synapse*. *Neuron*, 2004. **41**(3): p. 431-43.
8. Arikawa, K., et al., *Localization of peripherin/rds in the disk membranes of cone and rod photoreceptors: relationship to disk membrane morphogenesis and retinal degeneration*. *J Cell Biol*, 1992. **116**(3): p. 659-67.
9. Bessant, D.A., R.R. Ali, and S.S. Bhattacharya, *Molecular genetics and prospects for therapy of the inherited retinal dystrophies*. *Curr Opin Genet Dev*, 2001. **11**(3): p. 307-16.
10. Dias, M.F., et al., *Molecular genetics and emerging therapies for retinitis pigmentosa: Basic research and clinical perspectives*. *Progress in Retinal and Eye Research*, 2018. **63**: p. 107-131.
11. *ASGCT Celebrates FDA Approval of Voretigene Neparvovec (Luxturna) as Treatment for Inherited Retinal Disease*. American Society of Gene & Cell Therapy [Internet] 2017 [cited 2018 September 8]; Available from: <https://www.asgct.org/research/news/december-2017/luxturna-fda-approval-spark>.
12. Fahim, A.T., S.P. Daiger, and R.G. Weleber, *Nonsyndromic Retinitis Pigmentosa Overview*, in *GeneReviews((R))*, M.P. Adam, et al., Editors. 1993: Seattle (WA).
13. Aït-Ali, N., et al., *Rod-Derived Cone Viability Factor Promotes Cone Survival by Stimulating Aerobic Glycolysis*. *Cell*, 2015. **161**(4): p. 817-832.
14. Leveillard, T., et al., *Identification and characterization of rod-derived cone viability factor*. *Nat Genet*, 2004. **36**(7): p. 755-9.
15. Gu, S., et al., *Autosomal recessive retinitis pigmentosa locus RP28 maps between D2S1337 and D2S286 on chromosome 2p11-p15 in an Indian family*. *J Med Genet*, 1999. **36**(9): p. 705-7.
16. Ziviello, C., et al., *Molecular genetics of autosomal dominant retinitis pigmentosa (ADRP): a comprehensive study of 43 Italian families*. *J Med Genet*, 2005. **42**(7): p. e47.
17. *RetNet: Summaries of Genes and Loci Causing Retinal Diseases*. Stephen P. Daiger, PhD and The University of Texas Health Science Center, Houston, Texas [Internet] August 2018 [cited 2018 September 8]; Available from: <https://sph.uth.edu/retnet/sum-dis.htm#A-genes>.
18. Sanyal, S. and H.G. Jansen, *Absence of receptor outer segments in the retina of rds mutant mice*. *Neurosci Lett*, 1981. **21**(1): p. 23-6.
19. Jansen, H.G. and S. Sanyal, *Development and degeneration of retina in rds mutant mice: electron microscopy*. *J Comp Neurol*, 1984. **224**(1): p. 71-84.
20. Reuter, J.H. and S. Sanyal, *Development and degeneration of retina in rds mutant mice: the electroretinogram*. *Neurosci Lett*, 1984. **48**(2): p. 231-7.

21. Molday, R.S., D. Hicks, and L. Molday, *Peripherin. A rim-specific membrane protein of rod outer segment discs*. Invest Ophthalmol Vis Sci, 1987. **28**(1): p. 50-61.
22. Boon, C.J., et al., *The spectrum of retinal dystrophies caused by mutations in the peripherin/RDS gene*. Prog Retin Eye Res, 2008. **27**(2): p. 213-35.
23. Connell, G.J. and R.S. Molday, *Molecular cloning, primary structure, and orientation of the vertebrate photoreceptor cell protein peripherin in the rod outer segment disk membrane*. Biochemistry, 1990. **29**(19): p. 4691-8.
24. Travis, G.H., J.G. Sutcliffe, and D. Bok, *The retinal degeneration slow (rds) gene product is a photoreceptor disc membrane-associated glycoprotein*. Neuron, 1991. **6**(1): p. 61-70.
25. Hemler, M.E., *Tetraspanin functions and associated microdomains*. Nat Rev Mol Cell Biol, 2005. **6**(10): p. 801-11.
26. Goldberg, A.F. and R.S. Molday, *Subunit composition of the peripherin/rds-rom-1 disk rim complex from rod photoreceptors: hydrodynamic evidence for a tetrameric quaternary structure*. Biochemistry, 1996. **35**(19): p. 6144-9.
27. Goldberg, A.F., et al., *Folding and subunit assembly of photoreceptor peripherin/rds is mediated by determinants within the extracellular/intradiskal EC2 domain: implications for heterogeneous molecular pathologies*. J Biol Chem, 2001. **276**(46): p. 42700-6.
28. Loewen, C.J., et al., *The role of subunit assembly in peripherin-2 targeting to rod photoreceptor disk membranes and retinitis pigmentosa*. Mol Biol Cell, 2003. **14**(8): p. 3400-13.
29. Goldberg, A.F., C.J. Loewen, and R.S. Molday, *Cysteine residues of photoreceptor peripherin/rds: role in subunit assembly and autosomal dominant retinitis pigmentosa*. Biochemistry, 1998. **37**(2): p. 680-5.
30. Chakraborty, D., et al., *Differential requirements for retinal degeneration slow intermolecular disulfide-linked oligomerization in rods versus cones*. Hum Mol Genet, 2009. **18**(5): p. 797-808.
31. Zulliger, R., et al., *Oligomerization of Prph2 and Rom1 is essential for photoreceptor outer segment formation*. Hum Mol Genet, 2018.
32. Chakraborty, D., et al., *Outer segment oligomerization of Rds: evidence from mouse models and subcellular fractionation*. Biochemistry, 2008. **47**(4): p. 1144-56.
33. Poetsch, A., L.L. Molday, and R.S. Molday, *The cGMP-gated channel and related glutamic acid-rich proteins interact with peripherin-2 at the rim region of rod photoreceptor disc membranes*. J Biol Chem, 2001. **276**(51): p. 48009-16.
34. Bascom, R.A., et al., *Cloning of the cDNA for a novel photoreceptor membrane protein (rom-1) identifies a disk rim protein family implicated in human retinopathies*. Neuron, 1992. **8**(6): p. 1171-84.
35. Moritz, O.L. and R.S. Molday, *Molecular cloning, membrane topology, and localization of bovine rom-1 in rod and cone photoreceptor cells*. Invest Ophthalmol Vis Sci, 1996. **37**(2): p. 352-62.
36. Clarke, G., et al., *Rom-1 is required for rod photoreceptor viability and the regulation of disk morphogenesis*. Nat Genet, 2000. **25**(1): p. 67-73.
37. Manes, G., et al., *High prevalence of PRPH2 in autosomal dominant retinitis pigmentosa in france and characterization of biochemical and clinical features*. Am J Ophthalmol, 2015. **159**(2): p. 302-14.
38. Goldberg, A.F., *Role of peripherin/rds in vertebrate photoreceptor architecture and inherited retinal degenerations*. Int Rev Cytol, 2006. **253**: p. 131-75.
39. Ferrari, S., et al., *Retinitis pigmentosa: genes and disease mechanisms*. Curr Genomics, 2011. **12**(4): p. 238-49.
40. Conley, S.M., et al., *Rom1 converts Y141C-Prph2-associated pattern dystrophy to retinitis pigmentosa*. Hum Mol Genet, 2017.
41. Dryja, T.P., et al., *Dominant and digenic mutations in the peripherin/RDS and ROM1 genes in retinitis pigmentosa*. Invest Ophthalmol Vis Sci, 1997. **38**(10): p. 1972-82.
42. Kajiwara, K., E.L. Berson, and T.P. Dryja, *Digenic retinitis pigmentosa due to mutations at the unlinked peripherin/RDS and ROM1 loci*. Science, 1994. **264**(5165): p. 1604-8.

43. Sullivan, L.S., et al., *Prevalence of disease-causing mutations in families with autosomal dominant retinitis pigmentosa: a screen of known genes in 200 families*. Invest Ophthalmol Vis Sci, 2006. **47**(7): p. 3052-64.
44. Goldberg, A.F. and R.S. Molday, *Defective subunit assembly underlies a digenic form of retinitis pigmentosa linked to mutations in peripherin/rds and rom-1*. Proc Natl Acad Sci U S A, 1996. **93**(24): p. 13726-30.
45. Kedzierski, W., et al., *Deficiency of rds/peripherin causes photoreceptor death in mouse models of digenic and dominant retinitis pigmentosa*. Proc Natl Acad Sci U S A, 2001. **98**(14): p. 7718-23.
46. Daya, S. and K.I. Berns, *Gene Therapy Using Adeno-Associated Virus Vectors*. Clinical Microbiology Reviews, 2008. **21**(4): p. 583-593.
47. Schön, C., M. Biel, and S. Michalakis, *Retinal gene delivery by adeno-associated virus (AAV) vectors: Strategies and applications*. European Journal of Pharmaceutics and Biopharmaceutics, 2015. **95**: p. 343-352.
48. Balaji, B. and R.J. Giridhara, *Basic Biology of Adeno-Associated Virus (AAV) Vectors Used in Gene Therapy*. Current Gene Therapy, 2014. **14**(2): p. 86-100.
49. Allocca, M., et al., *Novel Adeno-Associated Virus Serotypes Efficiently Transduce Murine Photoreceptors*. Journal of Virology, 2007. **81**(20): p. 11372-11380.
50. Petrs-Silva, H., et al., *High-efficiency Transduction of the Mouse Retina by Tyrosine-mutant AAV Serotype Vectors*. Molecular Therapy, 2009. **17**(3): p. 463-471.
51. Kotterman, M.A. and D.V. Schaffer, *Engineering adeno-associated viruses for clinical gene therapy*. Nature Reviews Genetics, 2014. **15**: p. 445.
52. Koch, S., et al., *Gene therapy restores vision and delays degeneration in the CNGB1(-/-) mouse model of retinitis pigmentosa*. Hum Mol Genet, 2012. **21**(20): p. 4486-96.
53. Michalakis, S., et al., *Restoration of cone vision in the CNGA3-/- mouse model of congenital complete lack of cone photoreceptor function*. Mol Ther, 2010. **18**(12): p. 2057-63.
54. Boye, S.E., et al., *A comprehensive review of retinal gene therapy*. Mol Ther, 2013. **21**(3): p. 509-19.
55. Michalakis, S., et al., *Gene therapy for achromatopsia*. J Gene Med, 2017. **19**(3).
56. McClements, M.E. and R.E. MacLaren, *Adeno-associated Virus (AAV) Dual Vector Strategies for Gene Therapy Encoding Large Transgenes*. Yale J Biol Med, 2017. **90**(4): p. 611-623.
57. Salganik, M., M.L. Hirsch, and R.J. Samulski, *Adeno-associated Virus as a Mammalian DNA Vector*. Microbiol Spectr, 2015. **3**(4).
58. Allocca, M., et al., *Novel adeno-associated virus serotypes efficiently transduce murine photoreceptors*. J Virol, 2007. **81**(20): p. 11372-80.
59. Petrs-Silva, H., et al., *High-efficiency transduction of the mouse retina by tyrosine-mutant AAV serotype vectors*. Mol Ther, 2009. **17**(3): p. 463-71.
60. Vandenberghe, L.H. and A. Auricchio, *Novel adeno-associated viral vectors for retinal gene therapy*. Gene Ther, 2012. **19**(2): p. 162-8.
61. Gao, G.P., et al., *Novel adeno-associated viruses from rhesus monkeys as vectors for human gene therapy*. Proc Natl Acad Sci U S A, 2002. **99**(18): p. 11854-9.
62. Auricchio, A., et al., *Isolation of highly infectious and pure adeno-associated virus type 2 vectors with a single-step gravity-flow column*. Hum Gene Ther, 2001. **12**(1): p. 71-6.
63. Livak, K.J. and T.D. Schmittgen, *Analysis of relative gene expression data using real-time quantitative PCR and the 2(-Delta Delta C(T)) Method*. Methods, 2001. **25**(4): p. 402-8.
64. Riedmayr, L.M., Böhm, S., Michalakis, S. and Becirovic, E., *Construction and Cloning of Minigenes for in vivo Analysis of Potential Splice Mutations*. Bio-protocol, 2018.
65. Graham, F.L. and A.J. van der Eb, *A new technique for the assay of infectivity of human adenovirus 5 DNA*. Virology, 1973. **52**(2): p. 456-67.
66. Bradford, M.M., *A rapid and sensitive method for the quantitation of microgram quantities of protein utilizing the principle of protein-dye binding*. Anal Biochem, 1976. **72**: p. 248-54.

67. Wu, C. and Y. Lu, *Inclusion of high molecular weight dextran in calcium phosphate-mediated transfection significantly improves gene transfer efficiency*. Cell Mol Biol (Noisy-le-grand), 2007. **53**(4): p. 67-74.
68. Akimoto, M., et al., *Targeting of GFP to newborn rods by Nrl promoter and temporal expression profiling of flow-sorted photoreceptors*. Proc Natl Acad Sci U S A, 2006. **103**(10): p. 3890-5.
69. Fei, Y. and T.E. Hughes, *Transgenic expression of the jellyfish green fluorescent protein in the cone photoreceptors of the mouse*. Vis Neurosci, 2001. **18**(4): p. 615-23.
70. Becirovic, E., et al., *In Vivo Analysis of Disease-Associated Point Mutations Unveils Profound Differences in mRNA Splicing of Peripherin-2 in Rod and Cone Photoreceptors*. PLoS Genet, 2016. **12**(1): p. e1005811.
71. Butz, E.S., et al., *Quantifying macromolecular interactions in living cells using FRET two-hybrid assays*. Nat Protoc, 2016. **11**(12): p. 2470-2498.
72. Griesbeck, O., et al., *Reducing the environmental sensitivity of yellow fluorescent protein. Mechanism and applications*. J Biol Chem, 2001. **276**(31): p. 29188-94.
73. Rizzo, M.A., et al., *An improved cyan fluorescent protein variant useful for FRET*. Nat Biotechnol, 2004. **22**(4): p. 445-9.
74. Erickson, M.G., et al., *FRET two-hybrid mapping reveals function and location of L-type Ca<sup>2+</sup> channel CaM preassociation*. Neuron, 2003. **39**(1): p. 97-107.
75. Ben Johny, M., et al., *Dynamic switching of calmodulin interactions underlies Ca<sup>2+</sup> regulation of CaV1.3 channels*. Nat Commun, 2013. **4**: p. 1717.
76. Shaltiel, L., et al., *Complex regulation of voltage-dependent activation and inactivation properties of retinal voltage-gated Cav1.4 L-type Ca<sup>2+</sup> channels by Ca<sup>2+</sup>-binding protein 4 (CaBP4)*. J Biol Chem, 2012. **287**(43): p. 36312-21.
77. Stricker, H.M., et al., *The Cys214-->Ser mutation in peripherin/rds causes a loss-of-function phenotype in transgenic mice*. Biochem J, 2005. **388**(Pt 2): p. 605-13.
78. Nour, M., S.J. Fliesler, and M.I. Naash, *Genetic supplementation of RDS alleviates a loss-of-function phenotype in C214S model of retinitis pigmentosa*. Adv Exp Med Biol, 2008. **613**: p. 129-38.
79. Yanagihashi, S., et al., *Autosomal dominant central areolar choroidal dystrophy and a novel Arg195Leu mutation in the peripherin/RDS gene*. Arch Ophthalmol, 2003. **121**(10): p. 1458-61.
80. Coco, R.M., et al., *PRPH2 (Peripherin/RDS) mutations associated with different macular dystrophies in a Spanish population: a new mutation*. Eur J Ophthalmol, 2010. **20**(4): p. 724-32.
81. Budu, et al., *Peripherin/RDS gene mutation (Pro210Leu) and polymorphisms in Japanese patients with retinal dystrophies*. Jpn J Ophthalmol, 2001. **45**(4): p. 355-8.
82. Felbor, U., H. Schilling, and B.H. Weber, *Adult vitelliform macular dystrophy is frequently associated with mutations in the peripherin/RDS gene*. Hum Mutat, 1997. **10**(4): p. 301-9.
83. Saga, M., et al., *A novel Cys-214-Ser mutation in the peripherin/RDS gene in a Japanese family with autosomal dominant retinitis pigmentosa*. Hum Genet, 1993. **92**(5): p. 519-21.
84. Payne, A.M., et al., *Founder effect, seen in the British population, of the 172 peripherin/RDS mutation-and further refinement of genetic positioning of the peripherin/RDS gene*. Am J Hum Genet, 1998. **62**(1): p. 192-5.
85. Jacobson, S.G., et al., *Photoreceptor function in heterozygotes with insertion or deletion mutations in the RDS gene*. Invest Ophthalmol Vis Sci, 1996. **37**(8): p. 1662-74.
86. Rodriguez, J.A., A.M. Gannon, and S.P. Daiger, *Screening for mutations in rhodopsin and peripherin/RDS in patients with autosomal dominant retinitis pigmentosa*. Vol. 55. 1994.
87. Kohl, S., et al., *RDS/peripherin gene mutations are frequent causes of central retinal dystrophies*. J Med Genet, 1997. **34**(8): p. 620-6.

88. Renner, A.B., et al., *Phenotypic variability and long-term follow-up of patients with known and novel PRPH2/RDS gene mutations*. *Am J Ophthalmol*, 2009. **147**(3): p. 518-530 e1.
89. Becirovic, E., et al., *Peripherin-2 couples rhodopsin to the CNG channel in outer segments of rod photoreceptors*. *Hum Mol Genet*, 2014. **23**(22): p. 5989-97.
90. Seigneuret, M., et al., *Structure of the tetraspanin main extracellular domain. A partially conserved fold with a structurally variable domain insertion*. *J Biol Chem*, 2001. **276**(43): p. 40055-64.
91. Chakraborty, D., et al., *Structural characterization of the second intra-discal loop of the photoreceptor tetraspanin RDS*. *FEBS J*, 2013. **280**(1): p. 127-38.
92. Roy, A., *Chapter Three - Membrane Preparation and Solubilization*, in *Methods in Enzymology*, A.K. Shukla, Editor. 2015, Academic Press. p. 45-56.
93. Ding, X.Q., H.M. Stricker, and M.I. Naash, *Role of the second intradiscal loop of peripherin/rds in homo and hetero associations*. *Biochemistry*, 2005. **44**(12): p. 4897-904.
94. Nguyen, O.N., et al., *Peripherin-2 differentially interacts with cone opsins in outer segments of cone photoreceptors*. *Hum Mol Genet*, 2016. **25**(12): p. 2367-2377.
95. Patterson, G.H., D.W. Piston, and B.G. Barisas, *Förster Distances between Green Fluorescent Protein Pairs*. *Analytical Biochemistry*, 2000. **284**(2): p. 438-440.
96. Ding, X.Q., et al., *The R172W mutation in peripherin/rds causes a cone-rod dystrophy in transgenic mice*. *Hum Mol Genet*, 2004. **13**(18): p. 2075-87.
97. Loewen, C.J. and R.S. Molday, *Disulfide-mediated oligomerization of Peripherin/Rds and Rom-1 in photoreceptor disk membranes. Implications for photoreceptor outer segment morphogenesis and degeneration*. *J Biol Chem*, 2000. **275**(8): p. 5370-8.
98. Goldberg, A.F., O.L. Moritz, and R.S. Molday, *Heterologous expression of photoreceptor peripherin/rds and Rom-1 in COS-1 cells: assembly, interactions, and localization of multisubunit complexes*. *Biochemistry*, 1995. **34**(43): p. 14213-9.
99. Sanyal, S., A. De Ruiter, and R.K. Hawkins, *Development and degeneration of retina in rds mutant mice: light microscopy*. *J Comp Neurol*, 1980. **194**(1): p. 193-207.
100. Nir, I. and D.S. Papermaster, *Immunocytochemical localization of opsin in the inner segment and ciliary plasma membrane of photoreceptors in retinas of rds mutant mice*. *Invest Ophthalmol Vis Sci*, 1986. **27**(5): p. 836-40.
101. Farjo, R., et al., *Retention of function without normal disc morphogenesis occurs in cone but not rod photoreceptors*. *J Cell Biol*, 2006. **173**(1): p. 59-68.
102. Nour, M., et al., *Modulating expression of peripherin/rds in transgenic mice: critical levels and the effect of overexpression*. *Invest Ophthalmol Vis Sci*, 2004. **45**(8): p. 2514-21.
103. Conley, S., et al., *Late-Onset Cone Photoreceptor Degeneration Induced by R172W Mutation in Rds and Partial Rescue by Gene Supplementation*. *Investigative Ophthalmology & Visual Science*, 2007. **48**(12): p. 5397-5407.
104. Rossmiller, B., H. Mao, and A.S. Lewin, *Gene therapy in animal models of autosomal dominant retinitis pigmentosa*. *Mol Vis*, 2012. **18**: p. 2479-96.
105. Petrs-Silva, H. and R. Linden, *Advances in gene therapy technologies to treat retinitis pigmentosa*. *Clin Ophthalmol*, 2014. **8**: p. 127-36.
106. Ali, R.R., et al., *Restoration of photoreceptor ultrastructure and function in retinal degeneration slow mice by gene therapy*. *Nat Genet*, 2000. **25**(3): p. 306-10.
107. Conley, S.M., M.W. Stuck, and M.I. Naash, *Structural and functional relationships between photoreceptor tetraspanins and other superfamily members*. *Cellular and Molecular Life Sciences*, 2012. **69**(7): p. 1035-1047.
108. Loewen, C.J., O.L. Moritz, and R.S. Molday, *Molecular characterization of peripherin-2 and rom-1 mutants responsible for digenic retinitis pigmentosa*. *J Biol Chem*, 2001. **276**(25): p. 22388-96.
109. Bernstein, H.S., et al., *Fabry disease: six gene rearrangements and an exonic point mutation in the alpha-galactosidase gene*. *The Journal of Clinical Investigation*, 1989. **83**(4): p. 1390-1399.

110. Lee, S., et al., *Exonic point mutations of human tau enhance its toxicity and cause characteristic changes in neuronal morphology, tau distribution and tau phosphorylation in the lamprey cellular model of tauopathy*. J Alzheimers Dis, 2009. **16**(1): p. 99-111.
111. Fukuda, S., et al., *Mucopolysaccharidosis type IVA. N-acetylgalactosamine-6-sulfate sulfatase exonic point mutations in classical Morquio and mild cases*. The Journal of Clinical Investigation, 1992. **90**(3): p. 1049-1053.





Mutation	ASSEDA (fold change to WT)										NNSplice Score	
	Donor	Acceptor	Donor <sub>genom</sub>	Acceptor <sub>genom</sub>	SC35	SRp40	SRp55	SF2_ASF	hnRNP A1	Donor	Acceptor	
<b>P219R</b>	n.c.	↓ 2.4x CATCCAGT ↓ 1.9x GTATCAGA	n.c.	n.c.	↑ 16.5x	1.7x ↓	n.c.	n.c.	n.c.	n.c.	n.c.	
<b>R220W</b>	n.c.	↓ 1.3x CATCCAGT ↓ 1.1x GTATCAGA	n.c.	n.c.	n.c.	41.0x ↓	3.3x ↓	n.c.	n.c.	n.c.	n.c.	
<b>R220Q</b>	n.c.	↓ 1.5x CATCCAGT ↑ 9.0x GCCACGGC (G>A)	n.c.	n.c.	↑ 3.9x	14.8x ↓	7.3x ↓	1.4x ↓	n.c.	n.c.	n.c. Novel AS GCCACAGGC Score = 0.68	
<b>Q226E</b>	↑ (10.3x) TCCA <b>GT</b> ATC	↓ 1.8x GTATCAGA	↑ (4.2x) TCCA <b>GT</b> ATC	n.c.	n.c.	1.7x ↓	n.c.	n.c.	↑ 45.6x	n.c.	n.c.	
<b>N244H</b>	n.c.	↑ 1.4x GCTGCAGG	n.c.	n.c.	2.5x ↓	n.c.	n.c.	n.c.	n.c.	n.c.	n.c.	
<b>N244K (AAC&gt;AAG)</b>	↓ 2.2x AACCT <b>GT</b> G	↓ 2.0x GCTGCAGG	↓ 2.0x AACCT <b>GT</b> G	n.c.	5.8x ↓ ↑ 3.0x	n.c.	n.c.	n.c.	n.c.	n.c.	n.c.	
<b>N244K (AAC&gt;AAA)</b>	n.c.	↓ 1.7x GCTGCAGG	n.c.	n.c.	2.4x ↓	↑ 7.9x	n.c.	n.c.	14.1x ↓	n.c.	n.c.	
<b>W246R</b>	↑ 3.0x TGTGG <b>GT</b> G ↓ 28.3x AACCT <b>GT</b> G	n.c.	↑ 3.0x TGTGG <b>GT</b> G ↓ 4.5x AACCT <b>GT</b> G	n.c.	1.3x ↓	n.c.	↑ 3.3x 3.3x ↓	↑ 2.7x	n.c.	n.c. Novel DS TGTGG <b>GT</b> G Score = 0.41	n.c.	
<b>G249S</b>	↓ 1.3x TGTGG <b>GT</b> G	n.c.	n.c.	n.c.	7.8x ↓ 2.5x ↓	n.c.	↑ 3.3x 7.8x ↓	n.c.	↑ 3.7x	n.c. Novel DS TGTGG <b>GT</b> G Score = 0.65	n.c.	
<b>G266D</b>	n.c.	n.c.	n.c.	n.c.	↑ 4.6x	2.2x ↓	2.0x ↓	2.3x ↓	n.c.	n.c.	n.c.	
<b>V268I</b>	n.c.	n.c.	n.c.	n.c.	3.1x ↓	n.c.	n.c.	2.3x ↓	n.c.	n.c.	n.c.	

**Supplementary Table 2 Relative intensity percentages of peripherin-2 isoforms obtained for per<sup>WT</sup> and per<sup>MT</sup> minigenes (cf. Figure 7). MV, mean value; SEM, standard error of the mean; n.s., not significant.**

		rods										cones					
		C214S	P210L	S198R	Q226E	W246R	G249S	WT	V209I	R195L	R220Q	S212T	R220W	WT			
unspliced	MV	7.48	6.79	6.17	6.41	7.22	8.53	7.54	65.0	58.0	46.2	84.7	86.7	87.1			
	SEM	1.00	1.85	1.25	1.43	1.70	1.84	1.19	2.25	1.60	2.86	1.78	1.24	1.12			
	Dunnett's test	n.s.	n.s.	n.s.	n.s.	n.s.	n.s.	n.s.	n.s.	n.s.	n.s.	n.s.	n.s.	n.s.			
intron 1 retention	MV	25.6	24.2	25.3	22.8	23.7	25.7	22.4	14.5	14.9	17.3	13.0	11.3	11.3			
	SEM	3.40	2.15	2.38	2.99	1.77	2.64	2.26	1.38	1.26	1.50	1.97	0.95	1.06			
	Dunnett's test	n.s.	n.s.	n.s.	n.s.	n.s.	n.s.	n.s.	n.s.	n.s.	n.s.	n.s.	n.s.	n.s.			
correctly spliced	MV	66.9	69.1	68.6	70.8	69.1	56.2	70.1	20.5	27.1	36.5	2.25	2.01	1.64			
	SEM	2.65	3.21	3.09	4.16	3.39	1.31	2.09	1.59	2.04	2.89	0.39	0.43	0.42			
	Dunnett's test	n.s.	n.s.	n.s.	n.s.	n.s.	p<0.05		p<0.0001	p<0.0001	p<0.0001	n.s.	n.s.	n.s.			

**Supplementary Table 3 FRET measurements from HEK293T cells and isolated rescued rod OSs (cf. Figure 15 and Figure 19). n, number of cells/rod OSs.**

	HEK293T										rod OSs		
	WT-WT	WT-P210L	WT-C214S	P210L-P210L	P210L-C214S	C214S-C214S	WT-Rom-1	Rom-1-P210L	Rom-1-C214S	WT-WT	WT-P210L	WT-C214S	
$E_{Amax}$	34.2	9.44	8.58	30.7	26.5	15.6	6.58	6.32	26.0	37.1	26.5		
% of WT-WT or WT-Rom-1	-	28	25	90	77	-	42	40	-	143	102		
n	53	53	50	53	54	48	48	48	45	32	44		

**Supplementary Table 4 Quantification of the SDGC experiments.** Values are given as mean values  $\pm$  SEM.

		Immunoreactivity (% of Total)											
		1	2	3	4	5	6	7	8	9	10	11	
n = 3	WT	Non-covalent	0.00	0.00	0.00	2.78 $\pm$ 2.78	9.33 $\pm$ 0.71	11.53 $\pm$ 1.38	11.70 $\pm$ 2.15	10.98 $\pm$ 2.06	2.65 $\pm$ 2.65	2.76 $\pm$ 2.76	1.68 $\pm$ 1.68
		Disulfide bond	0.00	2.05 $\pm$ 2.05	4.73 $\pm$ 2.39	7.97 $\pm$ 1.60	11.78 $\pm$ 1.26	12.46 $\pm$ 1.50	7.61 $\pm$ 0.57	0.00	0.00	0.00	0.00
n = 4	P210L	Non-covalent	0.00	0.00	0.00	0.00	0.00	0.00	0.00	0.00	2.10 $\pm$ 2.10	20.35 $\pm$ 4.66	19.00 $\pm$ 6.53
		Disulfide bond	0.00	0.00	0.00	0.00	2.86 $\pm$ 2.86	5.44 $\pm$ 3.16	4.81 $\pm$ 2.79	5.78 $\pm$ 2.13	2.67 $\pm$ 2.67	1.78 $\pm$ 1.78	0.00
n = 3	C214S	Aggregate	0.00	0.00	2.08 $\pm$ 2.08	8.28 $\pm$ 3.17	10.83 $\pm$ 1.53	8.80 $\pm$ 3.07	3.18 $\pm$ 2.67	2.02 $\pm$ 1.78	0.00	0.00	0.00
		Non-covalent	0.00	0.00	0.00	0.00	2.61 $\pm$ 2.61	4.36 $\pm$ 4.36	3.42 $\pm$ 3.42	3.34 $\pm$ 3.34	18.23 $\pm$ 13.07	27.29 $\pm$ 14.59	5.20 $\pm$ 5.20
n = 5	P210L + WT IB: anti-myc	Aggregate	7.28 $\pm$ 3.77	7.65 $\pm$ 4.20	5.27 $\pm$ 5.27	4.03 $\pm$ 4.03	6.78 $\pm$ 6.78	4.53 $\pm$ 4.53	0.00	0.00	0.00	0.00	0.00
		Non-covalent	0.00	1.74 $\pm$ 1.74	2.84 $\pm$ 2.84	3.13 $\pm$ 3.13	5.13 $\pm$ 3.15	4.33 $\pm$ 2.80	2.07 $\pm$ 2.07	4.45 $\pm$ 2.73	23.39 $\pm$ 4.14	27.42 $\pm$ 5.71	12.38 $\pm$ 5.53
n = 4	P210L + WT IB: anti-myc	Disulfide bond	0.00	0.00	0.00	0.00	0.00	0.00	0.00	0.00	0.00	0.00	0.00
		Aggregate	0.00	1.36 $\pm$ 1.36	0.00	2.01 $\pm$ 1.27	3.57 $\pm$ 2.37	3.94 $\pm$ 2.49	2.23 $\pm$ 2.23	0.00	0.00	0.00	0.00
n = 3	P210L + WT IB: anti-flag	Non-covalent	0.00	0.00	0.00	0.00	2.37 $\pm$ 2.37	1.85 $\pm$ 1.85	9.13 $\pm$ 1.95	11.07 $\pm$ 4.26	10.79 $\pm$ 5.76	11.68 $\pm$ 3.67	0.00
		Disulfide bond	3.68 $\pm$ 3.68	4.67 $\pm$ 4.67	6.60 $\pm$ 3.45	7.86 $\pm$ 4.13	12.61 $\pm$ 0.59	11.95 $\pm$ 2.62	3.35 $\pm$ 3.35	2.40 $\pm$ 2.40	0.00	0.00	0.00
n = 4	C214S + WT IB: anti-myc	Non-covalent	0.00	0.00	0.00	0.00	4.45 $\pm$ 2.64	5.22 $\pm$ 3.09	5.91 $\pm$ 3.74	16.61 $\pm$ 3.49	12.33 $\pm$ 4.41	20.32 $\pm$ 4.78	19.65 $\pm$ 10.11
		Aggregate	0.00	0.00	5.87 $\pm$ 3.60	7.81 $\pm$ 2.74	1.82 $\pm$ 1.82	0.00	0.00	0.00	0.00	0.00	0.00
n = 3	WT + Rom-1 IB: anti-myc	Non-covalent	0.00	0.00	0.00	0.00	1.45 $\pm$ 1.45	1.67 $\pm$ 1.12	5.95 $\pm$ 1.39	3.40 $\pm$ 1.90	6.41 $\pm$ 0.57	7.52 $\pm$ 0.92	4.11 $\pm$ 4.11
		Disulfide bond	5.51 $\pm$ 2.76	8.75 $\pm$ 1.12	10.40 $\pm$ 0.57	11.06 $\pm$ 0.38	11.38 $\pm$ 0.63	9.58 $\pm$ 0.63	7.24 $\pm$ 0.64	3.46 $\pm$ 1.90	2.11 $\pm$ 2.11	0.00	0.00
n = 3	P210L + Rom-1 IB: anti-myc	Non-covalent	0.00	0.00	0.00	0.00	8.22 $\pm$ 0.86	10.20 $\pm$ 1.46	6.34 $\pm$ 3.17	4.70 $\pm$ 4.70	2.77 $\pm$ 2.77	0.00	0.00
		Disulfide bond	8.48 $\pm$ 4.42	10.61 $\pm$ 1.81	10.18 $\pm$ 1.60	9.69 $\pm$ 1.87	10.50 $\pm$ 2.20	10.41 $\pm$ 1.38	7.92 $\pm$ 0.20	0.00	0.00	0.00	0.00
n = 3	C214S + Rom-1 IB: anti-myc	Non-covalent	0.00	0.00	0.00	1.45 $\pm$ 1.45	5.40 $\pm$ 2.89	14.96 $\pm$ 2.60	17.61 $\pm$ 1.74	18.26 $\pm$ 9.93	19.35 $\pm$ 3.61	8.99 $\pm$ 5.91	3.61 $\pm$ 3.61
		Disulfide bond	0.00	0.00	0.00	0.00	3.49 $\pm$ 1.85	4.55 $\pm$ 2.65	2.33 $\pm$ 2.33	0.00	0.00	0.00	0.00
n = 3	P210L + Rom-1 IB: anti-myc	Non-covalent	0.00	0.00	0.00	0.00	0.00	0.00	0.00	4.56 $\pm$ 4.56	22.76 $\pm$ 2.11	31.48 $\pm$ 6.45	28.67 $\pm$ 9.40
		Disulfide bond	0.00	0.00	0.00	0.00	0.00	0.00	0.00	0.00	0.00	0.00	0.00
n = 3	P210L + Rom-1 IB: anti-flag	Aggregate	0.00	5.60 $\pm$ 5.60	0.00	0.00	5.01 $\pm$ 5.01	1.93 $\pm$ 1.93	0.00	0.00	0.00	0.00	0.00
		Non-covalent	0.00	0.00	0.00	0.00	0.00	0.00	0.00	0.00	19.68 $\pm$ 9.84	43.50 $\pm$ 2.28	36.82 $\pm$ 12.12
n = 3	C214S + Rom-1 IB: anti-myc	Disulfide bond	0.00	0.00	0.00	0.00	0.00	0.00	0.00	0.00	0.00	0.00	0.00
		Non-covalent	0.00	0.00	0.00	0.00	0.00	4.59 $\pm$ 4.59	4.91 $\pm$ 4.91	0.00	29.00 $\pm$ 2.51	31.53 $\pm$ 3.67	24.34 $\pm$ 3.41
n = 3	C214S + Rom-1 IB: anti-myc	Aggregate	0.00	0.00	0.00	0.00	5.64 $\pm$ 5.64	0.00	0.00	0.00	0.00	0.00	0.00
		Non-covalent	0.00	0.00	0.00	0.00	0.00	0.00	0.00	2.43 $\pm$ 2.43	28.57 $\pm$ 6.38	26.46 $\pm$ 2.94	21.20 $\pm$ 2.41
n = 3	P210L + Rom-1 IB: anti-flag	Disulfide bond	0.00	0.00	0.00	0.00	0.00	0.00	1.75 $\pm$ 1.75	6.79 $\pm$ 4.15	10.18 $\pm$ 0.14	2.60 $\pm$ 2.60	0.00

**Supplementary Table 5 Primers used for cloning of the human peripherin-2 minigene.**

Primer name	Sequence 5' – 3'
hPrph2_BamHI_F	CCGGATCCGCCACCATGGCGCTACTGAAAGTCAAGT
hPrph2_NotI_R	GATCGCGGCCGCTCAGCCAGCCTCTGGGGCCTGG
OL_Prph2_In1_F	CCTCTTTGACCCATAAAAAATCGAGGAAGGCAGGGGCATTTA
OL_Prph2_In1_R	TAAATGCCCTGCCTTCCTCGATTTTTTATGGGTCAAAGAGG
OL_Prph2_In2_F	GGCCTCCACCTTTTGTATTTAGACATGAGGCTGGAGAAGAGT
OL_Prph2_In2_R	ACTCTTCTCCAGCCTCATGTCTAAATACAAAAGGTGGAGGCC

**Supplementary Table 6 Primers used for the introduction of the single point mutations in the human peripherin-2 minigene using side-directed mutagenesis.** The base pair required for the amino acid exchange is highlighted in red.

Primer name	Sequence 5' – 3'
hPrph2_R195L_F	TGTTTCCCTTTAAGTCTAATCAAGAGCAACGTG
hPrph2_R195L_R	CACGTTGCTCTTGATTAGACTTAAAGGGAAACA
hPrph2_S198R_F	TAAGTCGAATCAAGAGGAACGTGGATGGGCGGT
hPrph2_S198R_R	ACCGCCATCCACGTTCTCTTGATTCTGACTTA
hPrph2_V209I_F	GTACCTGGTGGACGGCATCCCTTTCAGCTGCTG
hPrph2_V209I_R	CAGCAGCTGAAAGGGATGCCGTCCACCAGGTAC
hPrph2_P210L_F	CTGGTGGACGGCGTCCTTTTTCAGCTGCTGCAAT
hPrph2_P210L_R	ATTGCAGCAGCTGAAAAGGACGCCGTCCACCAG
hPrph2_S212T_F	GACGGCGTCCCTTTTCACTGCTGCAATCCTAGC
hPrph2_S212T_R	GCTAGGATTGCAGCAGGTGAAAGGGACGCCGTG
hPrph2_C214S_F	GTCCCTTTCAGCTGCTCCAATCCTAGCTCGCCA
hPrph2_C214S_R	TGGCGAGCTAGGATTGGAGCAGCTGAAAGGGAC
hPrph2_R220Q_F	AATCCTAGCTCGCCACAGCCCTGCATCCAGTAT
hPrph2_R220Q_R	ATACTGGATGCAGGGCTGTGGCGAGCTAGGATT
hPrph2_R220W_F	CAATCCTAGCTCGCCATGGCCCTGCATCCAGTA
hPrph2_R220W_R	TACTGGATGCAGGGCCATGGCGAGCTAGGATTG
hPrph2_Q226E_F	GCCCTGCATCCAGTATGAGATCACCAACAACCTC
hPrph2_Q226E_R	GAGTTGTTGGTGTCTCATACTGGATGCAGGGC
hPrph2_W246R_F	GGAGGAGCTCAACCTGCGGGTGCCTGGCTGCAG
hPrph2_W246R_R	CTGCAGCCACGCACCCGCAGGTTGAGCTCCTCC
hPrph2_G249S_F	CAACCTGTGGGTGCGTAGCTGCAGGGCTGCCCT
hPrph2_G249S_R	AGGGCAGCCCTGCAGCTACGCACCCACAGGTTG

**Supplementary Table 7 Primers used for the amplification of the splice isoforms resulting from the peripherin-2 minigenes (cf. Figure 7B).**

Primer name	Sequence 5' – 3'
Citr_End_Seq_F	GGCATGGACGAGCTATACAAG
hPrph2_E3_Seq_R	GGTTGGACACACCATCCAGCG

**Supplementary Table 8 Primers used for the detection of native murine (mP) and human (hP) peripherin-2 transcripts via qPCR (cf. Figure 9). cs, correctly spliced; us, unspliced.**

Primer name	Sequence 5' – 3'
Alas fwd	TCGCCGATGCCATTCTTATC
Alas rev	GGCCCCAACTTCCATCATCT
Rhodopsin fwd	GCCTCGAGAGCCGCAGCCATG
Rhodopsin rev	GCAGGAACATGTACGCTGCC
M-opsin fwd	GTTCCAGAGACAGTTTTCTAC
M-opsin rev	CAACGACCACAAGAATCATCC
mP-cs_F	TCTCCTCCAAGGAGGTCAAAG
mP-cs_R	GAGTCCGGCAGTGATGCTCAC
mP-us_F	GGGAGGATCTGCTGCTTGGTG
mP-us_R	GCTCACCAGGTCTGTCTTCAC
ALAS fwd	GATGTCAGCCACCTCAGAGAAC
ALAS rev	CATCCACGAAGGTGATTGCTCC
hP-cs_F	GTGGATCAGCAATCGCTACC
hP-cs_R	GGTTGGACACACCATCCAGCG
hP-us_F	GAAGTGGCCCCTGTTGAGAAG
hP-us_R	CATTAGACCCAAATGGGACCG

**Supplementary Table 9 Primers used for cloning of truncated peripherin-2 (cf. Figure 10).**

Primer name	Sequence 5' – 3'
hPrph2_trunc_F	CAGCAGCCTCATGAATTCCTAGGGCGTCGTCACACTTCTCG
hPrph2_trunc_R	CGAGAAGTGTGACGACGCCCTAGGAATTCATGAGGCTGCTG

## 9.2 Abbreviations

aa	amino acid
adRP	autosomal dominant retinitis pigmentosa
AFVD	adult-onset foveomacular vitelliform dystrophy
Alas	aminolevulinic acid synthase
APS	ammonium persulfate
2x BBS	2x BES buffered saline
BES	N,N-bis(2-hydroxyethyl)-2-aminoethanesulfonic acid
bp	base pair
CaCl <sub>2</sub>	calcium chloride
cap	genes for adeno viral packaging
cDNA	complementary DNA
cm	centimeter
CNGB1a	cyclic nucleotide gated channel beta 1a
CO <sub>2</sub>	carbon dioxide
co-IP	co-immunoprecipitation
CRISPR	clustered regularly interspaced short palindromic repeats
CT	cycle threshold
dk	donkey
DNA	deoxyribonucleic acid
H <sub>2</sub> O	water
DTT	dithiothreitol
$E_{Amax}$	maximal FRET efficiency
<i>E. coli</i>	Escherichia coli
EDTA	ethylenediaminetetraacetic acid
EGFP	enhanced green fluorescent protein
FACS	fluorescence-activated cell sorting
FBS	fetal bovine serum
FRET	Förster resonance energy transfer
g	gram
<i>g</i>	gravity
GCL	ganglion cell layer
gt	goat
h	hour
HCl	hydrochloric acid

---

HEK293T	human embryonic kidney cells expressing the SV40 large T antigen
HRP	horseradish peroxidase
hRHO	human rhodopsin promoter
INL	inner nuclear layer
IPL	inner plexiform layer
IS	inner segment
ITR	inverted terminal repeat
IRD	inherited retinal disease
kb	kilobase pair
KCl	potassium chloride
l	liter
M	molar
MgCl <sub>2</sub>	magnesium chloride
μg	microgram
μl	microliter
mg	milligram
min	minute
mM	millimolar
ml	milliliter
MOPS	3-morpholinopropane-1-sulfonic acid
mRNA	messenger RNA
mSws	murine short wavelength opsin promoter
MW	molecular weight
NaCl	sodium chloride
ng	nanogram
nm	nanometer
NMD	nonsense-mediated mRNA decay
ONL	outer nuclear layer
OPL	outer plexiform layer
OS	outer segment
pAD Helper	adenovirus helper plasmid
PAGE	polyacrylamide gel electrophoresis
PB	phosphate buffer
PBS	phosphate buffered saline
PCR	polymerase chain reaction

---

PFA	paraformaldehyde
PMMA	polymethyl methacrylate
<i>Prph2/PRPH2</i>	peripherin-2
PVDF	polyvinylidene fluoride
qPCR	quantitative real-time PCR
rAAV	recombinant adeno-associated virus
rb	rabbit
rep	genes for adeno viral replication
rds/RDS	retinal degeneration slow
RNA	ribonucleic acid
Rom-1	rod outer segment membrane protein 1
RPE	retinal pigment epithelium
rpm	revolutions per minute
RT	room temperature
RT-PCR	reverse transcription PCR
SDS	sodium dodecylsulfate
sec	second
SEM	standard error of the mean
SDGC	sucrose density gradient centrifugation
SV40	simian virus
T1-T4	transmembrane domain 1-4
TBE	tris-borate EDTA
TBST	tris-buffered saline with Tween20
TEMED	tetramethylethylenediamine
TRIS	tris(hydroxymethyl)aminomethane
WPRE	woodchuck hepatitis virus posttranscriptional regulatory element
WT	wild type

### 9.3 Curriculum vitae

#### Personal Details

---

Name Sybille Böhm

Nationality German

#### Education

---

Since 05/2015 Graduate School Life Science Munich (LSM)  
PhD program

Since 02/2015 Ludwig-Maximilians-University, Munich  
Department of Pharmacy  
Pharmacology for Natural Sciences  
PhD student

03/2013 – 09/2014 Technical University of Applied Sciences Georg Simon Ohm,  
Nuremberg  
Department of Applied Chemistry  
Master of Science Biochemistry

10/2009 – 03/2013 Technical University of Applied Sciences Georg Simon Ohm,  
Nuremberg  
Department of Applied Chemistry  
Bachelor of Science Biochemistry

09/2000 – 06/2009 Friedrich-Alexander-Gymnasium, Neustadt/Aisch  
A levels

#### Awards

---

04/2018 Scholarship from the “Deutscher Akademiker Austausch Dienst”  
(DAAD) for participation in the Association for Research in Vision and  
Ophthalmology Meeting,  
Honolulu, Hawaii

06/2016 Poster Award  
Life Science Munich (LSM) Retreat, Gut Schönwag, Germany

## 9.4 Lebenslauf

### Persönliche Daten

---

Name Sybille Böhm

Nationalität Deutsch

### Bildungsweg

---

Seit 05/2015 Graduate School Life Science Munich (LSM)  
Mitglied der Graduiertenschule

Seit 02/2015 Ludwig-Maximilians-Universität München  
Fakultät für Chemie und Pharmazie  
Pharmakologie für Naturwissenschaften  
Doktorand

03/2013 – 09/2014 Technische Hochschule Nürnberg Georg Simon Ohm  
Fakultät für angewandte Chemie  
Master of Science Biochemie

10/2009 – 03/2013 Technische Hochschule Nürnberg Georg Simon Ohm  
Fakultät für angewandte Chemie  
Bachelor of Science Biochemie

09/2000 – 06/2009 Friedrich-Alexander-Gymnasium, Neustadt/Aisch  
Abitur

### Auszeichnungen

---

04/2018 Stipendium vom "Deutscher Akademiker Austausch Dienst" (DAAD) für die Teilnahme am Association for Research in Vision and Ophthalmology Meeting, Honolulu, Hawaii

06/2016 Posterpreis  
Life Science Munich (LSM) Retreat, Gut Schönwag, Deutschland

## 9.5 List of publications

### Publications

---

- Riedmayr LM, **Böhm S**, Michalakis S, Becirovic E. (2018). Construction and Cloning of Minigenes for *in vivo* Analysis of Potential Splice Mutations. *Bio-protocol* 8(5): e2760.
- **Böhm S**, Riedmayr LM, Nguyen ONP, Gießl A, Liebscher T, Butz ES, Schön C, Michalakis S, Wahl-Schott C, Biel M, Becirovic E. Peripherin-2 and Rom-1 have opposing effects on rod outer segment targeting of retinitis pigmentosa-linked peripherin-2 mutants. *Sci Rep.* 2017 May 24;7(1):2321.
- Becirovic E, **Böhm S**, Nguyen ON, Riedmayr LM, Hammelmann V, Schön C, Butz ES, Wahl-Schott C, Biel M, Michalakis S. AAV Vectors for FRET-Based Analysis of Protein-Protein Interactions in Photoreceptor Outer Segments. *Front Neurosci.* 2016 Jul 28;10:356.
- Nguyen ON, **Böhm S**, Gießl A, Butz ES, Wolfrum U, Brandstätter JH, Wahl-Schott C, Biel M, Becirovic E. Peripherin-2 differentially interacts with cone opsins in outer segments of cone photoreceptors. *Hum Mol Genet.* 2016 Jun 15;25(12):2367-2377.
- Becirovic E, **Böhm S**, Nguyen ON, Riedmayr LM, Koch MA, Schulze E, Kohl S, Borsch O, Santos-Ferreira T, Ader M, Michalakis S, Biel M. *In Vivo* Analysis of Disease-Associated Point Mutations Unveils Profound Differences in mRNA Splicing of Peripherin-2 in Rod and Cone Photoreceptors. *PLoS Genet.* 2016 Jan; 12(1): e1005811.

## 9.6 Danksagung

Zu Beginn möchte ich mich recht herzlich bei Herrn Prof. Dr. Biel bedanken, dass ich diese Arbeit in seinem Arbeitskreis durchführen konnte.

Insbesondere danke ich dir Elvir, dass du mich damals mit ins Boot geholt hast ;). Deine Tür war immer offen und deine Ratschläge sowie deine enorme wissenschaftliche Expertise waren stets sehr hilfreich. Du bist nicht nur ein fairer Chef und super Betreuer, sondern auch ein echter Freund. Vielen Dank dafür!

Weiterhin bedanke ich mich bei all meinen Arbeitskollegen, die mir sehr ans Herz gewachsen sind und die ich nie hätte missen möchten, ein großes Lob an eure Freundlich- und Herzlichkeit sowie eure uneingeschränkte Hilfsbereitschaft. Die zahlreichen gemeinsamen Unternehmungen, die von einem Feierabendbierchen in der Küche über unser „wöchentliches“ Kicken bis hin zum Ski Trip nach Garmisch reichten, waren jedes Mal ein Highlight am Ende des Laboralltags. Es freut mich nicht nur Kollegen, sondern auch wahre Freunde in dieser aufregenden und auch manchmal schwierigen Zeit gefunden zu haben.

Hierbei sind besonders Vicky, Lisa und Schöttelinchen zu nennen. Vicky meine Liebe, ich weiß es ist nicht immer einfach zwischen uns, aber ich danke dir von Herzen für deine Freundschaft, die mir v.a. am Anfang das Einleben in München außerordentlich erleichtert hat. Lisa, „my partner in crime“, es war eine unglaubliche Bereicherung dich im Team Elvir zu haben, fachlich wie auch privat. Unsere eigenen kleinen „Meetings“ waren immer überaus konstruktiv und die gemeinsamen Konferenzen wurden durch dich nur noch besser. Verena, meine Platznachbarin, ich danke dir für dein immer offenes Ohr, die lustigen gemeinsamen Unternehmungen und ich vergesse nie die Zeit zusammen im dunklen Kämmerchen ;).

Ein enorm großer Dank geht auch an meine zwei Ladies von zu Hause, Angi und Judith. Euer Anhören meiner kleinen sowie großen Sorgen in manch mehr oder minder schwierigen Situation oder aber auch verzweifelten Lage hat mich stets über den Tag gerettet. Trotz der Entfernung seid und wart ihr immer für mich da und dafür schätze ich euch sehr.

Schlussendlich komme ich zu den Menschen, ohne die es überhaupt nie so weit gekommen wäre und denen ich diese Arbeit widmen möchte, meiner Familie. Ohne eure tatkräftige Unterstützung und euren Beistand würde ich heute nicht an diesem Punkt in meinem Leben stehen. Das Wissen, dass ihr immer für mich da seid und sein werdet, bestärkt mich jeden Tag in all dem was ich tue. Ich danke euch!